

1-1-2004

Electric field alignment of diblock copolymer thin films.

Ting, Xu

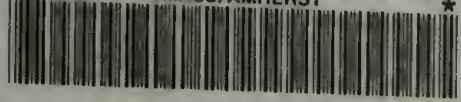
University of Massachusetts Amherst

Follow this and additional works at: https://scholarworks.umass.edu/dissertations_1

Recommended Citation

Xu, Ting,, "Electric field alignment of diblock copolymer thin films." (2004). *Doctoral Dissertations 1896 - February 2014*. 1059.
https://scholarworks.umass.edu/dissertations_1/1059

This Open Access Dissertation is brought to you for free and open access by ScholarWorks@UMass Amherst. It has been accepted for inclusion in Doctoral Dissertations 1896 - February 2014 by an authorized administrator of ScholarWorks@UMass Amherst. For more information, please contact scholarworks@library.umass.edu.



312066 0288 9968 4



**ELECTRIC FIELD ALIGNMENT OF
DIBLOCK COPOLYMER THIN FILMS**

A Dissertation Presented

by

TING XU

Submitted to the Graduate School of the
University of Massachusetts Amherst in partial fulfillment
of the requirements for the degree of

DOCTOR OF PHILOSOPHY

May 2004

Polymer Science and Engineering

© Copyright by Ting Xu 2004

All Rights Reserved

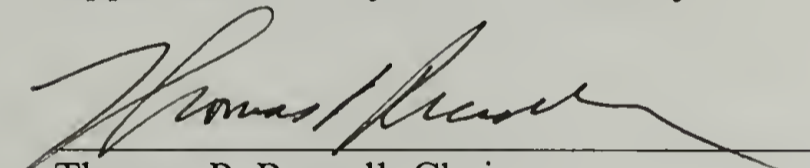
**ELECTRIC FIELD ALIGNMENT OF DIBLOCK COPOLYMER THIN
FILMS**

A Dissertation Presented

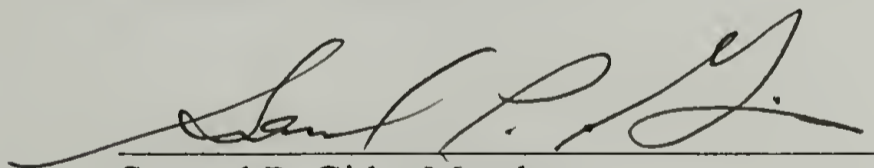
by

TING XU

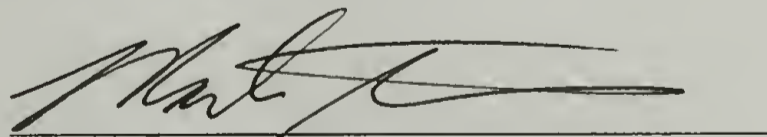
Approved as to style and content by:



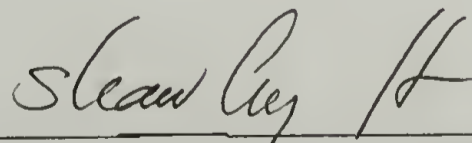
Thomas P. Russell, Chair



Samuel P. Gido, Member



Mark Tuominen, Member



Shawling Hsu, Interim Department Head
Polymer Science and Engineering

To my parents
To all the people that love me

ACKNOWLEDGEMENTS

Becoming a Ph.D graduate has been expected for so long that when it comes, it seems unreal. I am going to finish my graduate student career and start another leg of the journey. I indulge myself to enjoy the moment. At the same time, I can feel pain in my heart to say good-bye to everybody who loves me and all the people I love. In a way, I wish I could stay.

The past four and a half years rewinds like a movie. I was fortunate to be admitted to PSE, join Prof. Thomas P. Russell's group, work with excellent researchers and make friends. It was the happiest time in my life and it is definitely my advisor Prof. Thomas P. Russell who made it happen. I am grateful to Tom for his vast amount of knowledge, creativity, enthusiasm in science and endless efforts and patience to educate and promote students. As a mentor, he gave me complete freedom to explore the world of polymer physics. I will benefit from his unique approach to problems and persistence in pursuing cutting edge science for the rest of my life. He is the best role model for me to become a scientist, an educator and most importantly, a person.

I would like to thank my committee members, Prof. Samuel P. Gido and Prof. Mark Tuominen for their time, useful suggestions and discussions. A great portion of the thesis work was done using transmission electron microscopy. Prof. Gido and his groupmembers, especially Yuqing Zhu gave me lots of help. Prof. Tuominen's research group and I had close collaborations and they gave me lots of insights and assistance with my research work. I also would like to thank the entire faculty in the department, not only for their excellent teaching in the first year classes, but also for

their unconditional help over the years. Prof. Shaw Ling Hsu helped me with my visa problems even before I came to the country. Once I joined PSE, the faculty were always happy to help me using their expertise. Discussions, especially those with Prof. Winter, Hoagland and McCarthy, widened my horizons. Besides, their friendly greetings and care definitely made the long-distance study easier for a foreign student.

I lose my words when I think of how to say 'thank you' to my group members. Their wonderfulness makes leaving so hard. Here, I need to mention my dearest advisor, Tom, again who made the group like a family for everybody. Amanda, Irene and I started in the same year and became very good friends. Amanda helped me like a sister since the first time we met. She has always been there for me. Irene is another good friend over the years. The happy times we spent together will remain good memories for rest of my life. One of the many advantages of being in Tom's research group is the active interactions between group members. I benefited from all of the past and present postdoctoral researchers who shared their knowledge and useful suggestions. Particularly, I appreciate the help from Tobias, Hocheol, Shenda, Keisuke, Mashahiro, Jinkon, Dongha, Seunghyun, Hongqi, Alex and Brian. The past and present graduate students in our group are also great. It would have taken longer to finish my thesis work without help from Lee, Michael, Jason, Chris, Scott, James, Zhiqun, Matt, Yao, Kris, Julie, Jame, Suresh, Dongseok, Xiaochuan and Qingling. Especially, I thank Jason, Amanda, Matt, Jame, Dongseok and Seunghyun for the sleepless nights at the beam lines.

Our department has first class secretaries and staff. I was so lucky that I have been 'spoiled' since the first day I stepped into the PSE door. They took care of everything they could and let us concentrate on our research work. I would like to thank Linda, Eileen, Sophie, Ann, Susan and Joann. I also would like to thank Greg, John, Andre, Jack and Louis for their assistance over years. Lou helped me with TEM, which was essential to the whole work. John made the sample holders for the neutron scattering studies and Jack helped me with XPS measurements. Without Andre, I, probably, am still trying to fix my computers. It was also a great pleasure for me to work with the middle school teachers, Cathy, Jodi and Julieann from the research experience for teachers program.

My classmates are also an important part in my graduate school experience. We all became good friends and care for each other. Their friendship and encouragement, especially those from Chris, Amanda and Irene, will stay with me for the rest of my life.

I had the opportunity to work with the scientists, Ben and Oleg, at Brookhaven National Laboratory and Hammouda, Derek and Steve at the National Institute of Standards and Technology. It is the experimental results obtained at these beam lines that opened the door for the thesis. Without their help, the experiments were not able to be completed.

There is an important person in my life who guided me into the wonderful world of polymer physics. He is my previous advisor for my Master's degree in China, Prof. Bingzheng Jiang. The only pity for me is that he left before he could share this moment with me. I will miss him forever.

The page is too short to list all the people who helped me over the years. I am sure I did not include everybody here. I am sincerely grateful for every favor I got along the way.

Finally, I would like to thank my family. My parents devoted their whole life to my sisters and me. Their unconditional love and support made it possible for me to finish my Ph.D study. There is nothing in the world comparable to what I got from them. I will cherish their love for the rest of my life. My sisters and I have been very close over the years and they gave me a happy childhood. They are, and always will be, my best friends forever.

ABSTRACT

ELECTRIC FIELD ALIGNMENT OF DIBLOCK COPOLYMER THIN FILMS

MAY 2004

TING XU, B.S., DALIAN UNIVERSITY OF TECHNOLOGY

M.S., CHANGCHUN INSTITUTE OF APPLIED CHEMISTRY, CHINESE

ACADEMY OF SCIENCES

M.S., UNIVERSITY OF MASSACHUSETTS AMHESRT

Ph.D., UNIVERSITY OF MASSACHUSETTS AMHESRT

Directed by: Professor Thomas P. Russell

By anchoring random copolymers to the substrates, the interfacial interactions were tuned precisely and dependence of the orientation of lamellar microdomains in thin films on interfacial interactions was investigated quantitatively. A critical film thickness was found, below which a parallel alignment of the lamellar microdomains was seen throughout the film and depends upon the strength of the interfacial interactions.

The electric field alignment process is a competition between the applied electric field and surface fields. In the early stages, the surface field dominates. A mixture of orientations of the lamellae was found if the interfacial interactions were not balanced. However, in the presence of lithium ions (210ppm), lamellar microdomains were aligned along the applied electric field direction throughout the film, regardless of the strong interactions of blocks with substrate.

For cylindrical microdomain forming diblock copolymer thin films, starting from a poorly-ordered state, surface fields and opposed electric fields biased the cylinder orientation. With time upon annealing, the cylinders are locally disrupted to

form ellipsoidal shape microdomains that connected into cylinders in the applied field direction. Starting from an ordered state with cylinders parallel to the surface, the applied field enhanced fluctuations at the interfaces of the microdomains and disrupted cylinders into spheres. This transition is similar to thermoreversible cylinder-to-sphere order-order transition. With time, the spheres deformed into ellipsoids and reconnected forming cylindrical microdomains oriented at $\sim 45^\circ$ with respect to the applied field, which subsequently aligned along the field direction.

These studies were complemented by studies on an electric field induced disordered sphere-to-cylinder transition in thin films. Under an electric field, the asymmetric diblock copolymer formed spherical microdomains that were deformed into ellipsoids and, with time, interconnected into cylindrical microdomains oriented in the direction of the applied electric field.

A route to control the microdomain orientation in three dimensions in diblock copolymer thin films was also studied by use of two orthogonal, external fields. An elongational flow field was applied to obtain an in-plane orientation of the microdomains of the copolymer melt and an electric field, applied normal to the surface, was then used to further align the microdomains.

TABLE OF CONTENTS

	Page
ACKNOWLEDGEMENTS.....	v
ABSTRACT.....	ix
LIST OF FIGURES	xiv
CHAPTER	
1. EFFECT OF INTERFACIAL INTERACTIONS ON MICRODOMAIN ORIENTATION IN DIBLOCK COPOLYMER THIN FILMS	1
Introduction.....	1
Experimental	3
Materials	3
Sample Preparation	3
Results and Discussion	4
Conclusions.....	12
References.....	14
2. EFFECT OF INTERFACIAL INTERACTIONS ON ELECTRIC FIELD ALIGNMENT OF SYMMETRIC DIBLOCK COPOLYMER THIN FILMS	15
Introduction.....	15
Experimental	17
Materials	17
Sample Preparation	17
Results and Discussion	18
Conclusions.....	25
References.....	26
3. ELECTRIC FIELD ALIGNMENT OF SYMMETRIC DIBLOCK COPOLYMER THIN FILMS	28
Introduction.....	28
Experimental	31
Materials	31
Sample preparation	31

Results and Discussion	32
Conclusions.....	43
References.....	44
 4. EFFECT OF IONIC IMPURITIES IN ELECTRIC FIELD ALIGNMENT OF DIBLOCK COPOLYMER THIN FILMS.....	 46
Introduction.....	46
Experimental	48
Materials	48
Sample preparation	49
Results and Discussion	50
Conclusions.....	58
References.....	59
 5. ELECTRIC FIELD ALIGNMENT OF ASYMMETRIC DIBLOCK COPOLYMER THIN FILMS	 61
Introduction.....	61
Experimental	64
Materials	64
Sample preparation	65
Results and Discussion	65
Conclusions.....	79
References.....	81
 6. ELECTRIC FIELD INDUCED SPHERE TO CYLINDER TRANSITION IN DIBLOCK COPOLYMER THIN FILMS.....	 84
Introduction.....	84
Experimental	86
Materials	86
Sample preparation	86
Results and Discussion	87
Conclusions.....	94
References.....	95

7. SEQUENTIAL, ORTHOGONAL FIELDS: A PATH TO LONG-RANGE, 3-D ORDER IN BLOCK COPOLYMER THIN FILMS	97
Introduction.....	97
Experimental.....	99
Materials	99
Sample preparation	99
Results and Discussion	101
Conclusions.....	110
References.....	111
BIBLIOGRAPHY.....	113

LIST OF FIGURES

Figure	Page
1.1 Small angle neutron scattering profiles of <i>dPS-b-PMMA</i> thin films on Si substrate modified with random copolymers of (a) 58/42 (~320nm), (b) 65/35 (~320nm), and (c) 90/10 (~505nm) after annealing at 170°C under vacuum for 72hrs. The samples were tilted at 60° with respect to the incident beam. (d) shows the azimuthal angle integration of the SANS intensity in (a), (b) and (c).	7
1.2 (a) Small angle neutron scattering peak intensities of the <i>dPS-b-PMMA</i> thin films with different thicknesses. The films were on Si substrates modified with different random copolymers, 58/42, 65/35, 70/30, 90/10. (b) is the plot of the critical film thickness beyond which the parallel lamellar microdomains could not propagate throughout the whole film vs. interfacial interaction	8
1.3 Cross-sectional transmission electron microscopy images of annealed <i>PS-b-PMMA</i> thin films with different film thicknesses on Si substrates modified with random copolymers: (a) 58/42 (~400nm) (b) 70/30 (~430nm) (c) 70/30 (~800nm) (d) 90/10 (~800nm).....	10
1.4 Fraction of parallel lamellae microdomains vs. the distance from the copolymer/substrate interface. Each image was sectioned into slices of the equilibrium period thickness from the copolymer/substrate interface. The fraction of the parallel lamellae was counted in each slice and plotted vs. the distance from the copolymer/substrate interface. Each point was obtained by averaging ~20µm wide cross-sectional TEM images. The solid lines were plotted to guide the eye.....	12
2.1 Grazing incidence small angle x-ray scattering patterns of <i>PS-b-PMMA</i> (~900nm) films on silicon substrate with native oxide layer (a) after annealing under vacuum and (b) after annealing under ~40V/µm electric field	19
2.2 Transmission Electron Microscopy cross-section images of <i>PS-b-PMMA</i> thin films after (a) 90/10, annealed under vacuum for 48hrs and annealing under ~40V/µm electric field on the substrates modified with different random copolymers, (b) 58/42, $\delta \approx 0$, (c) 70/30, $\delta \approx 0.62$, (d) 80/20, $\delta \approx 0.73$, (e) 90/10, $\delta \approx 0.94$	21
2.3 Transmission Electron Microscopy cross-section images of <i>PS-b-PMMA</i> thin films (~3µm) after annealing under ~40V/µm electric field on the substrates modified with 90/10 random copolymers	22

2.4	Transmission Electron Microscopy cross-section images of PS- <i>b</i> -PMMA thin films after annealing under $\sim 40\text{V}/\mu\text{m}$ electric field for 1hr at $160\pm 5^\circ\text{C}$ on the substrates modified with 80/20 ($\delta\approx 0.73$) random copolymer	23
3.1	(a) The evolution of the SANS angular average intensity of the dPS- <i>b</i> -PMMA thin film ($\sim 110\text{nm}$) annealing under $\sim 40\text{V}/\mu\text{m}$ electric field. Solid line is the Gaussian fit of the data. (b) The evolution of the peak intensity with annealing time under electric field for the thin films.....	33
3.2	Cross-sectional TEM image of a $\sim 300\text{nm}$ PS- <i>b</i> -PMMA film annealed under $\sim 40\text{V}/\mu\text{m}$ electric field for (a) 3 hrs. (b) 6hrs. Scale bar: 100nm	35
3.3	The evolution of the SANS angular average intensity of the thick film ($\sim 700\text{nm}$) annealing under $\sim 40\text{V}/\mu\text{m}$ electric field. Solid line is the Gaussian fit of the data. (b) The evolution of the peak intensity with annealing time under electric field.....	36
3.4	Cross-sectional TEM image of a $\sim 700\text{nm}$ PS- <i>b</i> -PMMA film annealed under $\sim 40\text{V}/\mu\text{m}$ electric field for (a) 6hrs. (b) 16hrs. Scale bar: 100nm	37
3.5	The evolution of the SANS angular average intensity of the thicker film ($\sim 3\mu\text{m}$) annealing under $\sim 40\text{V}/\mu\text{m}$ electric field. Solid line is the Gaussian fit of the data. (b) The evolution of the peak intensity with annealing time under electric field	39
3.6	Cross-sectional TEM images of PS- <i>b</i> -PMMA films annealed under $\sim 40\text{V}/\mu\text{m}$ electric field for (a) 3hrs. (b) 6hrs. (c) 16hrs. Scale bar: 200nm	41
4.1	Cross-sectional TEM images of $\sim 800\text{ nm}$ PS- <i>b</i> -PMMA films (a) before and (b) after lithium ions extraction. The films were annealed at 170°C for 72 hrs under vacuum.....	51
4.2	Cross-sectional TEM image of a $\sim 1\mu\text{m}$ PS- <i>b</i> -PMMA film after annealed at 170°C under a $\sim 40\text{V}/\mu\text{m}$ DC electric field for 16hrs. The copolymer has been cleaned off lithium ions.....	52
4.3	(a) Cross-sectional TEM and (b) height and phase AFM images of a $\sim 300\text{nm}$ PS- <i>b</i> -PMMA film after annealed at 170°C under a $\sim 40\text{V}/\mu\text{m}$ DC electric field for 16hrs. (c) Cross-sectional TEM image of a $\sim 1\mu\text{m}$ PS- <i>b</i> -PMMA thin film with the same treatment. The copolymer contains 210 ppm lithium residual impurity	54
4.4	Cross-sectional TEM image of a $\sim 300\text{ nm}$ PS- <i>b</i> -PMMA film after annealed at 170°C under a $\sim 40\text{V}/\mu\text{m}$ DC electric field for (a) 6 hrs, (b) 9 hrs and (c) 12 hrs. The copolymer contains 210 ppm lithium residual impurity.....	56

5.1	Schematic diagram of hexagonally packed cylinders (a) parallel and (b) perpendicular to the surface in the real and reciprocal space. (c) The geometry of SANS measurement.....	66
5.2	2-D SANS patterns of a ~500 nm dPS- <i>b</i> -PMMA (47K) film annealed at 170°C under a ~40V/μm electric field for (a) 3, (b) 7, (c) 14 hrs. (d) The integrated peak intensity as a function of azimuthal angle of SANS patterns in a, b and c. (e) 2-D SANS pattern of another dPS- <i>b</i> -PMMA (47K) film annealed at 170°C under a ~40V/μm electric field for 16 hrs	69
5.3	(a) Schematic diagram of TEM sample preparation. Cross-sectional TEM images of ~700 nm PS- <i>b</i> -PMMA (120K) films after annealing at 185 ± 5°C under a ~40V/μm electric field for (b) 9, (c) 12, (d) 16 hrs. Scale bar: 100nm	71
5.4	(a) 2-D SANS pattern and (b) cross-sectional TEM image of a ~500nm dPS- <i>b</i> -PMMA (47K) film annealed at 170°C under vacuum for 72 hrs.....	73
5.5	2-D SANS patterns of a pre-annealed dPS- <i>b</i> -PMMA (47K) film annealed under a ~40V/μm electric field for (a) 3, (b) 7, (c) 14, (d) 29 hrs. (d) The integrated peak intensity as a function of azimuthal angle of SANS patterns in a, b, c and d. The plots were shifted 40 units with each other for clarity	75
5.6	Figure 5.6. Cross-sectional TEM images of a ~500 nm pre-annealed dPS- <i>b</i> -PMMA (47K) thin film after annealing under a ~40V/μm electric field for (a) 7, (c) 7, (d) 29 hrs. Scale bar: 100nm.....	77
6.1	(a) AFM phase image of a ~50nm PS- <i>b</i> -PMMA film annealed 48hrs at 170°C under vacuum, then exposed to UV and rinsed with acetic acid. Image size: 1X1μm ² . (b) Cross-sectional TEM image and (c) Grazing incidence small angle x-ray scattering pattern of a ~400 nm PS- <i>b</i> -PMMA film annealed 48hrs at 170°C under vacuum. Scale bar: 100 nm	88
6.2	(a) Grazing incidence small angle x-ray scattering pattern of a ~400nm PS- <i>b</i> -PMMA film annealed at 170°C under ~40V/μm electric field for 24hrs. (b) The q_y scan at $q_z \approx 0.022 \text{ \AA}^{-1}$ of the left side of the GISAXS pattern of the films annealed with and without electric field.....	90
6.3	AFM phase image of a ~400nm PS- <i>b</i> -PMMA film annealed at 170°C under ~40V/μm electric field for 24hrs. (a) before and (b) after UV exposure and acetic acid rinsing to remove PMMA blocks. (c) cross-sectional TEM image of the film.....	92

6.4	Cross-sectional TEM image of a ~400nm PS- <i>b</i> -PMMA film annealed at 170°C under ~40V/μm electric field for ~10hrs. Different morphologies are discernable. Region A, B: undeformed spherical microdomains. Region C, D; deformed spherical microdomains. Region E: deformed spherical microdomain connected into cylinders	93
7.1	(a) Schematic drawing of the roll-pressing and (b) the typical shape of copolymer thin films after roll-pressing	100
7.2	(a) SAXS pattern of a copolymer thin film after roll-pressing and (b) the integrated peak intensity as a function of azimuthal angle Ω	101
7.3	(a) SAXS pattern of copolymer thin films after roll-pressing and applying a subsequent electric field normal to the film surface. (b) The integrated peak intensity as a function of azimuthal angle Ω	102
7.4	TEM cross-sectional images of (a) the copolymer/substrate interface and (b) the interior of the film	104
7.5	FFT patterns of TEM images at different positions of the film. The TEM images were taken every ~3μm (a) normal to the film surface (along the Z direction in Fig. 7.4a), the first images on the left side of the sequence was taken right after Fig. 7.4a., and subsequent images were taken towards the other side of the film. The last image on the right of the z-axis sequence (top) exhibits a 4-point pattern due to the mixed orientation of the lamellar microdomains at the film edge. (b) The first image was taken in the center of the film and subsequent images were taken normal to the flow direction (along the X direction in Fig. 7.4a). The grain size is too large to be shown all and only small portion was shown.....	107
7.6	Cross-sectional TEM image of typical defects. While there were few defects, the defects shown were observed the most frequently	108

CHAPTER 1

EFFECT OF INTERFACIAL INTERACTIONS ON MICRODOMAIN ORIENTATION IN DIBLOCK COPOLYMER THIN FILMS

Introduction

In block copolymer thin films, the presence of a surface or interface can strongly influence the microdomain morphologies and the kinetics of microdomain ordering.¹⁻⁴ Much work has appeared on the influence of surfaces and interfaces on the ordering properties of symmetric diblock copolymers. Fredrickson studied the surface ordering phenomena in symmetric diblock copolymers near the microphase separation transition using mean field arguments. An oscillatory profile was found normal to the substrate where the amplitude of the oscillations decayed exponentially from the surface with a decay length that increased with increasing proximity to the microphase separation temperature, i.e. $\chi N - (\chi N)_s$ where χ is the segmental interaction parameter between the two blocks, and $(\chi N)_s$ is the value of χN at the microphase separation transition, and N is the number of the repeat units.^{5,6} In the disordered diblock copolymer thin film, the concentration of one block at the substrate interface is dictated by the difference in interfacial energies of the blocks with the substrate and the strength of segmental interactions. Experiments of Menelle *et al.* and Minsky *et al.* quantitatively described the concentration profiles of phase mixed symmetric diblock copolymers and found general agreement with the mean field arguments.^{7,8}

Experiments on the thin films of ordered symmetric diblock copolymer have typically focused on the behavior of copolymers at the interfaces where the

surface field strength is either large^{9,10} or zero.^{11,12} In the cases of a strong surface field, one block has much lower interfacial energy with the substrate and this block wets the substrate, inducing an orientation of the microdomains parallel to the substrate that propagate through the film. When the surface is neutral, i.e. where the interfacial interactions of both blocks with the substrate are the same, there is no preferential wetting and the microdomains orient normal to the substrate interface. This orientation persists a few periods from the interface before a randomization of the microdomain orientation occurs. While these phenomena result from the surface field, there has been no quantitative study on the extent to which interfacial energies can induce the propagation of microdomains orientation into a block copolymer film.

Here, the influence of interfacial interactions, a surface field, on the propagation of lamellar microdomain orientation parallel to the substrate in thin films of symmetric diblock copolymer polystyrene-block-poly(methyl methacrylate) thin films was quantitatively studied. By anchoring a random copolymer of styrene and methyl methacrylate onto the silicon substrates, the interfacial energy, *i.e.* the strength of the surface field was precisely tuned by varying the composition of the anchored random copolymer. It was found that the stronger the surface field, *i.e.*, the larger the difference in the interfacial energies between the blocks with the substrate, the further the orientation of the microdomains propagates into the films. For a specific surface field strength, a film thickness limit was found beyond which the orientation of the microdomains parallel to the surface was found throughout the film and above which a loss of

orientation was found in the center of the film. This thickness limit was found to be proportional to the strength of the surface field. In addition, the surface field was found to suppress the fluctuations at the interfaces between the microdomains in the vicinity of the interface, thereby retarding the formation of defects, and promoting the alignment of the microdomains parallel to the substrate interface.

Experimental

Materials

Diblock copolymers of polystyrene and polymethyl methacrylate, denoted as PS-*b*-PMMA, were made by conventional anionic polymerization procedures and were characterized by size exclusion chromatography using polystyrene as standard. The molecular weight was $M_n = 71,900$ g/mol with a polydispersity of 1.06. For small angle neutron scattering studies, the PS block was deuterated and the copolymer was denoted as dPS-*b*-PMMA. The molecular weight of dPS-*b*-PMMA was $M_n = 70,500$ g/mol with a polydispersity of 1.05.

The preparation of the narrow molecular weight distribution random copolymers of styrene and methyl methacrylate and modification of the silicon substrates has been described elsewhere.^{13,14} The volume fractions of styrene in the random copolymers were 0.58, 0.65, 0.30, 0.7, 0.90 with interfacial energy differences between PMMA and PS with the modified surface of approximately 0, 0.25, 0.45, 0.5, 0.75 dyne/cm, respectively.¹⁴

Sample Preparation

Films with thickness ranging from 100–900nm were spin coated onto silicon wafers modified with the random copolymers and annealed at 170°C

under vacuum for 3 days. All film thicknesses were measured with a Rudolph Research AutoEL®-II ellipsometer using a helium-neon laser ($\lambda=632.8\text{nm}$) at a 70° incidence angle. SANS experiments were performed on the 30-meter NG3-SANS instrument at National Institute of Standards and Technology (NIST) with a 1.25 cm pinhole at the sample defining a beam with a wavelength of $\lambda=6\text{\AA}$ and $\Delta\lambda/\lambda = 15\%$. The sample surface was either normal to the incident beam or tilted an angle of 60° with respect to the incident beam. Thin cross-sections (50-80 nm in thickness) were microtomed at room temperature using a diamond knife and placed on a copper grid. A thin layer of carbon (10-20nm) was coated on the surface and the film was embedded in epoxy and cured at 60°C for 12 hrs. The film was peeled off the substrate by dipping into liquid N_2 . The substrate was checked with ellipsometry and less than 5nm of film was left for all the samples shown here. The samples were exposed to ruthenium tetroxide for 35 minutes to enhance the contrast. The TEM images were taken on a JEOL 100CX at an accelerating voltage of 100kV.

Results and Discussion

The microdomains in block copolymer thin films are oriented parallel to the surface due to the preferential wetting of one block with the substrates. Islands and holes will form on the surface if the film thickness is not equal to nL_0 or $(n+1/2)L_0$ (where n is an integer, L_0 is the equilibrium period of the copolymer) depending on the boundary condition.¹⁵ This surface topography is a simple yet quantitative indicator of the orientation of the lamellar microdomains

parallel to substrate interface. Four samples, with similar thickness $\sim 10.3L_0$, were prepared on substrates modified with random copolymers having styrene fractions of 0.58, 0.65, 0.30, 0.90, where the differences in the interfacial energies were 0, 0.25, 0.45, 0.75 dyne/cm respectively. No islands or holes were found on the surface modified with 58/42 ($\Delta\gamma = 0$ dyne/cm) and 65/35 ($\Delta\gamma = 0.25$ dyne/cm) random brushes, whereas, islands and holes were clearly seen on the surfaces modified with 30/70 ($\Delta\gamma = 0.45$ dyne/cm) and 90/10 ($\Delta\gamma = 0.75$ dyne/cm) random brushes. By varying the film thickness, the absence of a surface topography on films prepared on substrates coated with a 58/42 random copolymer brush can be attributed to an orientation of the microdomains normal to the surface. In the case of the 65/35 surface, the PS block preferentially wets the substrate. However, the strength of the surface field is weak and the preferential orientation of the microdomains parallel to the interface is lost with increasing distance from the substrate. In both cases, the orientation of the microdomains normal the surface, or at least at orientations that are not parallel to the surface, alleviates commensurability constraints between the film thickness and L_0 and, consequently, the surface of the film remains smooth.

Shown in Figure 1.1a (58/42), 1.1b (65/35) and 1.1c (90/10) are the small angle neutron scattering profiles of three films on substrates with different surface fields. Figure 1.1d shows the integration of the SANS intensity over q as a function of the azimuthal angle. The samples were tilted at 60° with respect to the incident beam. In this case, the scattering arises from microdomains oriented

at angles more than 60° away from the surface planes. The azimuthal angle dependence of the scattering reflects the different orientations of the lamellar microdomains. Clearly, the overall intensities decrease with increasing surface field strength. Even with much thicker films ($\sim 500\text{nm}$), the intensity of scattering for the film on the 90/10 substrate is much lower than that for films on either the 58/42 or 65/35 substrates. Thus, the extent to which the orientation of the microdomains is maintained parallel to the surface increases with increasing strength of the surface field. In all three cases, the majority of the microdomains that are not parallel to the surface have orientations close to being normal to the surface.

To assess the orientation of the microdomains quantitatively SANS was performed with the beam normal to the substrate surface. Since the diffraction vector is oriented parallel to the surface, the intensity of the scattering maximum corresponds to the number of lamellar microdomains oriented normal to the substrate surface. Figure 1.2a shows the peak intensity for samples with different thicknesses on different substrates. For films with a similar thickness, the peak intensity decreases as the strength of the surface field increases. The film thickness dependence of the SANS on any given surface shows that no SANS is observed until a specific thickness is reached. Then, with increasing film thickness, the peak intensity increases. Thus, for very thin films on any particular surface, the lamellae are oriented parallel to the film surface throughout the entire film. However, above a critical film thickness, the influence of the surface is lost and the lamellae orient normal to the interface in the film interior. This critical

film thickness is directly related to the strength of the surface field. Shown in Figure 1.2b is the critical film thickness as a function of the strength of the surface field. Essentially a linear relationship is seen.

Figure 1.1 Small angle neutron scattering profiles of dPS-*b*-PMMA thin films on Si substrate modified with random copolymers of (a) 58/42 (~320nm), (b) 65/35 (~320nm), and (c) 90/10 (~505nm) after annealing at 170°C under vacuum for 72hrs. The samples were tilted at 60° with respect to the incident beam. (d) shows the azimuthal angle integration of the SANS intensity in (a), (b) and (c).

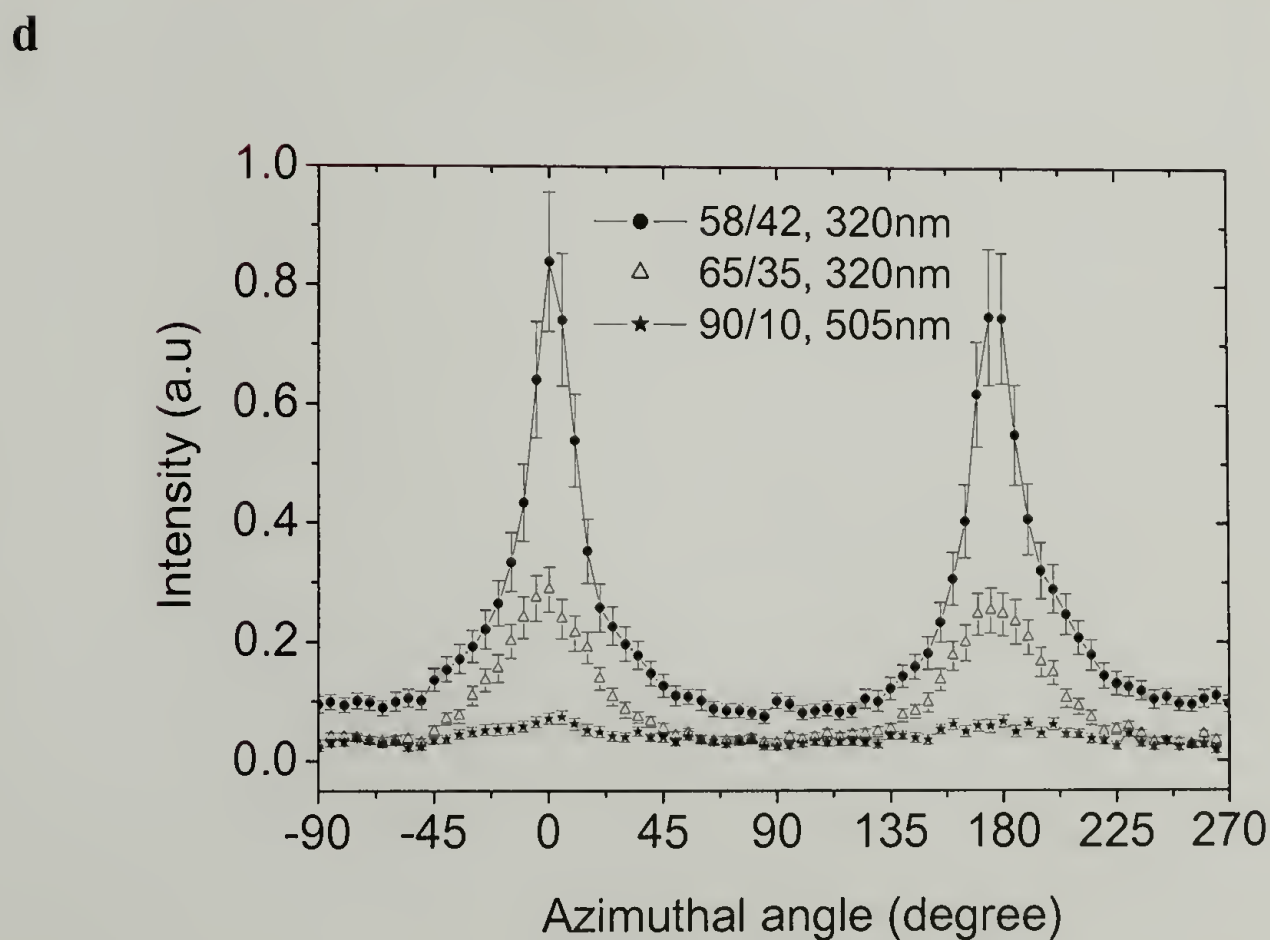
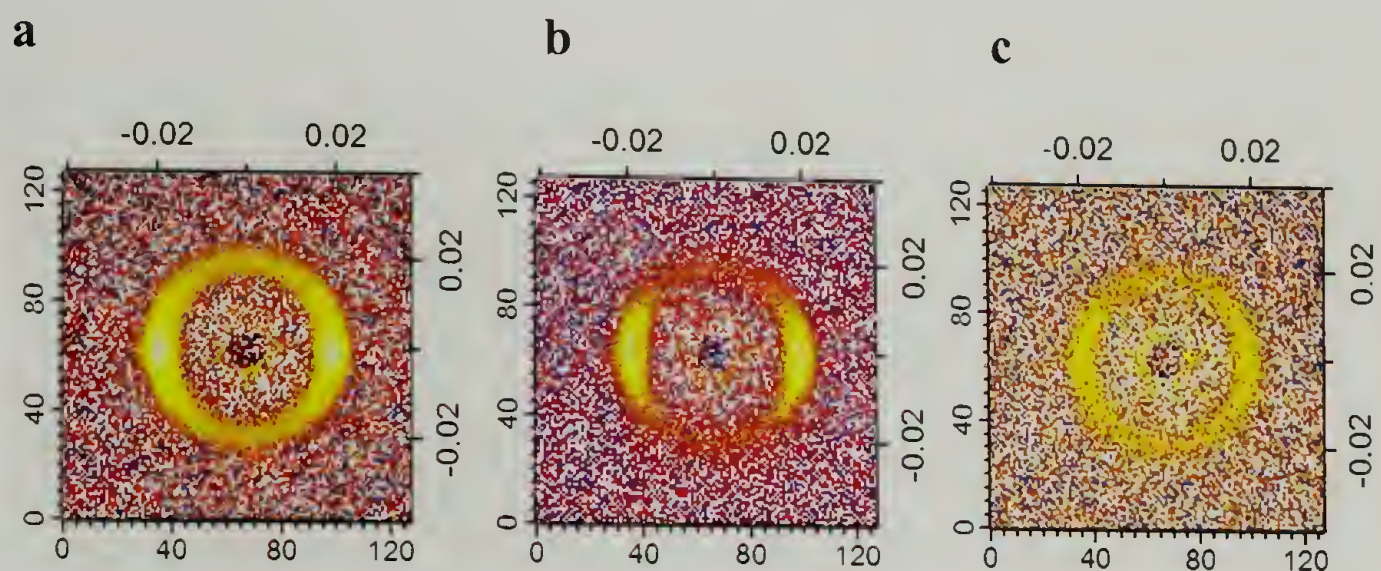
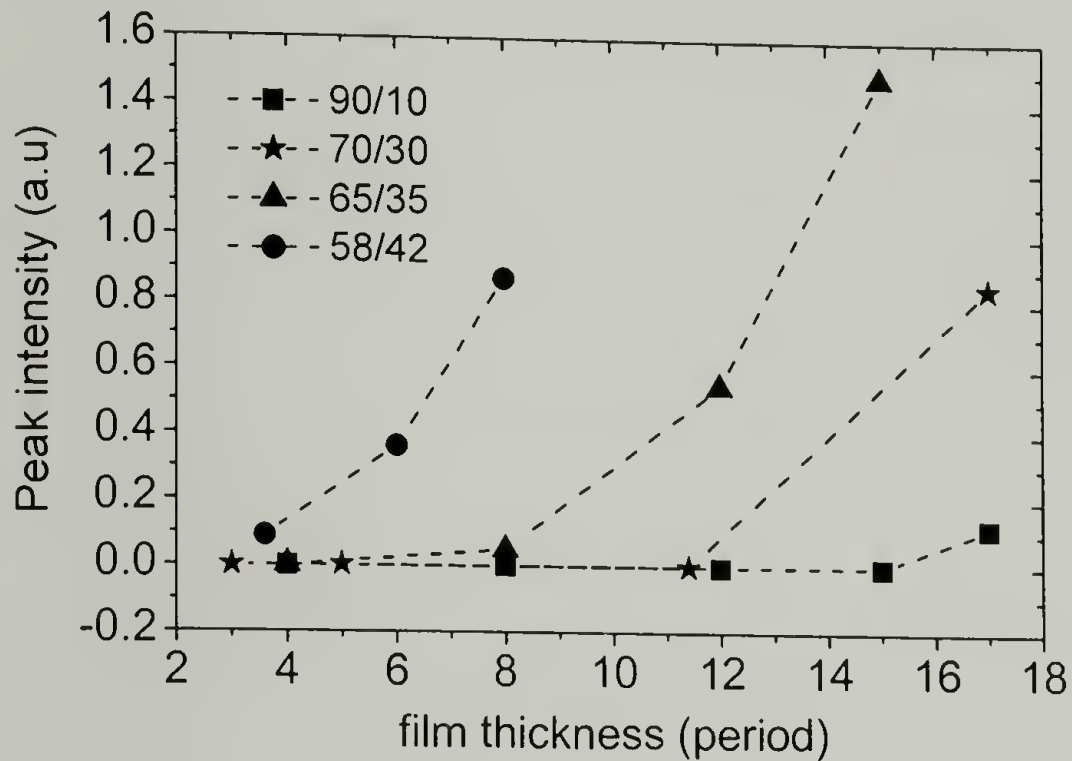


Figure 1.2(a) Small angle neutron scattering peak intensities of the dPS-*b*-PMMA thin films with different thicknesses. The films were on Si substrates modified with different random copolymers, 58/42, 65/35, 70/30, 90/10. (b) is the plot of the critical film thickness beyond which the parallel lamellar microdomains could not propagate throughout the whole film vs. interfacial interaction.

a



b

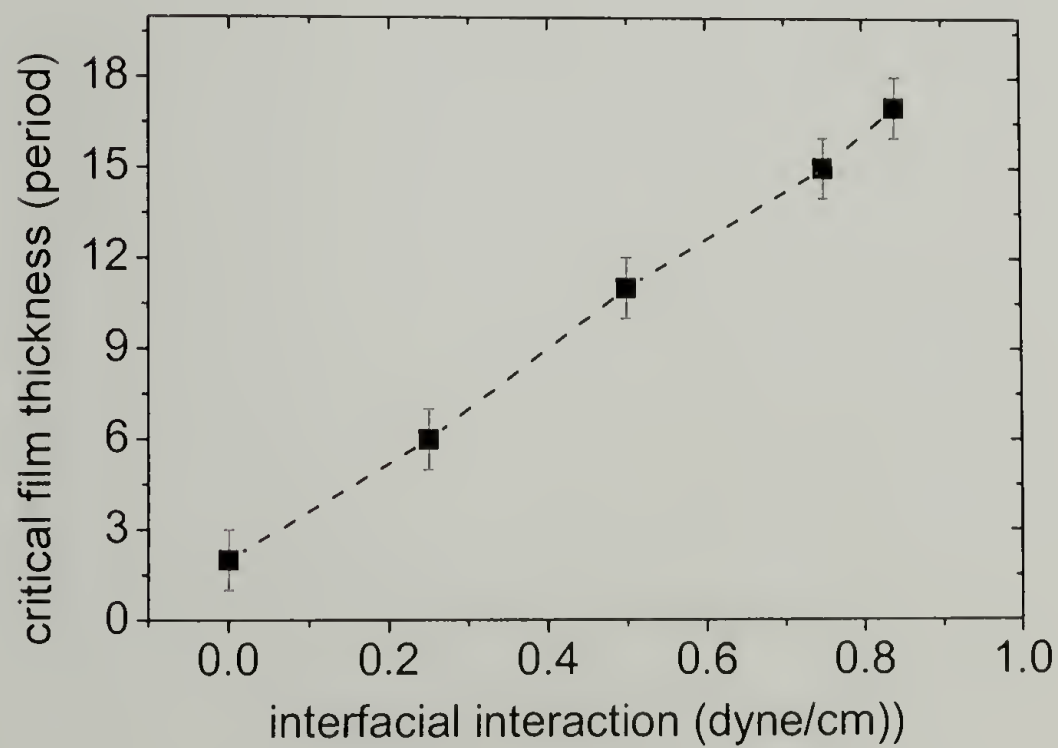
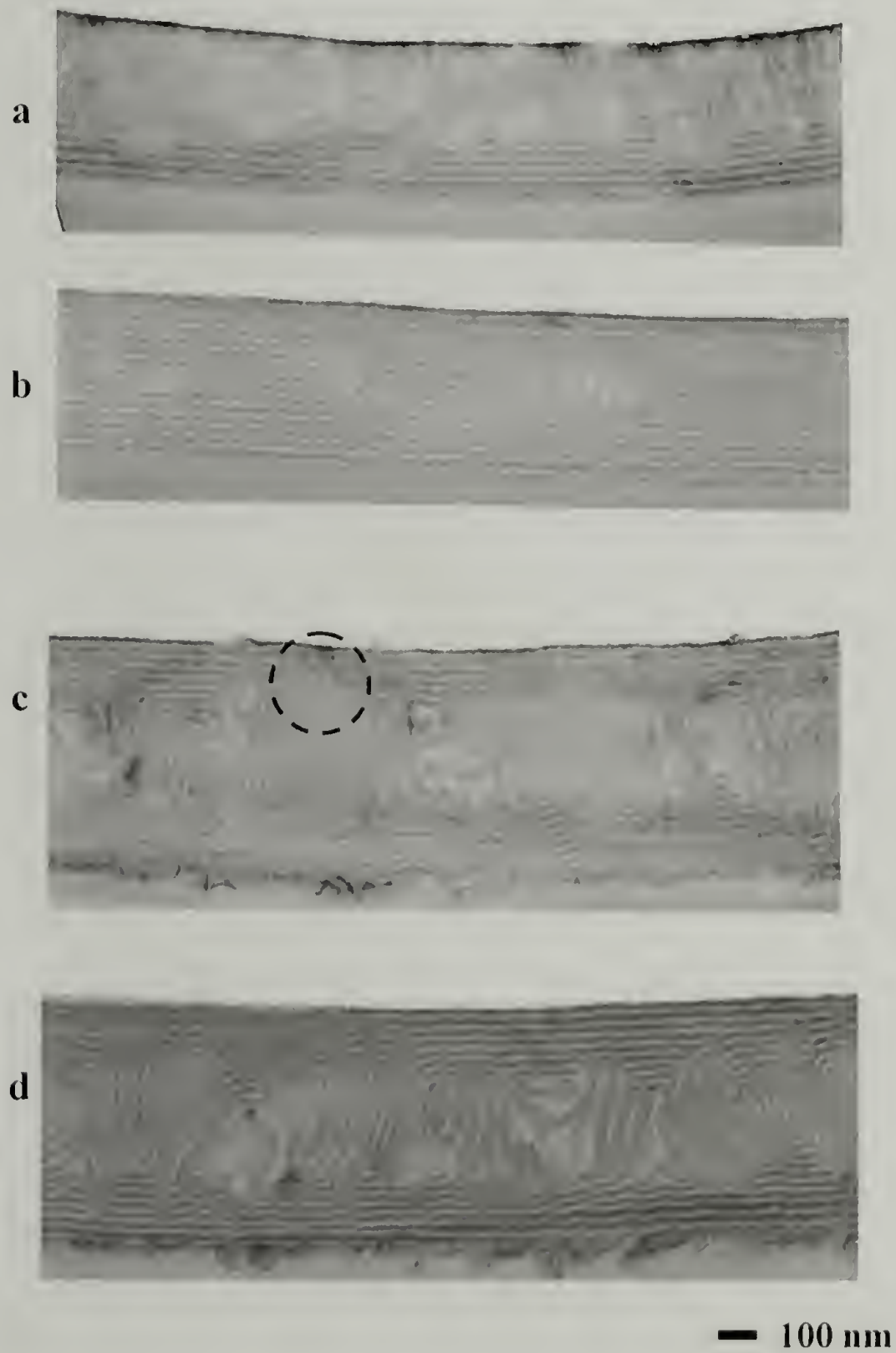


Figure 1.3 shows typical cross-section TEM images of the samples in this study. Figure 1.3a shows a $\sim 400\text{nm}$ film on a neutral surface (58/42). From the TEM sample preparation, the top surface corresponds to the copolymer/modified Si substrate interface. The lamellar microdomains are oriented normal to the interface and propagate into the film. At the air/polymer surface, the microdomains are parallel, due to the lower surface tension of PS. Figure 1.3b is a $\sim 430\text{nm}$ film on the substrate modified with 70/30 random copolymer. As seen before, the lamellae are oriented parallel to the substrate due to the preferential wetting of PS on the modified substrate. This orientation propagates through the entire film for the thinner films (no shown). However, for thicker films, the parallel orientation is lost after a given distance from the surface and in the middle of the film, different microdomain orientations appear as shown in Figure 1.3b. Mixed orientations become obvious when the film gets thicker as shown in Figure 1.3c. The parallel orientation was seen at copolymer/substrate interface. However, the coherence of the orientation across the films is lost after $\sim 3L_0$. Defects in the structure appear (highlighted by the circle) and lamellar with mixed orientations are dominant in the center of the film. Figure 1.3d shows the cross-section TEM image of a film with a thickness similar to that of the samples in Figure 1.3c prepared on a substrate modified with the 90/10 random copolymer. The parallel alignment of the lamellae propagates further into the samples. In the center of the films, a mixed microdomain orientation is seen. This microdomain orientation in the film did not change significantly with further annealing. In keeping with the SANS results, the TEM images show that there is

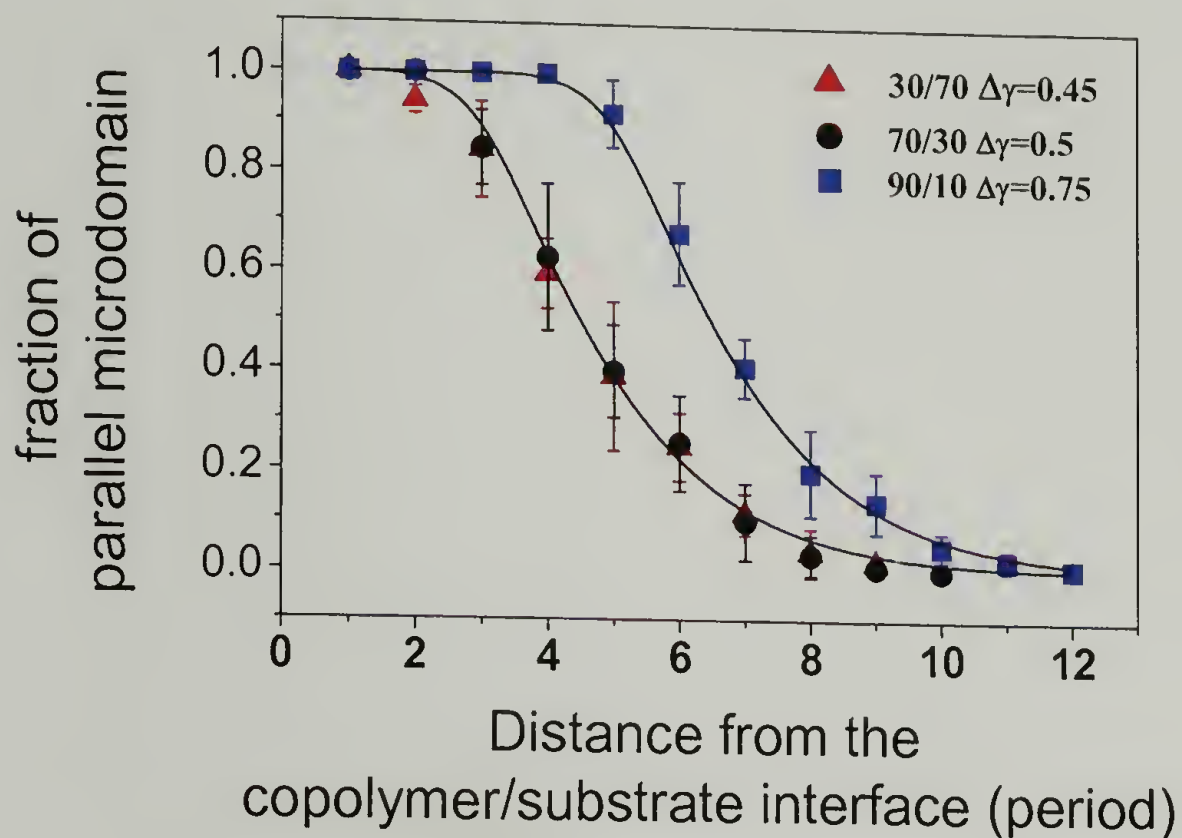
a distance from the substrate where the orientation of the copolymer microdomains persists and this distance increases with increasing strength of the interactions between the copolymer and the modified substrate surface.

Figure 1.3 Cross-sectional transmission electron microscopy images of annealed PS-*b*-PMMA thin films with different film thicknesses on Si substrates modified with random copolymers: (a) 58/42 (~400nm) (b) 70/30 (~430nm) (c) 70/30 (~800nm) (d) 90/10 (~800nm).



The TEM images were used to quantify the persistence of orientation of the copolymer microdomains as a function of distance from the surface. By projecting the contrast of the TEM image onto a line oriented normal to the surface, the projected amplitude of the contrast is a direct measure of the copolymer orientation. An alternate approach used here was to determine the linear fraction of lamellae oriented parallel to the surface of the TEM images as a function of distance from the surface. This is shown in Figure 1.4. Films (~800nm) on three substrates modified with 30/70 ($\Delta\gamma = 0.45 \text{ dyne/cm}$), 70/30 ($\Delta\gamma = 0.5 \text{ dyne/cm}$), 90/10 ($\Delta\gamma = 0.75 \text{ dyne/cm}$) random copolymers were analyzed. Each point was obtained from ~20 μm wide cross-section TEM images. The results in Figure 1.4 are quite revealing. First, the shapes of the profiles are similar. Adjacent to the surface, the profiles are flat, indicating the parallel alignment of the copolymer microdomains. The persistence of the orientation was found to depend on the strength of the interfacial interactions. The 70/30 and 30/70 cases are identical where the orientation extends only ~1 period from the surface. For the 90/10 case, the parallel alignment extends ~5 periods from the surface, as would be expected from the stronger interfacial interaction. The transition of the orientation from parallel to random is essentially the same in all cases, i.e. the profiles can be horizontally shifted and superposed. Such behavior has been predicted theoretically and indicates that the decay in orientation is a characteristic of the copolymer.⁵

Figure 1.4 Fraction of parallel lamellae microdomains vs. the distance from the copolymer/substrate interface. Each image was sectioned into slices of the equilibrium period thickness from the copolymer/substrate interface. The fraction of the parallel lamellae was counted in each slice and plotted vs. the distance from the copolymer/substrate interface. Each point was obtained by averaging $\sim 20\mu\text{m}$ wide cross-sectional TEM images. The solid lines were plotted to guide the eye.



Conclusions

It is well known that the preferential wetting of one block with the substrate induces the parallel alignment of the lamellar microdomains. Here, by modifying a surface with random copolymer brushes, interfacial energies were controlled and the influence of interfacial energy on the lamellar microdomain orientation of PS-*b*-PMMA thin films was studied quantitatively. Mixed lamellar microdomain orientations were found when the surface field, i.e. the difference in the interfacial energies between each block with the substrate, is not strong enough to orient the lamellar parallel to the substrates throughout the film. The critical film thickness, below which the lamellar microdomains are parallel to the

substrate throughout the film, is proportional to the surface field strength. TEM images indicate that the presence of a surface field suppresses microdomain fluctuations and defect formation, thereby promoting the propagation of orientation into the films. A linear relationship is found between the strength of interfacial interactions and the distance over which the orientation of the microdomains persists. These results have direct bearing on the strength of fields necessary to induce orientation in thin block copolymer thin films.¹⁶

References

- (1) Hasegawa, H.; Hashimoto, T. *Macromolecules* **1985**, *18*, 589.
- (2) Henkee, C. S.; Thomas, E. L.; Fetters, L. J. *J Mater Sci* **1988**, *23*, 1685.
- (3) Winey, K. I.; Patel, S. S.; Larson, R. G.; Watanabe, H. *Macromolecules* **1993**, *26*, 4373.
- (4) Yokoyama, H.; Mates, T. E.; Kramer, E. J. *Macromolecules* **2000**, *33*, 1888.
- (5) Fredrickson, G. H. *Macromolecules* **1987**, *20*, 2535.
- (6) Milner, S. T.; Morse, D. C. *Physical Review E* **1996**, *54*, 3793.
- (7) Menelle, A.; Russell, T. P.; Anastasiadis, S. H.; Satija, S. K.; Majkrzak, C. F. *Physical Review Letters* **1992**, *68*, 67.
- (8) Mansky, P.; Russell, T. P.; Hawker, C. J.; Mays, J.; Cook, D. C.; Satija, S. K. *Physical Review Letters* **1997**, *79*, 237.
- (9) Anastasiadis, S. H.; Russell, T. P.; Satija, S. K.; Majkrzak, C. F. *Physical Review Letters* **1989**, *62*, 1852.
- (10) Karim, A.; Singh, N.; Sikka, M.; Bates, F. S. *Journal of Chemical Physics* **1994**, *100*, 1620.
- (11) Huang, E.; Rockford, L.; Russell, T. P.; Hawker, C. J. *Nature* **1998**, *395*, 757.
- (12) Huang, E.; Russell, T. P.; Harrison, C.; Chaikin, P. M.; Register, R. A.; Hawker, C. J.; Mays, J. *Macromolecules* **1998**, *31*, 7641.
- (13) Hawker, C. J. *Macromolecules* **1996**, *29*, 2686.
- (14) Mansky, P.; Liu, Y.; Huang, E.; Russell, T. P.; Hawker, C. *Science* **1997**, *275*, 1458.
- (15) Coulon, G.; Deline, V. R.; Russell, T. P.; Green, P. F. *Macromolecules* **1989**, *22*, 2581.
- (16) Thurn-Albrecht, T.; DeRouchey, J.; Russell, T. P.; Jaeger, H. M. *Macromolecules* **2000**, *33*, 3250.

CHAPTER 2

EFFECT OF INTERFACIAL INTERACTIONS ON ELECTRIC FIELD ALIGNMENT OF SYMMETRIC DIBLOCK COPOLYMER THIN FILMS

Introduction

Thin films of block copolymers, have attracted significant attention due to their potential uses as templates and scaffolds for nanostructured materials.¹⁻³ However, a crucial element for the success of such strategies is the complete alignment of the copolymer microdomains. The interfacial energies of the blocks of the copolymer play a key role in achieving full alignment of the copolymer microdomains. The preferential segregation of one block to the substrate will orient the microdomains parallel to the substrate surface.⁴⁻⁶ To overcome such surface directed orientation, external fields have been used.⁷⁻¹⁰ For example, lamellar and cylindrical microdomains in thin films of polystyrene-*b*-poly(methyl methacrylate) (PS-*b*-PMMA) can be oriented normal to the substrate with an electric field, achieving complete orientation in the direction of the applied field.^{2,10-13}

Several theoretical studies have appeared addressing the alignment of symmetrical diblock copolymers in thin films by an electric field.¹⁴⁻¹⁶ The roles of the applied electric field strength, interfacial energies, film thickness, dielectric constant difference between the two blocks, and commensurability of the film thickness and the natural period of the copolymer, have been investigated.^{16,17} From these, however, the interfacial energies of the blocks emerge as the critical parameter or impediment in achieving complete alignment of the domains. A parallel orientation of the microdomains is favored when there is a difference in the interfacial energies, whereas a normal orientation of the microdomains is favored by the applied electric field. Under certain conditions, a

mixed orientation of the microdomains is predicted. Here, parallel orientation of the microdomains at the surface occurs, whereas, away from the surface, the influence of the applied electric field dominates and the microdomains orient in the direction of the applied electric field. With such mixed orientations, however, 'T' junctions form when the lamellae, oriented in orthogonal directions meet. These defects represent a significant energetic penalty. A dimensionless parameter δ can be defined as $\delta = (\gamma_{AS} - \gamma_{BS}) / \gamma_T$, where γ_{AS} and γ_{BS} are the interfacial energies of block A and B with the substrate respectively, and γ_T is the interfacial energy between block A and block B. Theoretical calculation done by Pereira, *et al.* predict that in the strong segregation limit, for $\delta \leq 1$, only normal orientation is favored, whereas, for $\delta > 1$, a mixed orientation is predicted.¹⁵ It should be noted that Tsori and Andelmann, using the identical variables predict normal orientations when $\delta < 2$ and a mixed orientation when $\delta > 2$.¹⁴

Here, an experimental study on the influence of the interfacial energies on the alignment of symmetric diblock copolymers, of polystyrene-*b*-poly(methyl methacrylate), PS-*b*-PMMA, is shown as a function of δ . Complete alignment of the lamellar microdomains normal to the surface, i.e. in the direction of the applied field, is found only when the interactions of the blocks with the substrate are balanced ($\delta=0$). In all other cases, a mixed orientation of the microdomains was found. This very narrow window in δ contradicts theoretical predictions, but can be ascribed to a kinetic trapping of the microdomain orientation and a high activation energy associated with reorienting the microdomains.

Experimental

Materials

PS-*b*-PMMA was prepared by anionic synthetic routes and contained 50% (by volume) styrene. The number average molecular weight M_n is 7.19×10^4 with a polydispersity of 1.08 as measured by size exclusion chromatography using polystyrene standards. Silicon wafers were modified by anchoring hydroxyl terminated random copolymers of styrene and methyl methacrylate, prepared by living free radical procedures, to the substrate.¹⁸ Four random copolymers with styrene fractions of 0.58 (58/42), 0.7 (70/30), 0.8 (80/20) and 0.9 (90/10) were anchored to the surface, as described previously, to give a covalently attached random copolymer brush with thicknesses of approximately 6 nm. Using $\gamma_T=0.8$ dyne/cm, the respective values of δ are 0, 0.62, 0.73 and 0.94 respectively.¹⁹

Sample Preparation

Films of PS-*b*-PMMA, ~900nm in thickness, were prepared by spin coating ($\sim 10^3$ rpm) a 7% (w/v) toluene solution of the copolymer onto the substrate. An aluminized Kapton film comprised the top electrode, where a thin layer (20-25 μ m) of crosslinked PDMS (Sylgard™) was used as buffer layer between the Kapton electrode and the copolymer thin film. Crosslink PDMS (Sylgard 184™) was purchased from Dow Corning and used as received. The 10:1 mixture was mixed and spin coated on top of the aluminized Kapton, cured for 24hrs at 60°C. Then the crosslinked PDMS coated Kapton was annealed at 170°C under vacuum for 12hrs to remove the residue small molecules. The Si elemental concentration in the copolymer film after annealing in an electric field for 16hrs is less than 1% measured by X-ray photoelectron spectroscopy with probing

depth of 4.5nm. The PDMS layer conforms to the electrode surface, eliminates air gaps between the top electrode and the copolymer film, and maintains a smooth surface of the copolymer film. The copolymer films were heated to 170°C under N₂ with an applied electric field of ~40V/μm for 16hrs, and then quenched to room temperature before removing the electric field. The samples were embedded in epoxy, microtomed with a diamond knife at room temperature and transferred to a copper grid. A thin layer of carbon (10-20nm) was coated on the surface and the film was embedded with epoxy and cured at 60°C for 12 hrs. The film was peeled off the substrate by dipping into liquid N₂. The substrate was checked with ellipsometry and less than 5nm of film was left for all the samples shown here. The thin sections were exposed to ruthenium tetroxide for 35min to enhance the contrast. Electron microscopy experiments were performed on a JEOL 100CX TEM at the accelerating voltage of 100KV. Grazing incidence small angle x-ray scattering (GISAXS) was performed at the National Synchrotron Light Source, (Brookhaven National Laboratory), using x-rays with a wavelength of 1.567Å. Typical exposure times were 90 seconds per sample.

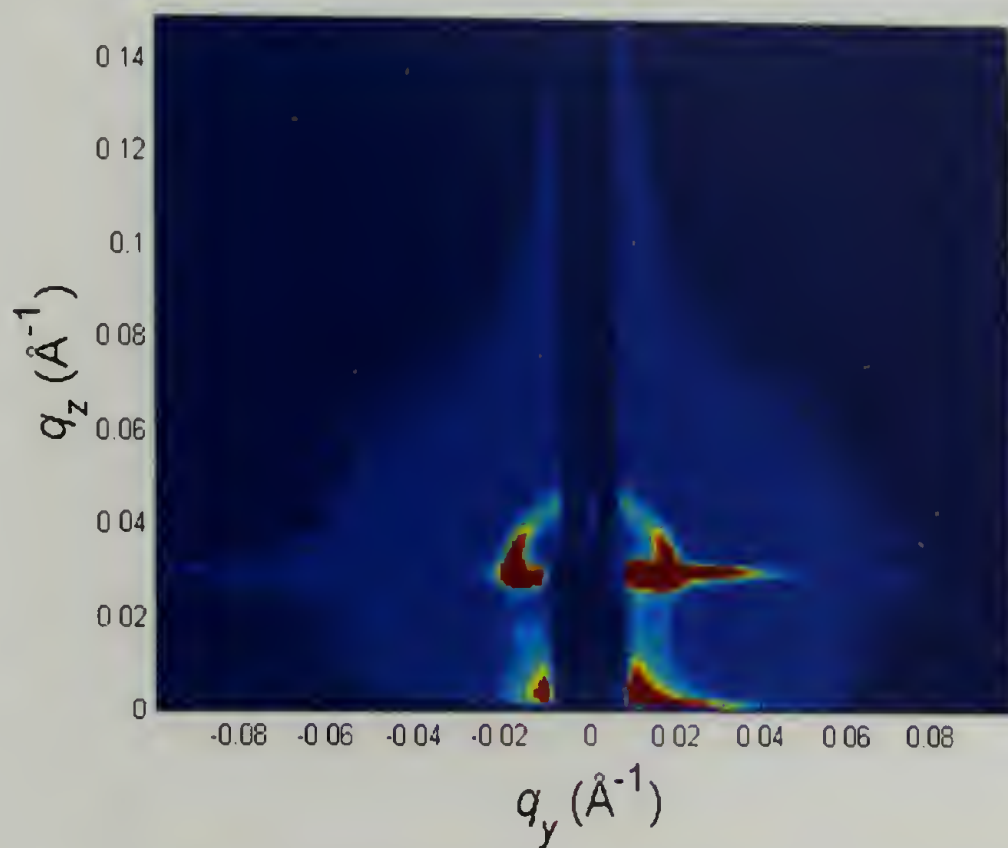
Results and Discussion

Shown in Figure 2.1 are the GISAXS patterns for a ~900nm thick PS-*b*-PMMA film on a silicon substrate with native oxide layer, obtained at a 0.2° incidental angle. Figure 2.1a is for the sample annealed at 170°C under vacuum for 48hrs with no applied field. The arc-like pattern indicates that the lamellar microdomains are randomly oriented in the film. The scattering from a similar sample annealed under an applied electric field (~40V/μm) is shown in Figure 2.1b. The two equatorial spots show that the lamellae orient normal to the

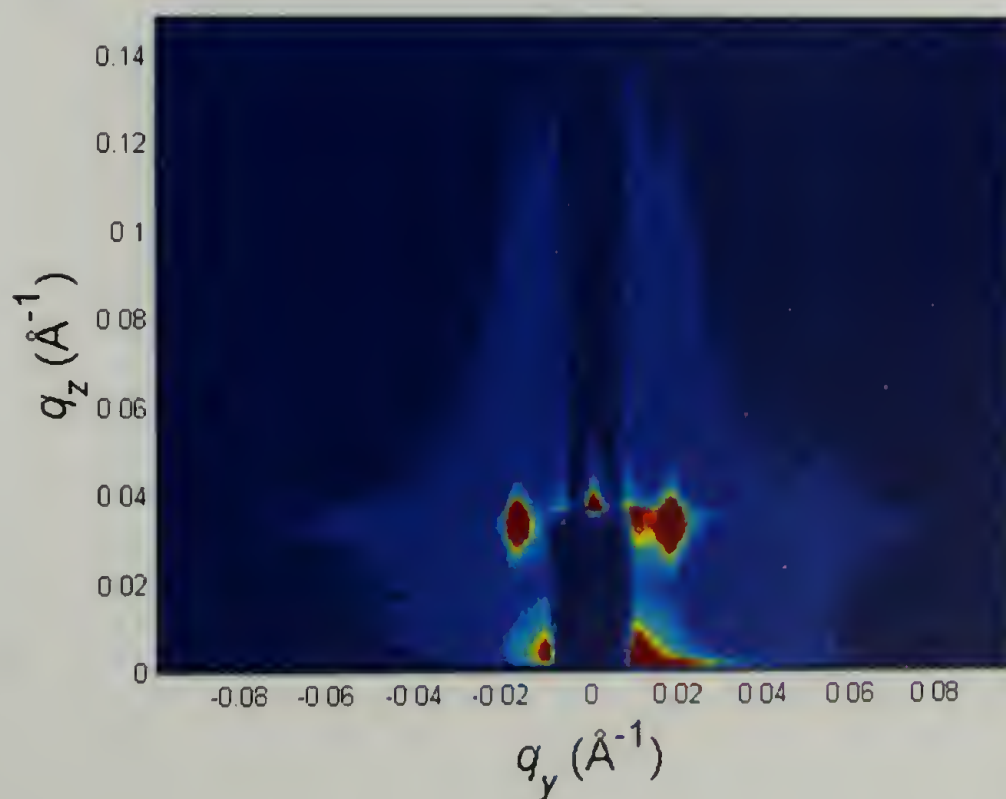
surface, in the direction of the applied field. However, with GISAXS, it is not possible to discern whether the alignment of the microdomains extends completely to the interfaces, only that the average degree of alignment is high.

Figure 2.1 Grazing incidence small angle x-ray scattering patterns of PS-*b*-PMMA (~900nm) films on silicon substrate with native oxide layer (a) after annealing under vacuum and (b) after annealing under ~40V/ μm electric field.

a

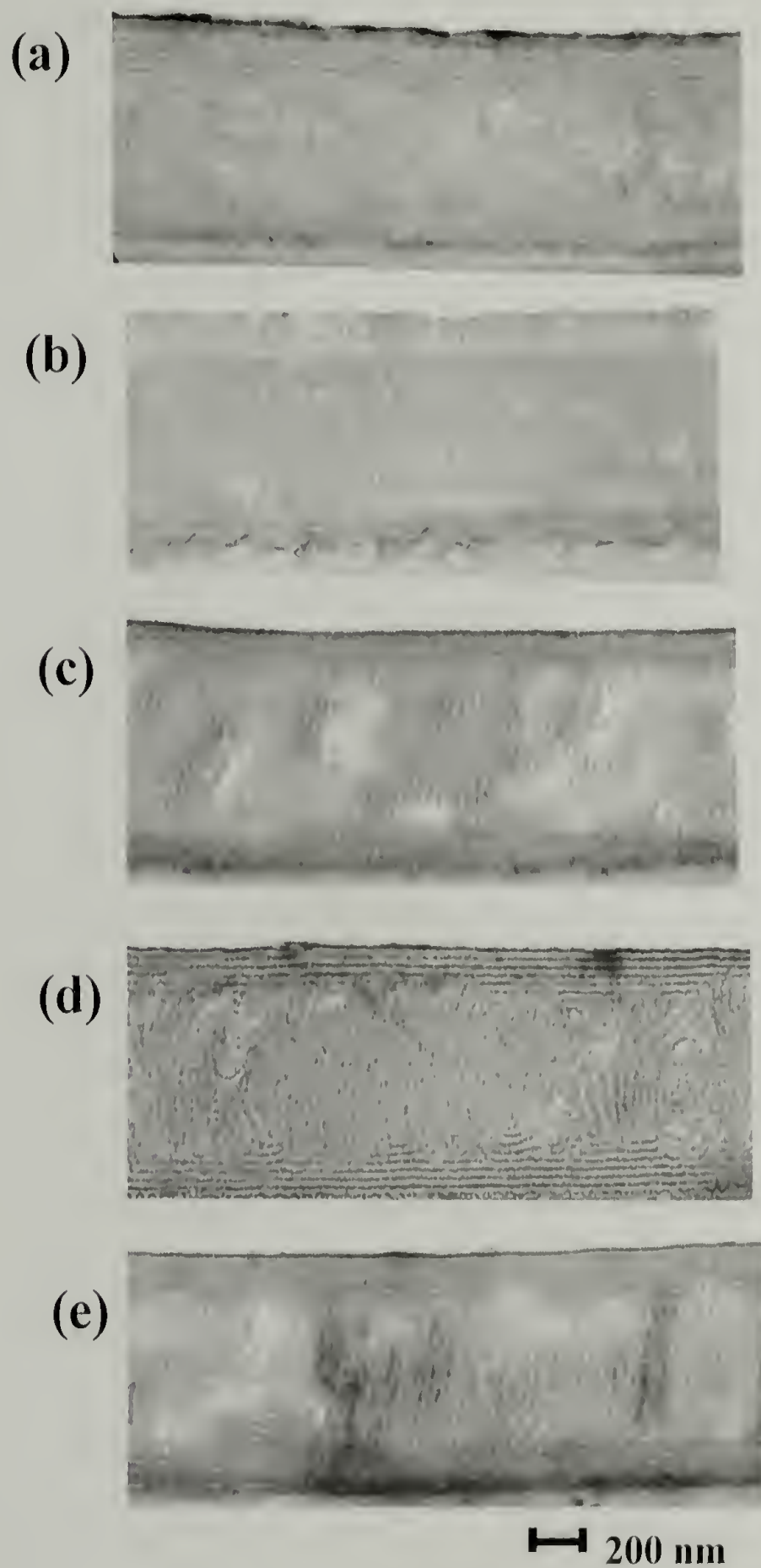


b



To examine the orientation of the microdomains at the interfaces, TEM was used. Figure 2.2a is the cross-section TEM image of PS-*b*-PMMA thin film after annealing under vacuum for 48hrs with no field applied. The film is on the substrate modified with 90/10 random copolymer with styrene fractions of 0.9. The lamellar microdomains are parallel to the substrate at both interfaces due to the preferential wetting of one block. Whereas, in the center of the film, the effect of the interface dissipates and the microdomains assume random orientations. Figure 2.2b, 2.2c, 2.2d, 2.2e show cross-section TEM images of PS-*b*-PMMA thin films after annealing under a $\sim 40\text{V}/\mu\text{m}$ electric field on four different substrates to which random copolymers with styrene fractions of 0.58, 0.7, 0.8 and 0.9 respectively were anchored. From the TEM sample preparation, the top of each image corresponds to the copolymer/substrate interface. An orientation of the lamellar microdomains in the direction of the applied field is seen in the middle of the films. Complete alignment of the lamellae extending to the interfaces was achieved only when $\delta=0$, i.e. when the interactions between the surface and the blocks were balanced. Mixed orientations were seen in all other cases, even when the difference in the interactions between the blocks and the substrate was much smaller than the interfacial energy between the two blocks.

Figure 2.2 Transmission Electron Microscopy cross-section images of PS-*b*-PMMA thin films after (a) 90/10, annealed under vacuum for 48hrs and annealing under $\sim 40\text{V}/\mu\text{m}$ electric field on the substrates modified with different random copolymers, (b) 58/42, $\delta \approx 0$, (c) 70/30, $\delta \approx 0.62$, (d) 80/20, $\delta \approx 0.73$, (e) 90/10, $\delta \approx 0.94$.



In comparison with the theoretical calculations, the observed range in δ to achieve complete orientation of the microdomains is much narrower. Figure 2.3

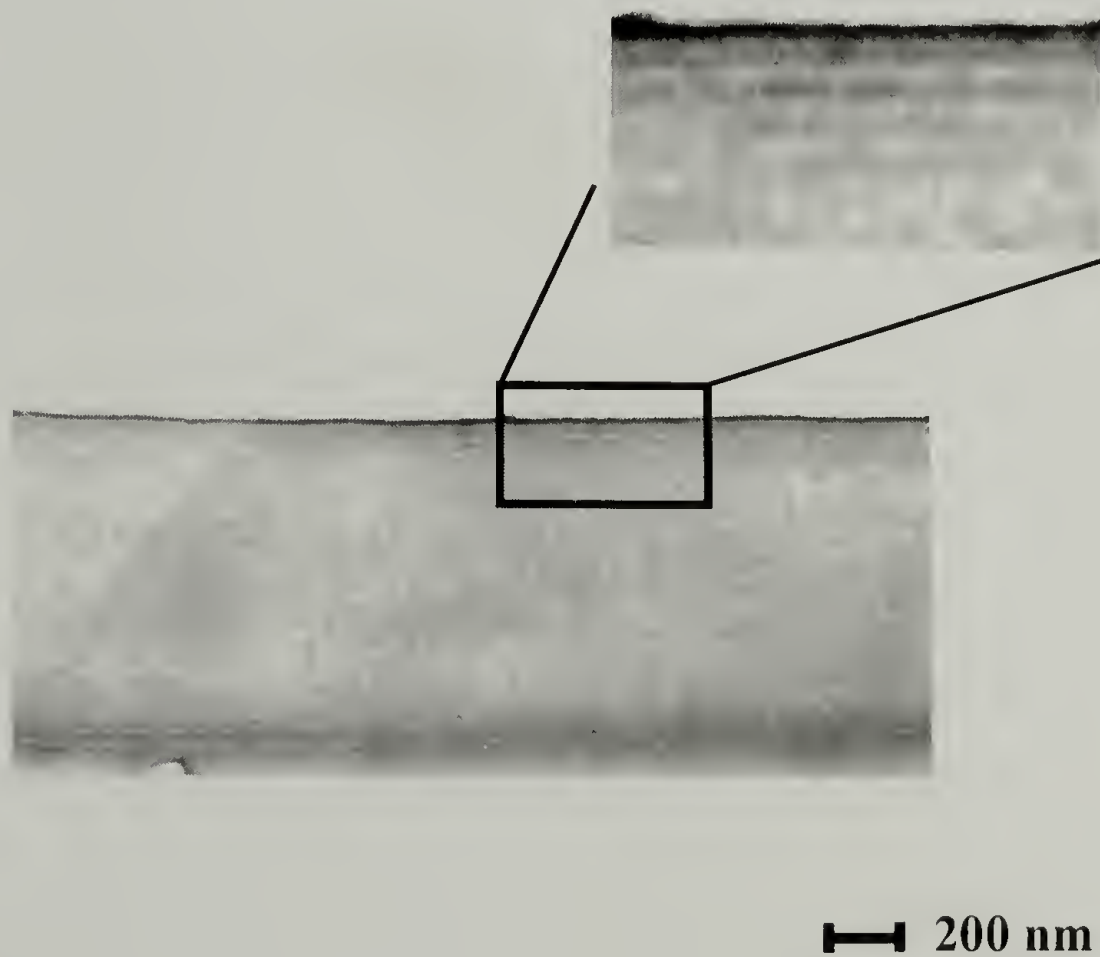
shows the cross-section TEM image of PS-*b*-PMMA thin film with film thickness $\sim 3\mu\text{m}$ annealed under $\sim 40\text{V}/\mu\text{m}$ electric field on the substrate modified with 90/10 random copolymers. Similar to the thinner films ($\sim 900\text{nm}$) in Figure 2.2, mixture orientations were seen. The lamellar microdomains were parallel to the surface at the copolymer/substrate interface and were aligned along the electric field direction in the middle of the film. Comparing Figure 2.2a, 2.2e and Figure 2.3, there is no dramatic change in the number of parallel lamellar microdomain at the copolymer/substrate interface.

Figure 2.3 Transmission Electron Microscopy cross-section images of PS-*b*-PMMA thin films ($\sim 3\mu\text{m}$) after annealing under $\sim 40\text{V}/\mu\text{m}$ electric field on the substrates modified with 90/10 random copolymers.



One explanation for the discrepancy between theory and experiment is a pathway dependence of the alignment process that is not considered theoretically. Figure 2.4 shows the cross-section TEM image of the thin film after annealing at $160\pm 5^\circ\text{C}$ under an electric field of $\sim 40\text{V}/\mu\text{m}$ for 1 hr. A random copolymer was anchored to the surface such that $\delta=0.73$. In this case, full alignment of the microdomains should occur. At the substrate interface, the lamellar microdomains are seen to orient parallel to the substrate initially, whereas, in the center of the film, the copolymer, while microphase separated, is not aligned. Further annealing of the sample under an electric field produced the film shown in Figure 2.2c.

Figure 2.4 Transmission Electron Microscopy cross-section images of PS-*b*-PMMA thin films after annealing under $\sim 40\text{V}/\mu\text{m}$ electric field for 1 hr at $160\pm 5^\circ\text{C}$ on the substrates modified with 80/20 ($\delta\approx 0.73$) random copolymer.



Based on these TEM images and others, it is evident that two kinetic processes are in competition, namely the alignment of the microdomains by the electric field and the surface induced alignment of the microdomains. While an electric field can bias concentration fluctuations of a disordered copolymer, it is apparent that the surface induced orientation is a stronger field initially.²⁰ This can be understood by the influence of a surface on the ordering of the copolymer. It has been shown that the order to disorder transition can be markedly increased in the vicinity of a surface.²¹ Consequently, the copolymers near the interface microphase separate initially with an orientation that is strongly biased by the interface. The influence of the interface, of course, dissipates with increasing distance from the surface and, in the absence of other fields, the copolymer orders and orients under the influence of the applied field. Consequently, in the center of the film, the copolymer microdomains are oriented parallel to the applied field, i.e. normal to the substrate surface. This structure does not correspond to the equilibrium structure, since the formation of T-junctions is energetically costly. However to fully orient the microdomains, the microdomains at the interface must be rotated 90°. A simple rotation of the microdomains is not feasible and an undulation of the microdomains is a more plausible route. This, however, increases the interfacial area between the microdomains and also necessitates the stretching and compression of the chains, since the substrate is flat. Thus, the energetic barrier to complete the transition to a fully aligned state is high, requiring a higher electric field than that predicted theoretically to achieve the perfectly aligned state.

Conclusions

In conclusion, the interfacial energy was controlled precisely by anchoring random copolymers to the substrate and the influence of interfacial energy on the electric field alignment of thin films of symmetric PS-*b*-PMMA thin films was studied. Complete alignment of symmetric diblock copolymer thin films was found only when the interactions between the blocks of copolymer and substrate were balanced. Mixed orientations were found in all other cases, even when the difference in the block-substrate interactions was smaller than the interfacial energy between two blocks. Electron microscopy results suggest a pathway dependence of the alignment process to explain the discrepancy between the experimental results and the theoretical predictions.

References

- (1) Park, M.; Harrison, C.; Chaikin, P. M.; Register, R. A.; Adamson, D. *Science* **1997**, *276*, 1401.
- (2) Thurn-Albrecht, T.; Steiner, R.; DeRouchey, J.; Stafford, C. M.; Huang, E.; Bal, M.; Tuominen, M.; Hawker, C. J.; Russell, T. P. *Adv. Mater.* **2000**, *12*, 1138.
- (3) Huang, E.; Rockford, L.; Russell, T. P.; Hawker, C. J. *Nature* **1998**, *395*, 757.
- (4) Anastasiadis, S. H.; Russell, T. P.; Satija, S. K.; Majkrzak, C. F. *Physical Review Letters* **1989**, *62*, 1852.
- (5) Anastasiadis, S. H.; Russell, T. P.; Satija, S. K.; Majkrzak, C. F. *Journal of Chemical Physics* **1990**, *92*, 5677.
- (6) Liu, Y.; Zhao, W.; Zheng, X.; King, A.; Singh, A.; Rafailovich, M. H.; Sokolov, J. *Macromolecules* **1994**, *27*, 4111.
- (7) Thurn-Albrecht, T.; DeRouchey, J.; Russell, T. P.; Jaeger, H. M. *Macromolecules* **2000**, *33*, 3250.
- (8) Morkved, T. L.; Lu, M.; Urbas, A. M.; Ehrichs, E. E.; Jaeger, H. M.; Mansky, P.; Russell, T. P. *Science* **1996**, *273*, 931.
- (9) Boker, A.; Knoll, A.; Elbs, H.; Abetz, V.; Muller, A. H. E.; Krausch, G. *Macromolecules* **2002**, *35*, 1319.
- (10) Thurn-Albrecht, T.; Schotter, J.; Kastle, C. A.; Emley, N.; Shibauchi, T.; Krusin-Elbaum, L.; Guarini, K.; Black, C. T.; Tuominen, M. T.; Russell, T. P. *Science* **2000**, *290*, 2126-2129.
- (11) Amundson, K.; Helfand, E.; Davis, D. D.; Quan, X.; Patel, S. S.; Smith, S. D. *Macromolecules* **1991**, *24*, 6546.
- (12) Amundson, K.; Helfand, E.; Quan, X.; Smith, S. D. *Macromolecules* **1993**, *26*, 2698.
- (13) Amundson, K.; Helfand, E.; Quan, X.; Hudson, S. D.; Smith, S. D. *Macromolecules* **1994**, *27*, 6559.
- (14) Tsori, Y.; Andelman, D. *Macromolecules* **2002**, *35*, 5161.
- (15) Pereira, G. G.; Williams, D. R. M. *Macromolecules* **1999**, *32*, 8115.
- (16) Onuki, A.; Fukuda, J. *Macromolecules* **1995**, *28*, 8788.

- (17) Ashok, B.; Muthukumar, M.; Russell, T. P. *Journal of Chemical Physics* **2001**, *115*, 1559.
- (18) Hawker, C. J. *Macromolecules* **1996**, *29*, 2686.
- (19) Mansky, P.; Liu, Y.; Huang, E.; Russell, T. P.; Hawker, C. *Science* **1997**, *275*, 1458.
- (20) Thurn-Albrecht, T.; DeRouchey, J.; Russell, T. P.; Kolb, R. *Macromolecules* **2002**, *35*, 8106.
- (21) Mansky, P.; Russell, T. P.; Hawker, C. J.; Mays, J.; Cook, D. C.; Satija, S. K. *Physical Review Letters* **1997**, *79*, 237.

CHAPTER 3

ELECTRIC FIELD ALIGNMENT OF SYMMETRIC DIBLOCK COPOLYMER THIN FILMS

Introduction

Block copolymers self-assemble into arrays of microdomains, *e.g.* lamellae, cylinders, or spheres depending on the volume fraction of the components. The sizes of the domains are dictated by the total molecular weight of the copolymer and, hence, are tens of nanometers in size. Locally, the ordering of the domains is high, but globally the arrays grains form where the orientation of the grains, on average, is random. External fields, such as shear,¹⁻³ electric^{4,5} and surface fields⁶ have been used in both the bulk and thin films to affect alignment.⁷⁻⁹ The preferential interaction and consequent segregation of one block to the substrate orients the microdomains parallel to the substrate surface.¹⁰⁻¹² Electric fields normal to the surface have been used to overcome interfacial interactions and orient the microdomains in the direction of the applied field. Neglecting confinement effects, the critical electric field strength needed to orient the microdomains is given by:^{13,14}

$$E_c = \Delta\gamma^{1/2} \cdot \frac{2(\epsilon_A + \epsilon_B)^{1/2}}{(\epsilon_A - \epsilon_B)} \cdot t^{-1/2} \quad (1)$$

where, $\Delta\gamma$ is the difference between the interfacial energies of each block with the substrate, ϵ_A , ϵ_B are the static dielectric constants of block A and B, respectively, and t is the film thickness. Thus, from equation (1), it is seen that either the film thickness or $\Delta\gamma$ can prevent or limit the orientation of the copolymer microdomains. If $\Delta\gamma$ is too large or the film is too thin, E_c is greater

than the dielectric break down and the copolymer orientation is not be possible. If $\Delta\gamma=0$, *i.e.* when, interfacial interactions are balanced, then $E_c=0$.

The orientation of diblock copolymers has been studied in both the bulk and in solution.^{9,15-19} Theoretically, Onuki and Fukuda investigated the dynamics of undulations in two-dimensional lamellar systems as a route toward alignment.²⁰ Amundson *et al.* studied the interactions of defects and defect mobility as a means of microdomain reorientation. Using TEM, they showed evidence of defect movement and subsequent annihilation of defect structures in bulk copolymer samples.¹⁹ Recently Krausch and coworkers studied the electric field alignment of concentrated copolymer solutions by the real-time synchrotron SAXS measurements and have shown that close to the order-disorder transition (ODT), migration of grain boundaries is the dominant mechanism, while rotation of grains dominates further away from the ODT, *i.e.*, under strongly segregating conditions.^{16,17} They argued that the viscosity plays a key role in determining the mechanism of the orientation. Zvelindovsky *et al.* simulated the same alignment process and showed that the mechanism by which the orientation occurs is determined by the magnitude of the interactions between the two blocks, which is related to the segmental interaction parameter χ_{AB} . In the strong segregation limit where χ_{AB} is large, it costs more energy to deform the microdomains due to the increase in interfacial area resulting from these deformations.²¹ They also studied dynamics of mesophase formation in the framework of dynamic density functional theory (DFT) for a diblock copolymer melt. Under an electric field, the domain alignment is achieved by a relatively local defect movement, *i.e.* the

lamellae locally break up and merge again.²² DeRouchey *et al.* have also recently argued, from small angle x-ray scattering results, that the copolymer domains in thick films are initially disrupted to create smaller grains that can rotate more easily in the field.^{15,23} The presence of two interfaces in thin films amplifies the importance of interfacial interactions that become increasingly more dominant as the film gets thinner. In addition, with decreasing thickness, confinement of the morphology in the thickness direction can present a geometric barrier. Grain rotation, for example, may not be possible due to this film thickness constraint.

In the present study the dependence of the electric field alignment of a symmetric diblock copolymer polystyrene-*b*-polymethyl methacrylate, PS-*b*-PMMA, was studied as a function of film thickness using *in-situ* small angle neutron scattering (SANS) and transmission electron microscopy (TEM). It is shown that the orientation in thin films is a competition between the applied electric field that aligns the microdomains normal to the surface and the surface fields that align the microdomains parallel to the surface. For very thin films, surface induced orientation dominates and the lamellar microdomains are always parallel to the substrate surface. With increasing film thickness, surface effects diminish with distance, and the applied field orients the lamellar microdomains in the center of the film in the direction of the applied field. The intermediate and late stages of the alignment were studied using transmission electron microscopy. Results from these studies indicate that the lamellae locally break up, then reform, in agreement with the arguments of DeRouchey *et al.* and Zvelindovsky *et al.*

Experimental

Materials

Symmetric diblock copolymers of polystyrene and poly(methyl methacrylate), PS-*b*-PMMA, with a number-average molecular weight of 7.19×10^4 g/mol and a PS volume fraction of 0.5 with a polydispersity of 1.09 were synthesized anionically. SANS studies were performed with PS-*b*-PMMA where the polystyrene block was deuterated, denoted as dPS-*b*-PMMA. The molecular weight of dPS-*b*-PMMA was 7.05×10^4 g/mol with a polydispersity of 1.05 and a dPS volume fraction of 0.5. Films were prepared by spin coating a toluene solution of the copolymer onto a substrate.

Sample Preparation

Film thickness was controlled by varying the solution concentration and spinning speed. An aluminized Kapton film was used as a top electrode, where a thin (20-25 μ m) layer of crosslinked polydimethylsiloxane (PDMS) (SylgardTM) was used as a buffer layer between the Kapton electrode and the copolymer thin film. The interfacial energy of PS with PDMS is lower than that of PMMA with PDMS as indicated by x-ray photoelectron spectroscopy. The preparation of the crosslinked PDMS layer has been described previously.

Transmission small angle neutron scattering (SANS) experiments were performed on beam-line NG-3, a 30 meter SANS instrument at National Institute of Standard Technology (NIST), using neutrons with a wavelength $\lambda = 0.6$ nm and $\Delta\lambda/\lambda = 0.15$. For the *in-situ* SANS studies, the spin coated samples were dried at 25°C under vacuum to remove solvent. In the SANS experiment, the samples were heated from room temperature to 170°C in less than ~5 minutes under N₂ under a ~40V/ μ m applied electric field, held at 170°C under the field and

scattering profiles were obtained every 5 minutes. Early stages of the development of order and orientation were examined as the copolymer was heated from a poorly ordered state into the ordered state under an applied external electric field ($\sim 40\text{V}/\mu\text{m}$). Real time small angle neutron scattering studies were performed on dPS-*b*-PMMA films on silicon substrates with the native oxide layer. Films having thicknesses of $\sim 110\text{nm}$, $\sim 700\text{nm}$ and $\sim 3\mu\text{m}$ were investigated.

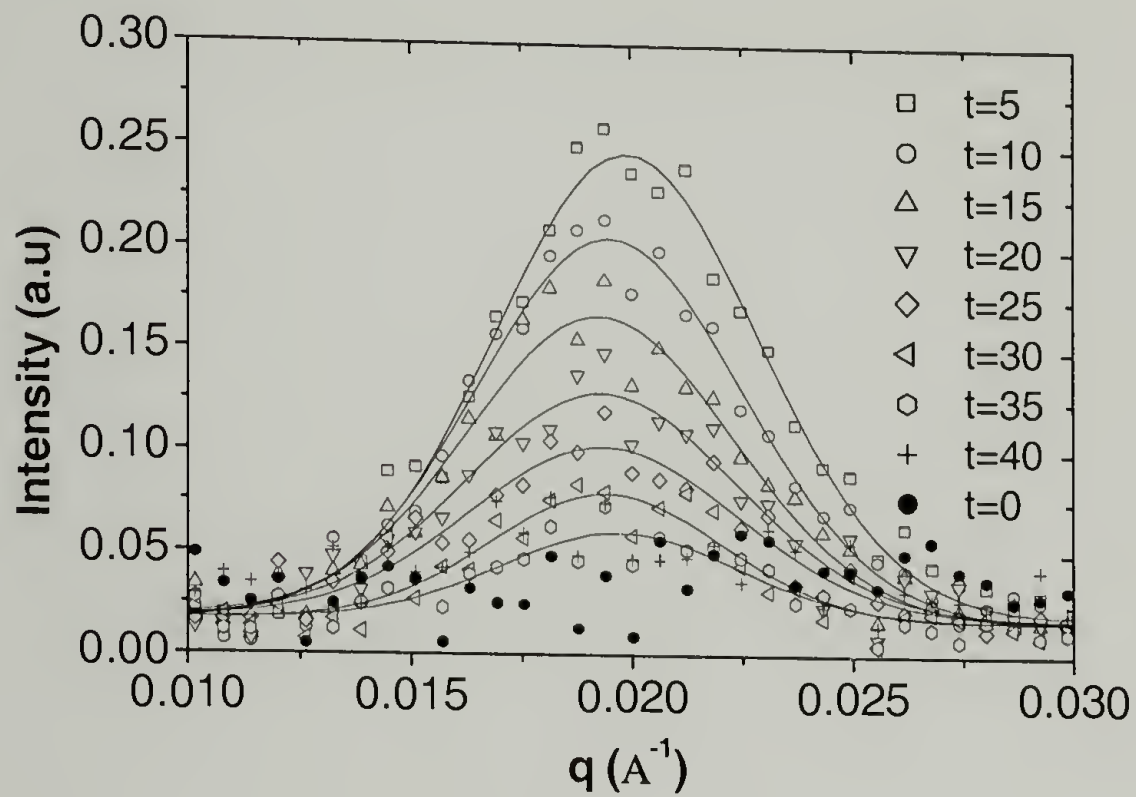
For TEM, the copolymer films were heated to 170°C under N_2 with a $\sim 40\text{V}/\mu\text{m}$ applied electric field for a predetermined time and then quenched to room temperature before removing the field. The films for TEM were prepared on a substrate modified with a random copolymer of styrene and methyl methacrylate having a 0.9 styrene fraction. A thin layer of carbon (10-20nm) was coated onto the surface before the film was embedded in epoxy and cured at 60°C for 12 hrs. The film was removed from the substrate by dipping into liquid N_2 , microtomed at room temperature with a diamond knife and transferred to a copper grid. The thin sections were exposed to ruthenium tetroxide vapor for 30-35min to enhance the contrast. Electron microscopy experiments were performed on a JEOL 100CX TEM at the accelerating voltage of 100KV.

Results and Discussion

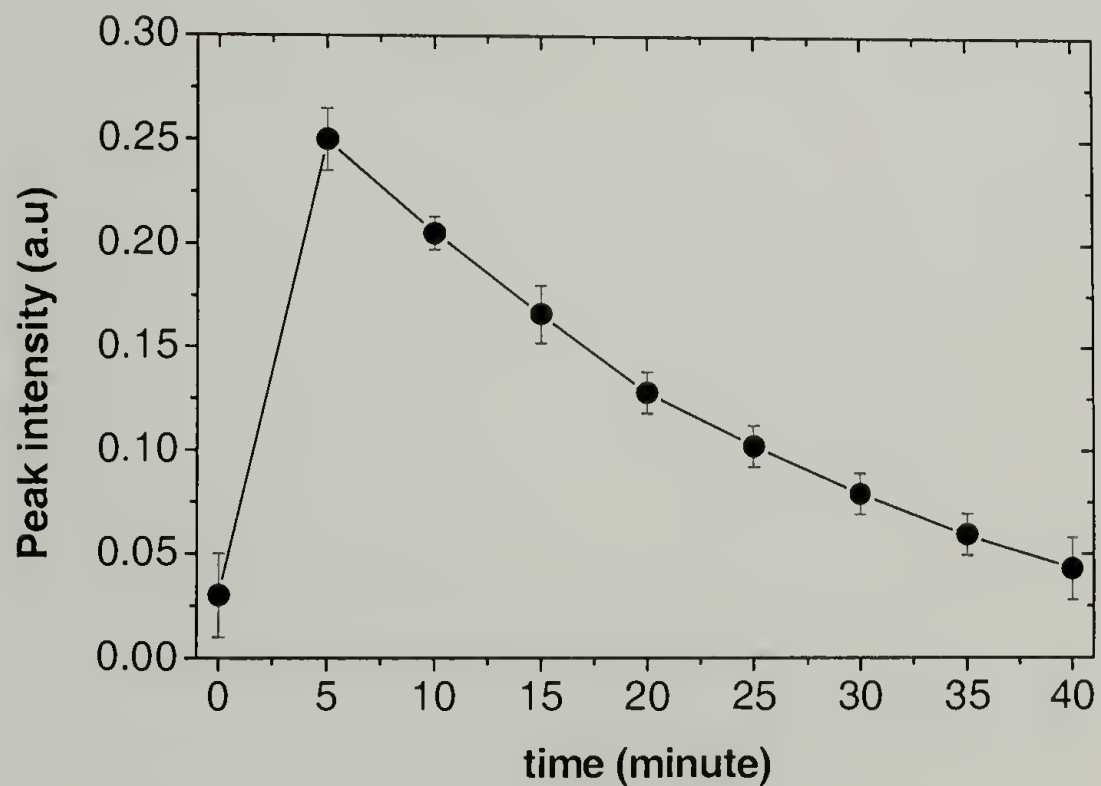
Figure 3.1a shows the evolution of the azimuthally averaged SANS intensity of a $\sim 110\text{nm}$ thick film at 170°C under $\sim 40\text{V}/\mu\text{m}$ electric field. At $t=0$, *i.e.* immediately after spin coating, a broad, weak peak is seen, indicating that the copolymer is poorly ordered.

Figure 3.1(a) The evolution of the SANS angular average intensity of the dPS-b-PMMA thin film ($\sim 110\text{nm}$) annealing under $\sim 40\text{V}/\mu\text{m}$ electric field. Solid line is the Gaussian fit of the data. (b) The evolution of the peak intensity with annealing time under electric field for the thin films.

a



b



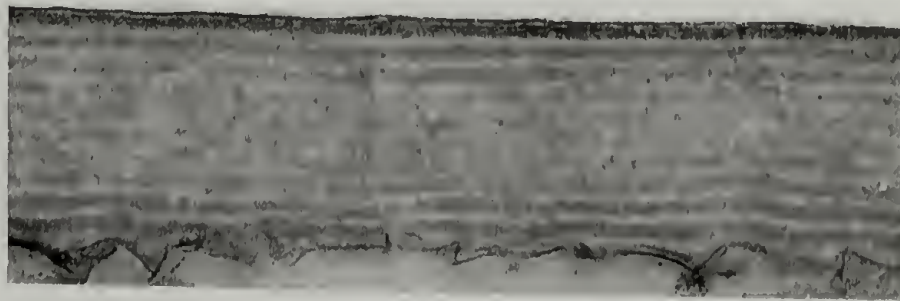
Upon heating to 170°C a sharp reflection is seen in the SANS at $q^* \approx 0.02 \text{ \AA}^{-1}$ ($q = \frac{4\pi}{\lambda} \sin \theta$, where λ is the neutron wavelength, and θ is the scattering angle), corresponding to a period of $\sim 31 \text{ nm}$. The peak intensity increased initially, reached a maximum, and then decreased with continued annealing. Shown in Figure 3.1b is the peak intensity as a function of time. The peak intensity at q^* is proportional to the number of microdomains oriented along the applied electric field direction, i.e. normal to the surface. Thus, there is a rapid orientation of the lamellar microdomains normal to the surface. However, with time, the microdomains reorient parallel to the surface, due to the preferential interactions of the PMMA with the oxide substrate. The evolution of the peak intensity reflects the competition between the applied electric field and interfacial interactions. For the 110nm films, approximately four periods in thickness, interfacial interactions are seen to dominate.

Figure 3.2a and 3.2b show the cross-sectional TEM images of $\sim 300 \text{ nm}$ thick *dPS-b-PMMA* films annealed under an electric field for 3hrs and 6hrs, respectively, on a silicon substrate that has been modified with a random copolymer of styrene and methyl methacrylate having a styrene fraction of 0.9. After 3hrs, the lamellar microdomains aligned parallel to both electrode interfaces, due to the preferential wetting of the PS blocks. In the center of the film, however, the microdomains have mixed orientations with very small grain sizes. After 6hrs, the lamellar microdomains are oriented parallel to the substrate interfaces throughout the film, even with the applied electric field normal to the interface. Annealing the film for 16hrs did not change the microdomain

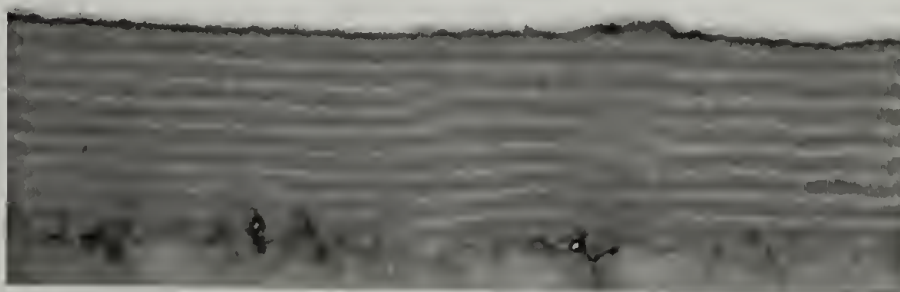
orientation. Results from the TEM studies also indicate that the applied electric field is not sufficiently high to overcome the interfacial interactions, and the lamellar microdomains orient parallel to the surface.

Figure 3.2 Cross-sectional TEM image of a $\sim 300\text{nm}$ PS-*b*-PMMA film annealed under $\sim 40\text{V}/\mu\text{m}$ electric field for (a) 3 hrs. (b) 6hrs. Scale bar: 100nm.

a



b

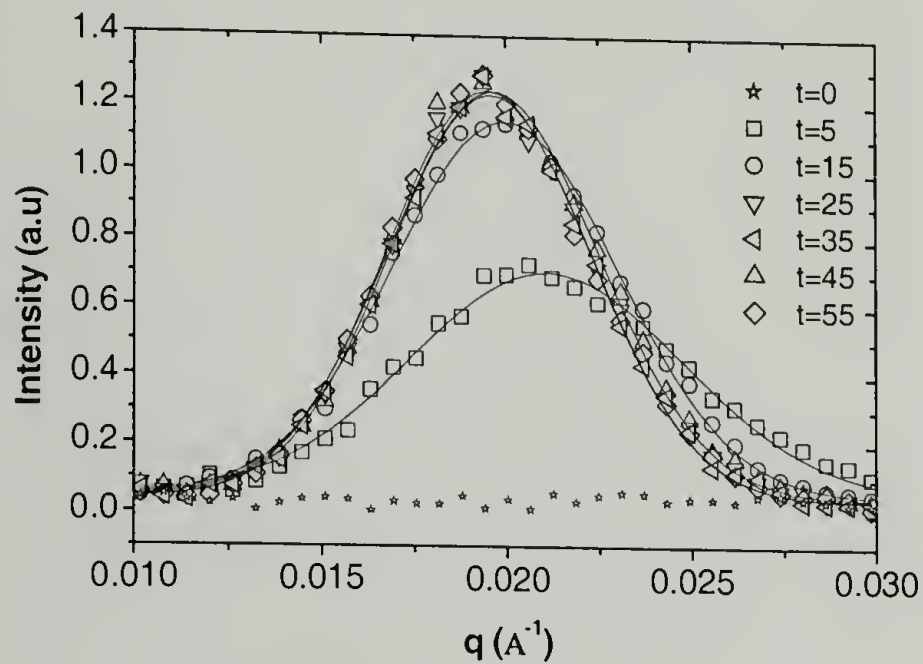


Previous studies have shown that interfacial interactions have a limited range over which orientation propagates into the film. The range depends on the strength of interfacial interactions. The stronger the interactions, the greater is the distance that the orientation propagates into the film. Beyond this range, however, fluctuations can not be suppressed by the interface and different orientations appear.²⁴ A second set of *in-situ* SANS experiments was performed to follow the alignment of a dPS-*b*-PMMA thick film ($\sim 700\text{nm}$). Figure 3.3a shows the time evolution of the circularly averaged SANS from a $\sim 700\text{nm}$ film on the Si substrate with native oxide layer. At $t=0$, i.e. after spin coating, a broad, weak maximum is seen, indicating the copolymer is poorly ordered. Once heated

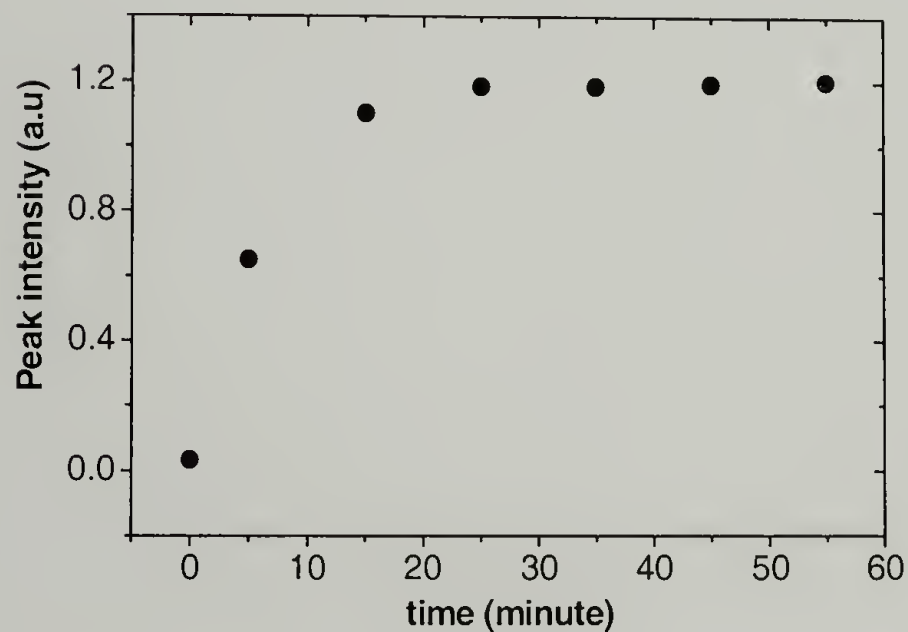
above the glass transition temperature, the polymer chains become mobile and microphase separate under the influence of the applied electric field.

Figure 3.3(a) The evolution of the SANS angular average intensity of the thick film ($\sim 700\text{nm}$) annealing under $\sim 40\text{V}/\mu\text{m}$ electric field. Solid line is the Gaussian fit of the data. (b) The evolution of the peak intensity with annealing time under electric field.

a



b



The peak is seen to intensify rapidly (within the first 5 minutes) with a maximum at $q^* \approx 0.021 \text{\AA}^{-1}$ and full width at half maximum (FWHM) of 0.0074\AA^{-1} .

^l. Further annealing causes the peak to intensify, shift to a smaller $q^* \approx 0.02 \text{ \AA}^{-1}$ and narrow with a full width at half maximum of 0.0055 \AA^{-1} at $t=25$ min. As shown in Figure 3b, the peak intensity initially increases rapidly indicating that the number of the microdomains aligned along the electric field direction has rapid increased. Subsequently, the intensity increases only slowly. In comparison to thin films where the interfacial interactions dominate, in thicker films the applied electric field is more effective in orienting the microdomains.

Figure 3.4 Cross-sectional TEM image of a $\sim 700\text{nm}$ PS-*b*-PMMA film annealed under $\sim 40\text{V}/\mu\text{m}$ electric field for (a) 6hrs. (b) 16hrs. Scale bar: 100nm.

a



b

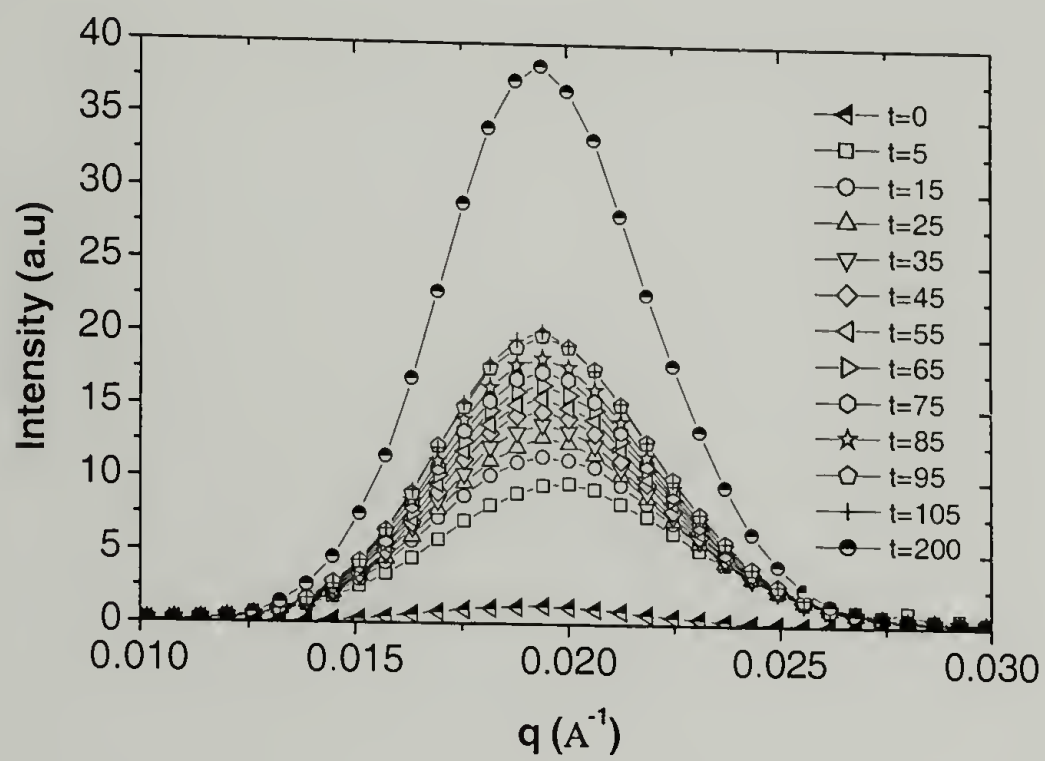


Shown in Figures 3.4a and 3.4b are cross-sectional TEM images of a $\sim 700\text{nm}$ thick PS-*b*-PMMA film on a silicon substrate (modified with 90/10 random copolymer) that had been annealed under electric field for 6 hrs and 16 hrs, respectively. Mixed orientations were observed and an orientation of the lamellar microdomains in the direction of the applied field is found in the middle of the films. This results from a kinetic trapping as discussed earlier.²⁵ After annealing for 6 hrs, the lamellar microdomains near the electrode interfaces are aligned parallel to the interfaces, due to the preferential wetting of PS blocks with the electrodes. However, in the center of the film, the lamellar microdomains formed small anisotropic grains. Within these small grains, the microdomains are, on average, oriented in the direction of the applied electric field. After 16 hrs, the orientation of the microdomains by both electrode interfaces and the applied electric field is evident as shown in Figure 3.4b. Consistent with previous studies, the parallel orientation extends $\sim 5L_0$ from both interfaces into the film before any orientation due to the applied field is evident.

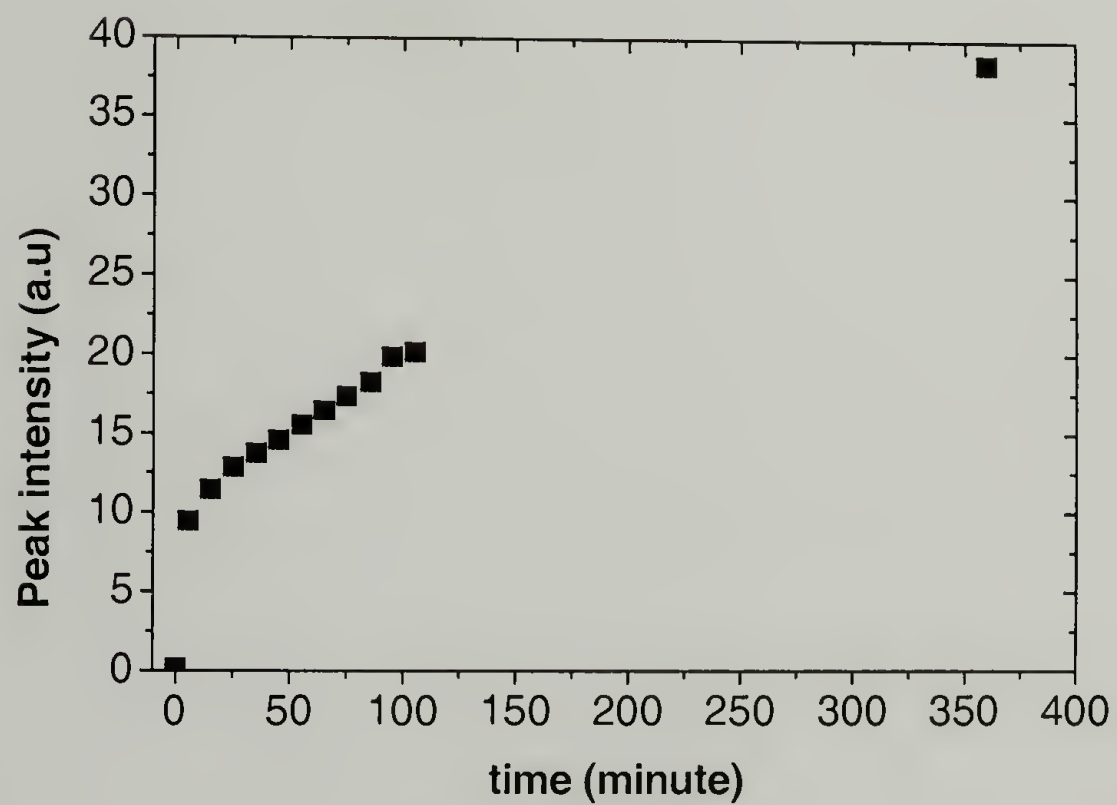
Figure 3.5a shows the evolution of the circularly averaged SANS intensity for a $\sim 3\mu\text{m}$ film. After spin coating, $t=0$, a diffuse, weak peak is seen at $q \approx 0.02 \text{ \AA}^{-1}$ with a FWHM of 0.005 \AA^{-1} . This is similar to the results observed for the thinner films. With increasing time, the peak intensifies, narrows and shifts to a slightly smaller q . From the peak intensity in Figure 3.5b, the orientation is seen to continue steadily, even after annealing under the applied field for 6 hrs.

Figure 3.5 The evolution of the SANS angular average intensity of the thicker film ($\sim 3\mu\text{m}$) annealing under $\sim 40\text{V}/\mu\text{m}$ electric field. Solid line is the Gaussian fit of the data. (b) The evolution of the peak intensity with annealing time under electric field.

a



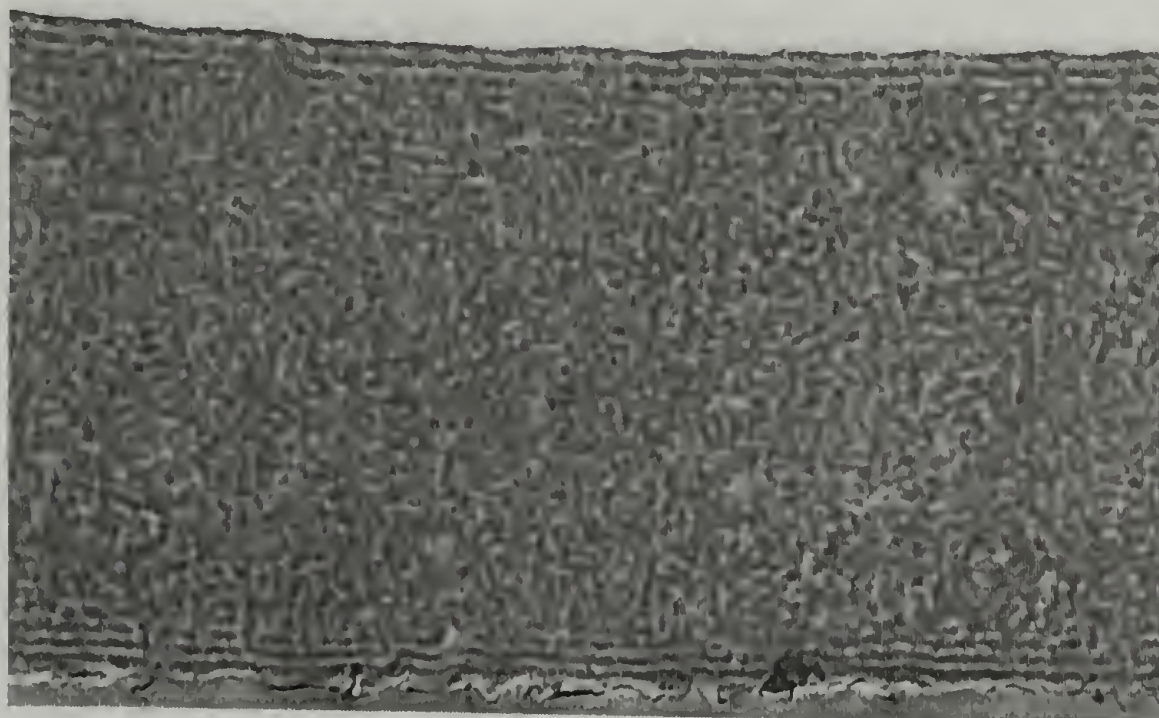
b



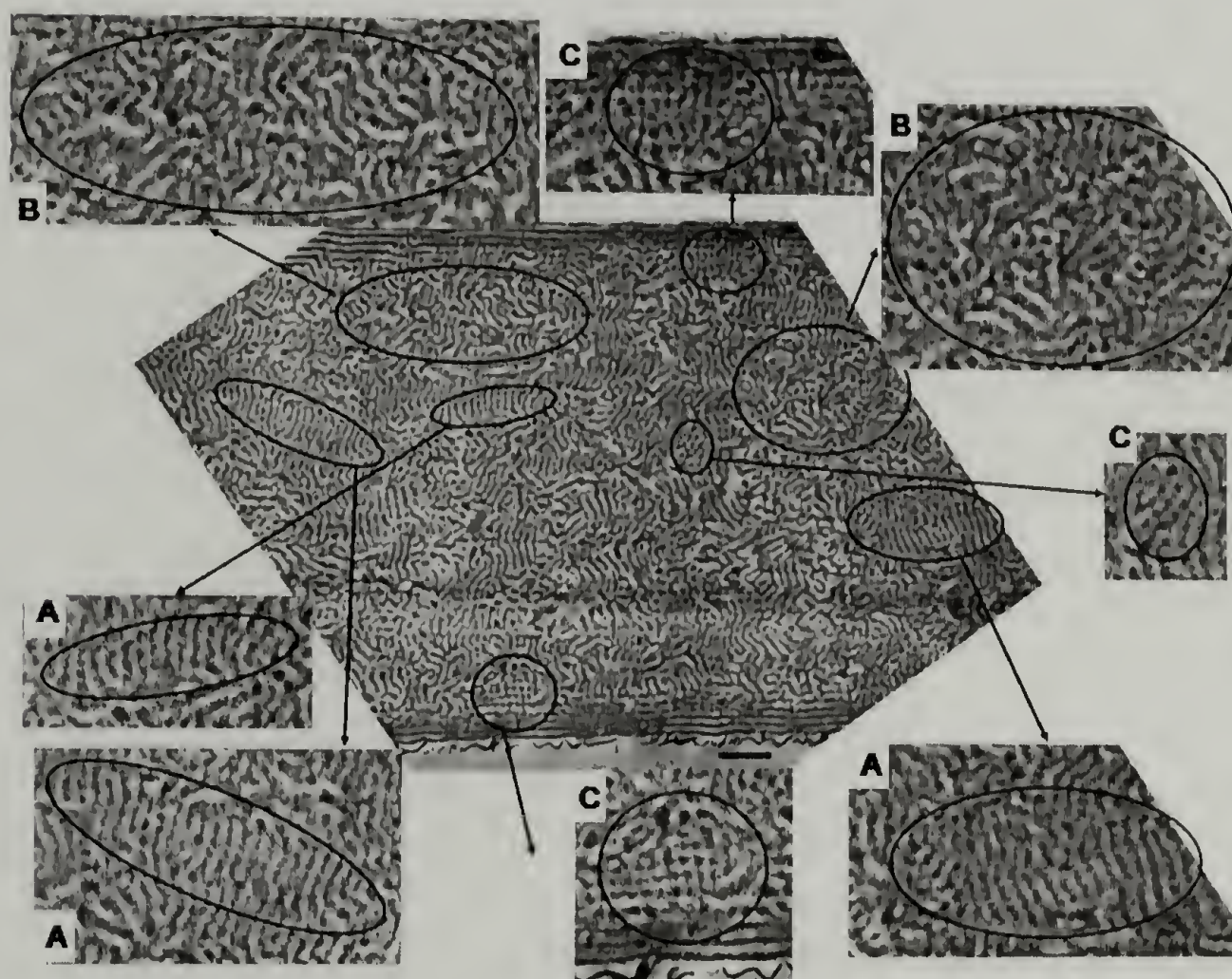
Shown in Figure 3.6a is the cross-sectional TEM images of a film annealed under electric field for 3 hrs. The microdomains adjacent to the interfaces are aligned parallel to the surface, due to the preferential wetting of PS blocks. Though SANS shows very strong scattering for the samples subjected to the same treatment, only very small grains were seen in the center of the film and the orientation of microdomains is not immediately clear. Figure 3.6b is the cross-sectional TEM images of a film annealed under electric field for 6 hrs. The lamellar microdomains are easily seen and the grain size has increased. The orientation of the microdomains is along the electric field direction, though there are still microdomains with no preferred orientation. In this image, there are several distinct features (labeled A, B, C) that provide insight into the alignment process. In all the A type regions, there are ellipsoidal grains with their long axis parallel to the surface. The lamellar microdomains within these grains are aligned parallel to the electric field direction. In regions marked B, the lamellar microdomains have random orientation. Here grains are very small with many defects in the stacking of the lamellae. Some of the lamellar microdomains are disrupted and are melding with nearby microdomains. In regions marked C, the disruption and melding process are clearly manifest. Fluctuations with a period similar to that of the equilibrium lamellar period are evident. Both conformal and nonconformal fluctuations in adjacent lamellae can be seen, with non-conformal fluctuations prevalent in the lamellae adjacent to the substrate.

Figure 3.6 Cross-sectional TEM images of PS-*b*-PMMA films annealed under $\sim 40\text{V}/\mu\text{m}$ electric field for (a) 3hrs. (b) 6hrs. (c) 16hrs. Scale bar: 200nm.

a



b



Continued next page

Figure 3.6, continued

c



There are striking similarities between the TEM images shown here and the images shown in the simulations of Zvelindovsky. The movement and coalescence of the defects, *i.e.* the local disruption and reformation of lamellae appears the dominant pathway in achieving alignment.

A cross-sectional TEM image of a film annealed under electric field for 16 hrs is shown in Figure 3.6c. Throughout the image, the lamellar microdomains are aligned parallel to the field direction. The number of defects is substantially reduced, though slight misalignment of adjacent grains still exists. Removal of

this misalignment, however, requires extended annealing, since the driving force to perfectly align the domains parallel to the applied field is small.

Conclusions

Electric field alignment of symmetric diblock copolymer thin films was studied using in-situ small angle neutron scattering and transmission electron microscopy. The early stage of the alignment process was found to be a competition between the applied electric field strength and the interfacial interactions. For thin films, the surface induced orientation dominates and the lamellar microdomains remain parallel to the substrate surface, independent of the strength of the applied electric field. With increasing film thickness, surface effects dissipate with distance from the surface and, in the interior of the film, the lamellar microdomains were oriented normal to the surface, i.e. parallel to the direction of the applied electric field. The migration and coalescence of the defects were found to be the dominant pathways to align the lamellar microdomains in the direction of the applied field.

References

- (1) Albalak, R. J.; Thomas, E. L. *J Polym Sci Pol Phys* **1993**, *31*, 37.
- (2) Albalak, R. J.; Thomas, E. L. *J Polym Sci Pol Phys* **1994**, *32*, 341.
- (3) Keller, A.; Pedemonte, E.; Willmouth, F. M. *Nature* **1970**, *225*, 538.
- (4) Amundson, K.; Helfand, E.; Davis, D. D.; Quan, X.; Patel, S. S.; Smith, S. D. *Macromolecules* **1991**, *24*, 6546.
- (5) Thurn-Albrecht, T.; Schotter, J.; Kastle, C. A.; Emley, N.; Shibauchi, T.; Krusin-Elbaum, L.; Guarini, K.; Black, C. T.; Tuominen, M. T.; Russell, T. P. *Science* **2000**, *290*, 2126.
- (6) Huang, E.; Rockford, L.; Russell, T. P.; Hawker, C. J. *Nature* **1998**, *395*, 757.
- (7) Mansky, P.; DeRouchey, J.; Russell, T. P.; Mays, J.; Pitsikalis, M.; Morkved, T.; Jaeger, H. *Macromolecules* **1998**, *31*, 4399.
- (8) Morkved, T. L.; Lu, M.; Urbas, A. M.; Ehrichs, E. E.; Jaeger, H. M.; Mansky, P.; Russell, T. P. *Science* **1996**, *273*, 931.
- (9) Thurn-Albrecht, T.; DeRouchey, J.; Russell, T. P.; Jaeger, H. M. *Macromolecules* **2000**, *33*, 3250.
- (10) Anastasiadis, S. H.; Russell, T. P.; Satija, S. K.; Majkrzak, C. F. *Phys Rev Lett* **1989**, *62*, 1852.
- (11) Anastasiadis, S. H.; Russell, T. P.; Satija, S. K.; Majkrzak, C. F. *J Chem Phys* **1990**, *92*, 5677.
- (12) Fredrickson, G. H. *Macromolecules* **1987**, *20*, 2535.
- (13) Tsori, Y.; Andelman, D. *Macromolecules* **2002**, *35*, 5161.
- (14) Pereira, G. G.; Williams, D. R. M. *Macromolecules* **1999**, *32*, 8115.
- (15) Thurn-Albrecht, T.; DeRouchey, J.; Russell, T. P.; Kolb, R. *Macromolecules* **2002**, *35*, 8106.
- (16) Boker, A.; Knoll, A.; Elbs, H.; Abetz, V.; Muller, A. H. E.; Krausch, G. *Macromolecules* **2002**, *35*, 1319.
- (17) Boker, A.; Elbs, H.; Hansel, H.; Knoll, A.; Ludwigs, S.; Zettl, H.; Urban, V.; Abetz, V.; Muller, A. H. E.; Krausch, G. *Phys Rev Lett* **2002**, *89*, 135502.

- (18) Amundson, K.; Helfand, E.; Quan, X.; Smith, S. D. *Macromolecules* **1993**, *26*, 2698.
- (19) Amundson, K.; Helfand, E.; Quan, X. N.; Hudson, S. D.; Smith, S. D. *Macromolecules* **1994**, *27*, 6559.
- (20) Onuki, A.; Fukuda, J. *Macromolecules* **1995**, *28*, 8788.
- (21) Zvelindovsky, A. V.; A., S. G. J. *Phys Rev Lett* **2003**, *90*, 49601.
- (22) Kyrylyuk, A. V.; Zvelindovsky, A. V.; Sevink, G. J. A.; Fraaije, J. G. E. M. *Macromolecules* **2002**, *35*, 1473.
- (23) DeRouchey, J.; Russell, T. P. *Unpublished results* **2003**.
- (24) Xu, T.; Hawker, C. J.; Russell, T. P., in preparation.
- (25) Xu, T.; Hawker, C. J.; Russell, T. P. *Macromolecules* **2003**, *36*, 6178.

CHAPTER 4

EFFECT OF IONIC IMPURITIES IN ELECTRIC FIELD ALIGNMENT OF DIBLOCK COPOLYMER THIN FILMS

Introduction

Thin films of block copolymers have attracted significant attention due to their potential use as templates and scaffolds for nanostructured materials.^{1,2} Controlling orientation of the copolymer microdomains, however, is crucial. Electric fields have been shown to be an effective route to achieve this control in thin films.³⁻⁸ By applying an electric field normal to the surface, the microdomains can be oriented along the applied field direction. The preferential interactions of either block with the interfaces present a barrier to this orientation that must be overcome to achieve the desired alignment.⁹⁻¹¹ The influence of interfacial energy on the microdomain orientation of symmetric diblock copolymers by an electric field has recently been discussed.¹² Complete alignment of the microdomains could be achieved only when the interfacial interactions were balanced. In all other cases, microdomains adjacent to the substrate were found to be oriented parallel to the substrate interface, whereas in the interior of the film the microdomains oriented in the direction of the applied field. These results were ascribed to a pathway-dependent alignment and a high energetic barrier to achieve complete re-orientation of the microdomains adjacent to the surface. At the early stages of alignment, the microdomains adjacent to the substrate were oriented parallel to the surface. The field strength required to achieve full alignment exceeded the dielectric breakdown of the copolymers. Therefore, relying strictly on the difference in the dielectric constants of the

microdomains to affect alignment was not possible. Consequently, an alternate alignment mechanism that requires lower electric field strength is needed.

Recently, we observed that an electric field could be used to introduce a transition in the morphology, from spherical to cylindrical microdomains.¹³ Tsori *et al.* calculated the electric field strength necessary to induce this transition based on the dielectric constant theory and found that the required electric field strength exceeded the dielectric breakdown of the copolymers. To explain the experimental observations, they proposed an alternate mechanism wherein the presence of ionic impurities may be responsible for inducing the observed morphological transition.¹⁴ The concentration of ionic impurities required to significantly reduce the critical field strength for alignment was quite low. These compelling arguments led us to undertake a systematic study of the influence of impurities on the microdomain alignment.

The effect of ionic impurities on the electric field alignment of lamellar microdomains of polystyrene-*block*-poly(methyl methacrylate) (PS-*b*-PMMA) in thin films was studied using transmission electron microscopy (TEM) and atomic force microscopy (AFM). At lithium ion concentrations greater than ~210 ppm, the microdomain morphology in block copolymers could be aligned in the direction of an applied electric field regardless of the strength of interfacial interactions. For thin films with thickness $\sim 10L_o$ (L_o is the equilibrium period of the copolymer in the bulk), where the lamellar microdomains are oriented parallel to the surface throughout the film, a re-orientation of the lamellar microdomains normal to the surface, i.e. in the direction of the applied field, was

observed wherein the applied field was seen to enhance fluctuations at the interfaces of the microdomains with a wavelength comparable to L_o , the equilibrium period of the copolymer. The enhancement in the fluctuations led to a disruption of the microdomains into microdomains $\sim L_o$ in size that, with time, reconnected to forming lamellar microdomains oriented in the direction of the applied field. This differentiates copolymers from polymer/polymer liquids, where the fluctuations enhanced by electric field vary with field strength, dielectric constants difference and interfacial energies between two polymers.^{15,16}

Experimental

Materials

Polystyrene-*block*-poly(methyl methacrylate) ($M_n = 6.4 \times 10^4$, PDI = 1.08), denoted as PS-*b*-PMMA, was prepared by anionic synthesis under a nitrogen atmosphere, using Schlenk techniques and contained 50% (by volume) styrene. Prior to polymerization, a small amount of lithium chloride (LiCl) (~0.5 g) was added to aid in the ion separation of the propagating end. Precipitation of the polymer was achieved by pouring the solution into 5 times its volume of methanol and filtering. Size exclusion chromatography was done versus polystyrene standards using a Knauer SEC system with K501 HPLC pump, K2301 RI detector and K2600 dual UV detector, equipped with 3 Plgel 5 μm columns (two mixed-D and one 50 Angstroms). The elemental concentration of lithium impurity of the PS-*b*-PMMA diblock copolymer prepared this way is 210 ppm as measured by Quantitative Technologies Inc. with 1 ppm resolution. The purified diblock copolymers used in this study were cleaned by running the

copolymer through 3 silica gel (70-230 mesh) plugs ($\frac{3}{4}$ " diam.x 5" tall). The polymer (0.5 g) was dissolved in 5 mL of HPLC grade toluene, passed through the plug once and the first 10 mL fraction containing polymer was precipitated into methanol. This was repeated 3 times using fresh silica gel each time. The elemental concentration of lithium after purification is lower than 1ppm.

Sample Preparation

Silicon substrates were modified by anchoring hydroxyl terminated random copolymers of styrene and methyl methacrylate with styrene fractions of 0.9, prepared by living free radical procedures.^{17,18} The interfacial interaction difference between PS and PMMA homopolymers with the modified substrates is approximately 0.9 dyne/cm ($\gamma_{\text{PMMA/sub}} - \gamma_{\text{PS/sub}} \approx 0.9$ dyne/cm). Films of PS-*b*-PMMA, ~300 nm, ~800 nm, ~1 μm in thickness, were prepared by spin coating toluene solution of the copolymers on to the substrates. Films of ~800 nm were annealed at 170°C for 3 days under vacuum.

The capacitor setup for the electric field alignment used an aluminized Kapton film as the top electrode (positive electrode). A thin layer (20-25 μm) of crosslinked PDMS (SylgardTM) was used as a buffer layer between the Kapton electrode and the copolymer thin film. The PDMS layer conforms to the electrode surface, eliminates air gaps between the top electrode and the copolymer film, and maintains a smooth surface of the copolymer film. The preparation of the crosslinked PDMS layer was described previously.¹² A conductive silicon substrate with a 2 nm native silicon oxide layer was used as the bottom electrode (ground/negative electrode). The silicon substrates were modified with a random copolymer of methyl methacrylate and styrene as described above. The copolymer films were heated to 170°C under N₂ with an applied DC electric field of ~40V/ μm for 16hrs, and then quenched to room

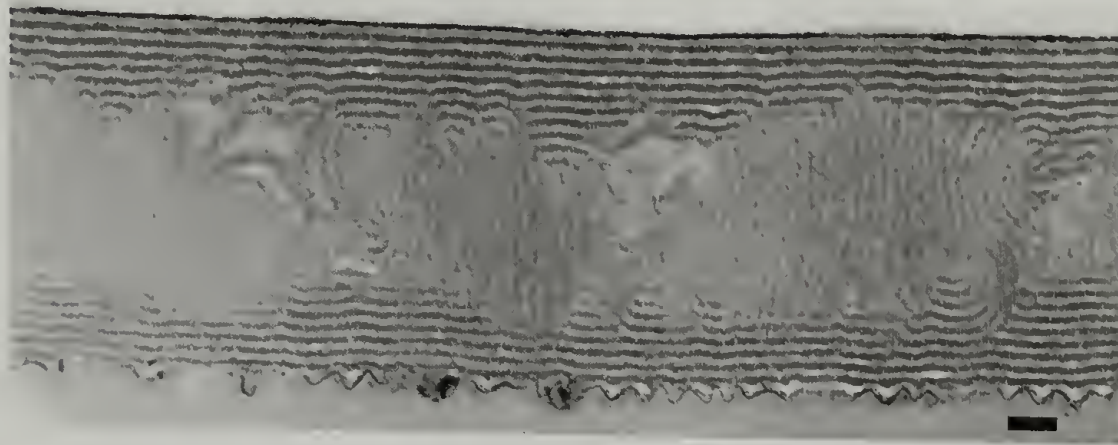
temperature before removing the electric field. Tapping mode AFM was performed with a Dimension 3100, Nanoscope III from Digital Instruments Corp. For TEM, the copolymer films were heated to 170 °C under N₂ with a ~40V/μm applied electric field for a predetermined time and then quenched to room temperature before removing the field. The samples were embedded in epoxy, microtomed with a diamond knife at room temperature and transferred to a copper grid. The thin sections were exposed to ruthenium tetroxide for 35min to enhance the contrast. Electron microscopy experiments were performed on a JEOL 100CX TEM at the accelerating voltage of 100KV.

Results and Discussion

Interfacial interactions and surface tension are sensitive to residual impurities in polymers and, to our knowledge, there is no report on whether the presence of lithium ions in PS-*b*-PMMA may significantly change interfacial interactions and surface tension in thin films. Films (~800 nm) of the copolymer before and after removal of lithium ions were prepared and annealed at 170°C for 72 hrs under vacuum. Figure 4.1 shows the cross-sectional TEM images of PS-*b*-PMMA thin films before (Figure 4.1a) and after (Figure 4.1b) lithium ion extraction. For both cases, lamellar microdomains were observed to be parallel at both, the air/polymer and polymer/substrate interface, indicating lower surface tension of PS and lower interfacial interactions between PS and the modified substrate. In this case, the presence of trace lithium ions (210 ppm) did not significantly change the interfacial interactions of each block with the substrate.

Figure 4.1 Cross-sectional TEM images of ~ 800 nm PS-*b*-PMMA films (a) before and (b) after lithium ions extraction. The films were annealed at 170°C for 72 hrs under vacuum.

a



b

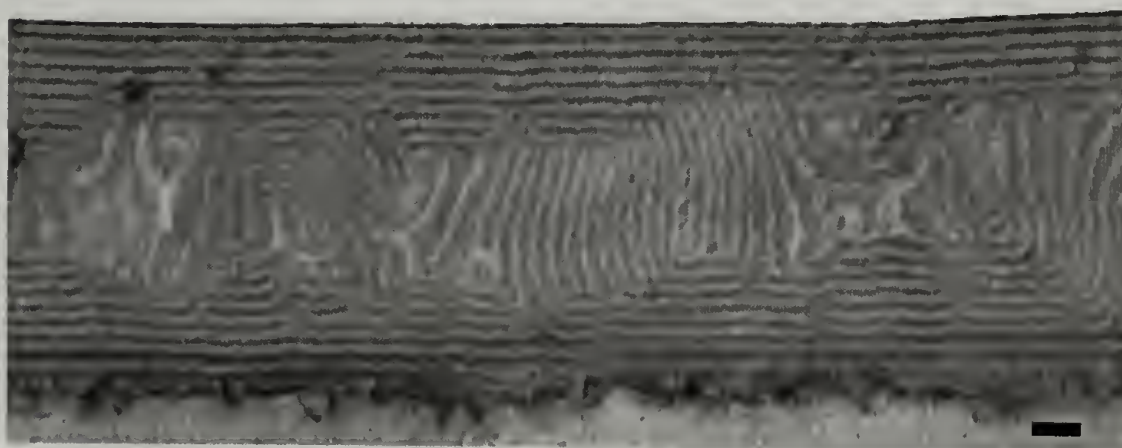
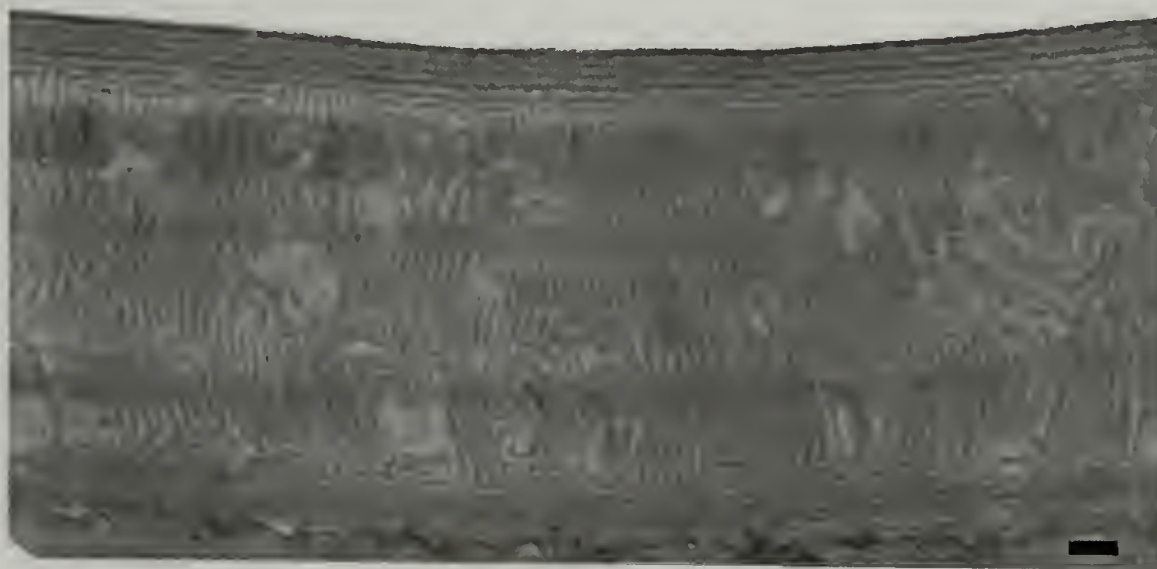


Figure 4.2 shows a cross-sectional TEM image of a ~ 1 μm film spin coated from a toluene solution of the copolymer after lithium ion extraction. The film was on a silicon substrate that had been modified with a random copolymer of styrene and methyl methacrylate having a styrene fraction of 0.9. Thus, the modified substrate had lower interfacial energy with PS than that of PMMA. Mixed orientations were seen after annealing at 170°C under a $\sim 40\text{V}/\mu\text{m}$ DC electric field for 16hrs. The film surface was covered by PS and showed no features except surface roughness as measured by AFM. For the film of ~ 300 nm

thickness, the lamellar microdomains were parallel to the surface regardless of the electric field applied normal to the surface (not shown). These TEM images show results consistent with previous studies based on a dielectric mechanism, where complete alignment of lamellar microdomains could not be achieved using an electric field if the interfacial interactions were not balanced.¹²

Figure 4.2 Cross-sectional TEM image of a $\sim 1 \mu\text{m}$ PS-*b*-PMMA film after annealed at 170°C under a $\sim 40\text{V}/\mu\text{m}$ DC electric field for 16hrs. The copolymer has been cleaned off lithium ions.



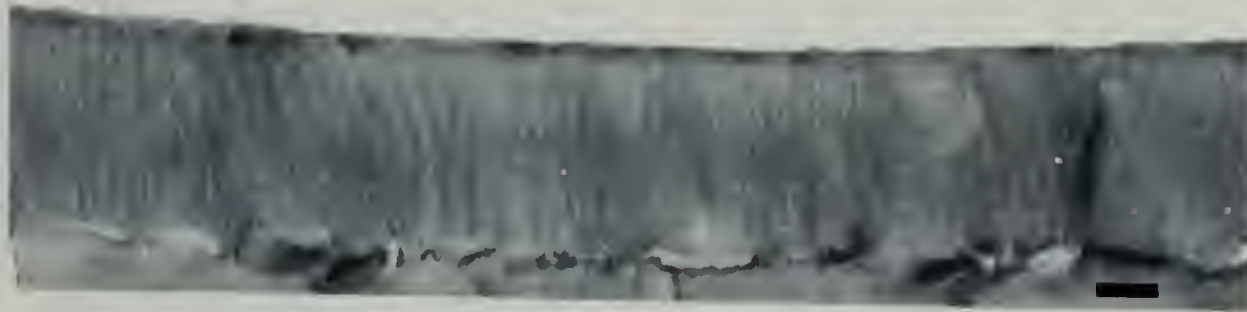
The mixed orientations were due to a pathway-dependent alignment and a high energetic barrier to achieve complete reorientation of the lamellae adjacent to the surface. The driving force for alignment, based on a dielectric constant difference between two blocks, is not strong enough to reorient the microdomains adjacent to the substrate, where the fluctuations were suppressed by surface field. With the presence of a trace amount of lithium ions, dissociated lithium ions reside predominantly within the PMMA domains due to $\text{Li} \leftarrow \text{O}=\text{C}$ coordination bridges as measured by Kim and Tsori *et al.*^{19,20} Under an electric field, there will be positive charges at one end of the PMMA microdomain and

negative charges at the other end, creating an effective dipole. Dipole-field interactions are known to be a much stronger driving force compared with that from a dielectric mechanism and may be able to reorient the lamellar microdomains adjacent to the substrate.

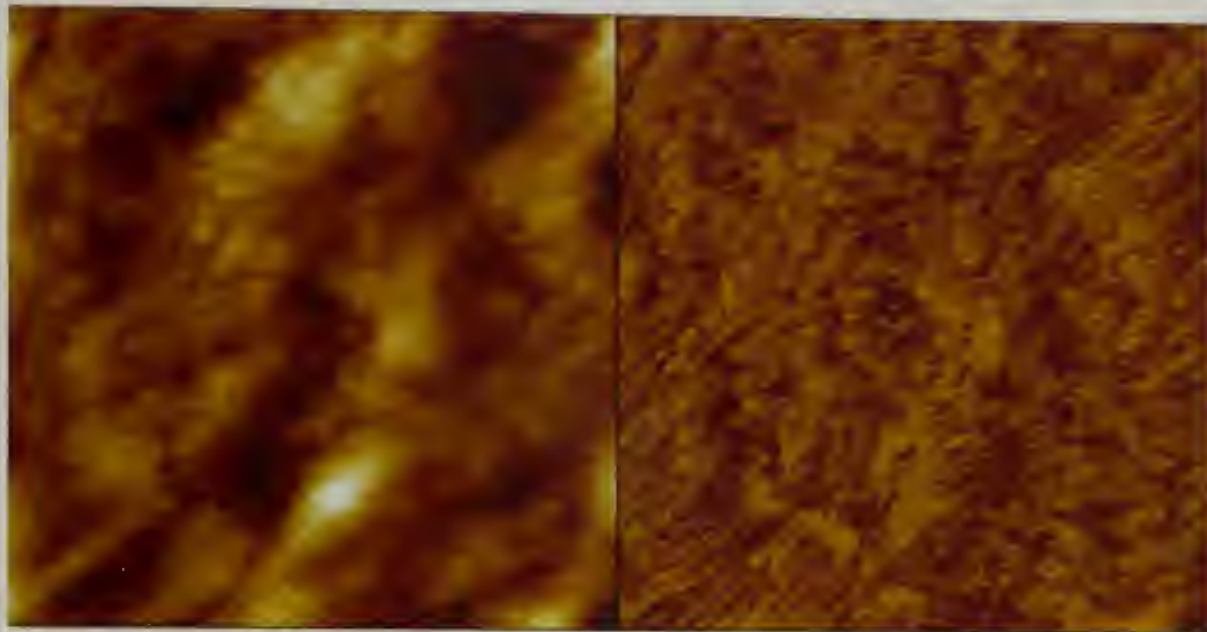
Figure 4.3a shows a cross-sectional TEM image of a ~ 300 nm PS-*b*-PMMA thin film after annealing at 170°C under a $\sim 40\text{V}/\mu\text{m}$ DC electric field for 16hrs. The substrate had been modified with the same random copolymers as that shown in Figure 4.2, thus having a lower interfacial interaction with the PS blocks. The diblock copolymer has not been purified and contained 210 ppm residual lithium impurities as measured by Quantitative Technology Inc. From the TEM image, it is clearly seen that lamellar microdomains were aligned along the applied electric field direction throughout the entire film. Figure 4.3b shows AFM height and phase images of the film surface. Both, PS (dark) and PMMA (bright) lamellae are visible on the surface, in agreement with a complete alignment. Figure 4.3c shows a cross-sectional TEM image of a ~ 1 μm film with the same treatment. Again, lamellar microdomains were aligned along the field direction completely. Thus, in the presence of lithium ions (210 ppm), the electric field can overcome the interfacial interactions to achieve complete alignment.

Figure 4.3 (a) Cross-sectional TEM and (b) height and phase AFM images of a $\sim 300\text{nm}$ PS-*b*-PMMA film after annealed at 170°C under an $\sim 40\text{V}/\mu\text{m}$ DC electric field for 16hrs. (c) Cross-sectional TEM image of a $\sim 1\ \mu\text{m}$ PS-*b*-PMMA film with the same treatment. The copolymer contains 210 ppm lithium residual impurity.

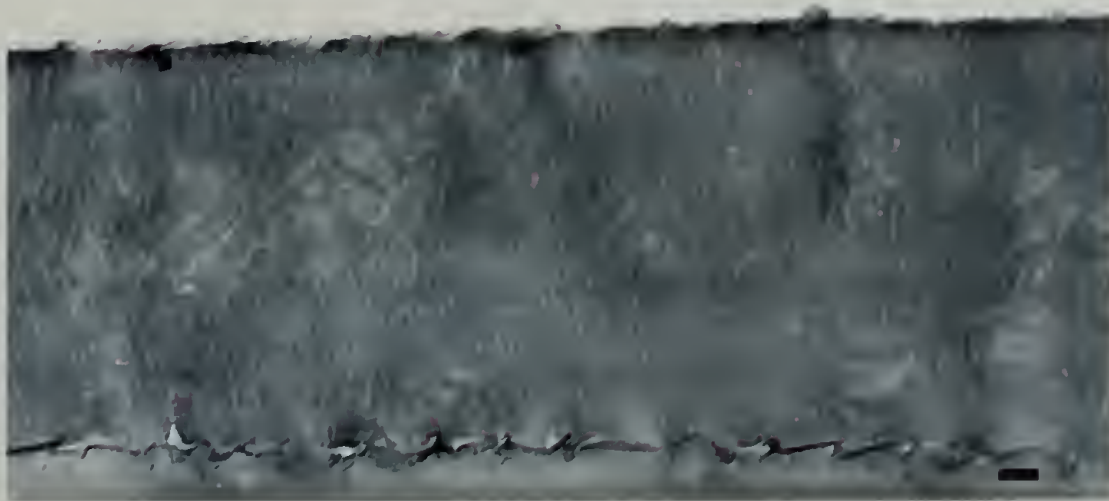
a



b



c

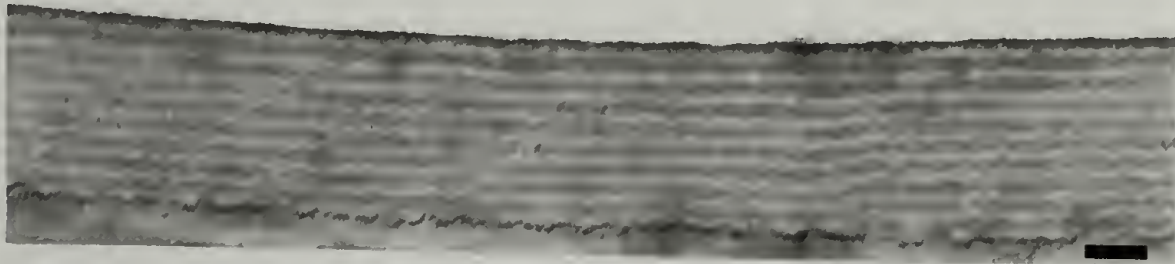


The effect of electric field induced transition of lamellar microdomains in diblock copolymer thin films ($\sim 10L_0$) from a parallel to perpendicular orientation was studied. Figure 4.4 shows cross-sectional TEM images of a ~ 300 nm film annealed at 170°C under a $\sim 40\text{V}/\mu\text{m}$ DC electric field for 6, 9, 12 hrs, respectively. The films were used after spin coating and were in a poorly ordered state. After 6hrs, the lamellar microdomains are oriented parallel to the substrate interfaces throughout the film, as seen in Figure 4.4a. This is due the dominance of the surface field in orienting the microdomains parallel to the surface initially. For copolymers without lithium ions, further annealing under an electric field did not change the microdomain orientation.²¹ However, with lithium ions present after an additional 3 hrs of annealing (total 9 hrs annealing under electric field), the applied electric field enhanced fluctuations at the microdomain interfaces with a wavelength comparable to L_0 , the equilibrium period of the copolymer, and the lamellar microdomains began to break up into microdomains L_0 in size as shown in Figure 4.4b.^{12,15,16,22-24} This mainly occurred in the center of the film, away from solid interfaces, where fluctuations are strongly suppressed by the surface field. With time, the electric field was able to enhance fluctuations on the lamellae adjacent to the substrate and broke them into small microdomains as shown in Figure 4.4c. With further annealing, these lamellar fragments reconnected and formed lamellar microdomains aligned along the applied field direction, similar to that shown in Figure 3a. For the study shown above (Figure 4.4), the diblock copolymer thin films were in a poorly ordered state initially.

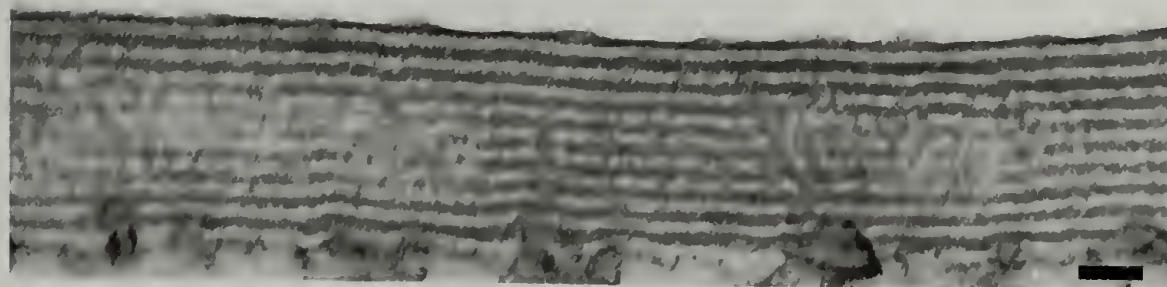
The same results were obtained by starting from a well-ordered state with lamellae parallel to the substrate throughout the film.

Figure 4.4 Cross-sectional TEM image of a ~300 nm PS-*b*-PMMA film after annealed at 170°C under a ~40V/μm DC electric field for (a) 6 hrs, (b) 9 hrs and (c) 12 hrs. The copolymer contains 210 ppm lithium residual impurity.

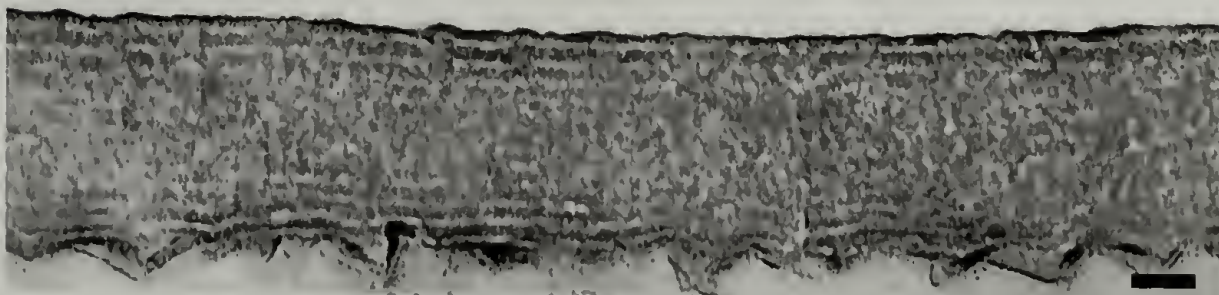
a



b



c



From the set of images in Figure 4, the parallel to perpendicular transition process is not a global coordination, but rather a local movement of polymer chains. For those microdomains in the center of the film, away from solid interfaces, it is easier for the electric field to enhance fluctuations. Thus, the reorientation is a faster process and only a minimum field strength is needed. However, for those adjacent to the interfaces, the fluctuations are suppressed and

consequently, the reorientation requires a much stronger driving force and is a much slower process. Having lithium ions changes the driving force from dielectric constant contrast to much stronger driving forces, dipole-field interactions. Thus, the applied electric field is able to enhance fluctuations at the interfaces of the microdomains with a wavelength comparable to L_0 and induce the transition from a parallel to a perpendicular orientation.

Two cases for the effect of lithium ions on the lamellar microdomain orientation under an electric field were presented. With very little to no lithium ions, the applied electric field ($\sim 40\text{V}/\mu\text{m}$) is not sufficient to reorient lamellar microdomains adjacent to the copolymer/substrate interface and only mixed orientation could be observed. With 210 ppm of lithium impurities, the electric field was able to reorient the parallel lamellar microdomains to achieve complete alignment. However, the limit in the concentration of lithium ions to achieve complete alignment was not determined. The interactions between ionic impurities and polymer chains need a more careful characterization. Our preliminary experimental results show that by adding LiCl salt back to the diblock copolymer after lithium ion extraction, the effect shown here could not be achieved.

The mechanism presented here should be applicable to other copolymer systems and opens a new route for controlling microdomain orientation in thin films by applying an electric field. Especially, for those copolymer systems where two blocks have little or no dielectric constant difference, electric field alignment may not occur based on a dielectric mechanism. The presence of

charged impurities in one block may be an effective and simple method to introduce electric field alignment.

Conclusions

The effect of ionic impurities on the electric field alignment of lamellar microdomains of polystyrene-*block*-poly(methyl methacrylate) (PS-*b*-PMMA) films was studied using TEM and AFM. At lithium ion concentration less than 1 ppm, a mixture of lamellar microdomain orientations was found if the preferential interfacial interactions exist between one block with the substrate. At the copolymer/substrate interface, lamellar microdomains were oriented parallel to the surface and the electric field showed no effect. At lithium ion concentrations greater than ~210 ppm, the microdomain morphology in block copolymers could be aligned in the direction of an applied electric field regardless of the strength of interfacial interactions. Complete alignment of the copolymer microdomains, even those adjacent to the polymer/substrate interface, occurred by a pathway where the applied electric field enhanced fluctuations at the interfaces of the microdomains with a wavelength comparable to L_0 , the equilibrium period of the copolymer. The enhancement in the fluctuations led to a disruption of the microdomains into smaller microdomains $\sim L_0$ in size that, with time, reconnected to forming microdomains oriented in the direction of the applied field.

References

- (1) Park, M.; Harrison, C.; Chaikin, P. M.; Register, R. A.; Adamson, D. *Science* **1997**, 276, 1401.
- (2) Huang, E.; Rockford, L.; Russell, T. P.; Hawker, C. J. *Nature* **1998**, 395, 757.
- (3) Amundson, K.; Helfand, E.; Davis, D. D.; Quan, X.; Patel, S. S.; Smith, S. D. *Macromolecules* **1991**, 24, 6546.
- (4) Amundson, K.; Helfand, E.; Quan, X.; Smith, S. D. *Macromolecules* **1993**, 26, 2698.
- (5) Amundson, K.; Helfand, E.; Quan, X. N.; Hudson, S. D.; Smith, S. D. *Macromolecules* **1994**, 27, 6559.
- (6) Boker, A.; Knoll, A.; Elbs, H.; Abetz, V.; Muller, A. H. E.; Krausch, G. *Macromolecules* **2002**, 35, 1319.
- (7) Morkved, T. L.; Lu, M.; Urbas, A. M.; Ehrichs, E. E.; Jaeger, H. M.; Mansky, P.; Russell, T. P. *Science* **1996**, 273, 931.
- (8) Thurn-Albrecht, T.; Schotter, J.; Kastle, C. A.; Emley, N.; Shibauchi, T.; Krusin-Elbaum, L.; Guarini, K.; Black, C. T.; Tuominen, M. T.; Russell, T. P. *Science* **2000**, 290, 2126.
- (9) Anastasiadis, S. H.; Russell, T. P.; Satija, S. K.; Majkrzak, C. F. *Physical Review Letters* **1989**, 62, 1852.
- (10) Fredrickson, G. H. *Macromolecules* **1987**, 20, 2535.
- (11) Xu, T.; Hawker, C. J.; Russell, T. P. **2003**, in preparation.
- (12) Xu, T.; Hawker, C. J.; Russell, T. P. *Macromolecules* **2003**, 36, 6178.
- (13) Xu, T.; Russell, T. P. **2003**, in preparation.
- (14) Tsori, Y.; Tournilhac, F.; Andelman, D.; Leibler, L. *Physical Review Letters* **2003**, 90, 145504.
- (15) Lin, Z. Q.; Kerle, T.; Baker, S. M.; Hoagland, D. A.; Schaffer, E.; Steiner, U.; Russell, T. P. *J Chem Phys* **2001**, 114, 2377.
- (16) Schafer, E.; Thurn-Albrecht, T.; Russell, T. P.; Steiner, U. *Europhys Lett* **2001**, 53, 518.

- (17) Mansky, P.; Liu, Y.; Huang, E.; Russell, T. P.; Hawker, C. *Science* **1997**, 275, 1458.
- (18) Hawker, C. J. *Macromolecules* **1996**, 29, 2686.
- (19) Xu, T.; Zhu, Y.; Gido, S. P.; Russell, T. P. *Macromolecules* **2003**, accepted.
- (20) Schaffer, E.; Thurn-Albrecht, T.; Russell, T. P.; Steiner, U. *Nature* **2000**, 403, 874.
- (21) Kyrylyuk, A. V.; Sevink, G. J. A.; Zvelindovsky, A. V.; Fraaije, J. G. E. M. *Macromol Theor Simul* **2003**, 12, 508.
- (22) Fukuda, J.; Onuki, A. *J Phys II* **1995**, 5, 1107.

CHAPTER 5

ELECTRIC FIELD ALIGNMENT OF ASYMMETRIC DIBLOCK COPOLYMER THIN FILMS

Introduction

Block copolymer thin films have significant potential for use as templates and scaffolds for the fabrication of arrays of nanometer-scale structures.¹⁻³ The microdomains are typically oriented parallel to the surface due to the preferential wetting of one block with the surface.^{4,5} Electric fields are an effective means to align microdomains, as shown experimentally and theoretically.^{3,6-15} For example, cylindrical microdomains in thin films of diblock copolymer polystyrene-*b*-poly(methyl methacrylate) can be oriented normal to the substrate using an electric field.^{3,13} Nanoporous films can be made subsequently by the selective removal of cylindrical component.¹⁶ The pore size can be easily tuned by varying molecular weight of the copolymer.¹⁷

Electric field alignment of lamellar and cylindrical microdomains in diblock copolymers has been studied in both the bulk and in thin films.^{3,6-15,18-24} Amundson suggested that, starting from a disordered state, the final oriented morphology was obtained by a simultaneous orientation and ordering of the lamellar microdomains, whereas, starting from randomly oriented lamellar microdomains, alignment would occur by movement of "grain boundaries" such that regions of favorable orientation grow at the expense of others.^{7,8} Krausch *et al.* and Zvelindovsky *et al.* found that with ordered lamellar microdomains in concentrated copolymer solutions, whether the orientation occurs through grain boundary migration or grain rotation is determined by the magnitude of the

interactions between two blocks.^{10,11} Thurn-Albrecht *et al.* followed the alignment process of cylindrical microdomains using *in-situ* small-angle x-ray scattering and found that the pathway depended upon the initial state.²⁰ From the disordered melt, the applied field biased concentration fluctuations that serve to template the formation of an oriented microphase-separated morphology. They assumed that the orientation of the copolymer obtained after spin-coating would occur by a similar route. For a copolymer having ordered microdomains normal to the field direction, the applied field leads to an instability that enables the large grains in the initial copolymer to be broken up into smaller sections. However, the wavelength of this instability was not determined.^{14,18} Recently, our transmission electron microscopy study on electric field alignment of lamellar microdomain in thin films showed that the applied electric field enhanced fluctuations at the interfaces of the microdomains with a wavelength comparable to L_0 , the equilibrium period of the copolymer. The enhancement in the fluctuations led to a disruption of the microdomains into microdomains $\sim L_0$ in size that, with time, reconnected to form microdomains oriented in the direction of the applied field.²⁴

Most of these studies were performed with films that were at least ~ 20 - $50\mu\text{m}$ thick using scattering techniques.^{6-8,10,13,20} For many applications, copolymer thin films having cylindrical microdomains with thickness less than $1\mu\text{m}$ are desirable. Interfacial interactions become increasingly more important with decreasing thickness and grain rotation is precluded due to the film thickness. Combining electron microscopy with scattering techniques,

information in both reciprocal space and real space could be attained to address the alignment process thoroughly. In particular, the length scale of the fluctuations, the effect of interfacial interactions and the formation of defects could be studied. Fully understanding the alignment process of these thin films with different initial states is key for success in generating nanoporous films with a desired orientation.

In the present study, electric field alignment of cylindrical microdomains in diblock copolymer thin films (~500 nm) of polystyrene-block-poly(methyl methacrylate) was studied using small angle neutron scattering (SANS) and transmission electron microscopy (TEM). Starting from a poorly ordered state (as cast), in the early stage, interfacial interactions induced a parallel orientation of the microdomains in the vicinity of the copolymer/substrate interfaces and the applied electric field biased the orientation of the cylindrical microdomain in the center of the film. With further annealing, the cylinders are locally disrupted to form, most likely, ellipsoidal microdomains that, with time, connect into cylindrical microdomains in the field direction. Starting from an ordered state with cylinders parallel to the surface, electric field enhanced fluctuations at the interfaces of the microdomains with a wavelength comparable to L_0 , the center to center distance of the cylindrical microdomains. The enhancement in the fluctuations led to a disruption of cylindrical microdomains and formation of spherical microdomains. This electric field induced sphere to cylinder transition is similar to the thermoreversible cylinder to sphere order-order transition. With time, the spheres deformed into ellipsoids and reconnected to form cylindrical

microdomains oriented at $\sim 45^\circ$ with respect to the applied field. Further annealing aligned the cylinders along the applied field direction. This reorientation process is much slower than that from poorly ordered state.

Experimental

Materials

Asymmetric diblock copolymers of polystyrene and poly(methyl methacrylate), PS-*b*-PMMA, with a number-average molecular weight of 1.2×10^5 g/mol (120K) and a PS volume fraction of 0.72 with a polydispersity of 1.05 were synthesized anionically. SANS studies were performed with PS-*b*-PMMA where the polystyrene block was deuterated, denoted as dPS-*b*-PMMA. The molecular weight of dPS-*b*-PMMA was 4.7×10^4 g/mol (47K) with a polydispersity of 1.04 and a dPS volume fraction of 0.7. The center to center distance, $D = 4\pi / \sqrt{3}q_{10}$, between cylindrical microdomains of dPS-*b*-PMMA (47K) is ~ 32 nm, corresponding to a scattering vector $q_{10} = 0.22 \text{ nm}^{-1}$. Here $q_{10} = 4\pi / \lambda \sin \theta$, where λ is the neutron wavelength and 2θ is the scattering angle. Films (~ 500 nm– 700 nm) were prepared by spin coating a toluene solution of the copolymer onto a silicon substrate. The silicon substrate was modified with a random copolymer of styrene and methyl methacrylate having a 0.7 volume fraction of styrene. The modified substrate has a lower interfacial interaction with PS than that of PMMA ($\gamma_{\text{PMMA}/\text{sub}} - \gamma_{\text{PS}/\text{sub}} \approx 0.45 \text{ dyne/cm}$).^{25,26} The copolymer thin films were annealed at 170°C for 72 hrs under vacuum.

Sample Preparation

For the electric field experiments, an aluminized Kapton film was used as the upper electrode, where a thin (20-25 μm) layer of crosslinked polydimethylsiloxane (PDMS) (SylgardTM) was used as a buffer layer between the Kapton electrode and the copolymer thin film. Preparation of the crosslinked PDMS layer has been described previously.²³ Thin films of dPS-*b*-PMMA (47K) were annealed at 170 $^{\circ}\text{C}$ under $\sim 40\text{V}/\mu\text{m}$ for a predetermined time and quenched to room temperature while the electric field was on. A small portion of the sample was removed for TEM studies. After the SANS measurements, the sample was put back to an oven preheated to 170 $^{\circ}\text{C}$ under the applied electric field. Transmission SANS experiments were performed on beam-line NG-3, a 30 meter SANS instrument at the National Institute of Standard and Technology (NIST), using neutrons with a wavelength $\lambda = 0.6 \text{ nm}$ and $\Delta\lambda/\lambda = 15\%$. The exposure time for each frame was 15 minutes. For TEM, a thin layer of carbon (10-20 nm) was coated onto the surface before the film was embedded in epoxy and cured at 60 $^{\circ}\text{C}$ for 12 hrs. The film was removed from the substrate by dipping into liquid N₂, microtomed at room temperature using a diamond knife and transferred to a copper grid. The cutting angle was $90 \pm 2^{\circ}$ with respect to the substrate (parallel to the electric field direction) as confirmed by optical microscopy. The thin sections were exposed to ruthenium tetroxide vapor for 15-20 min to enhance the contrast. Electron microscopy experiments were performed on a JEOL 200KV TEM with an accelerating voltage of 200KV.

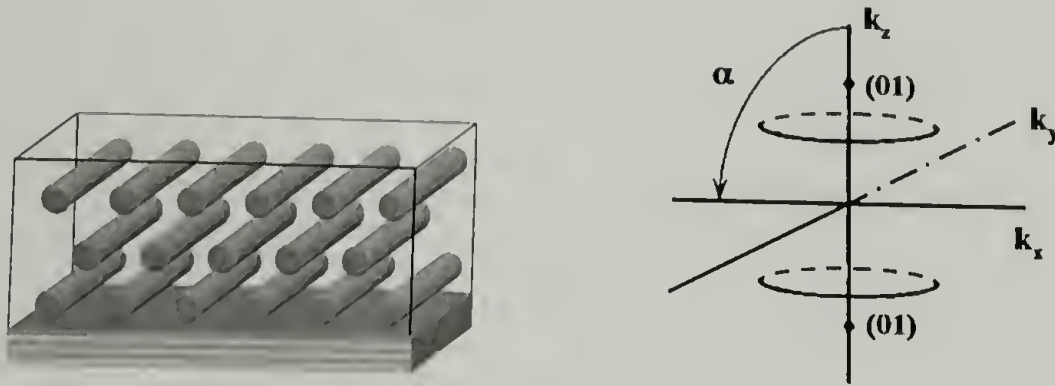
Results and Discussion

Shown in Figure 5.1a is a schematic diagram of hexagonally packed cylinders oriented parallel to the surface in real and reciprocal space,

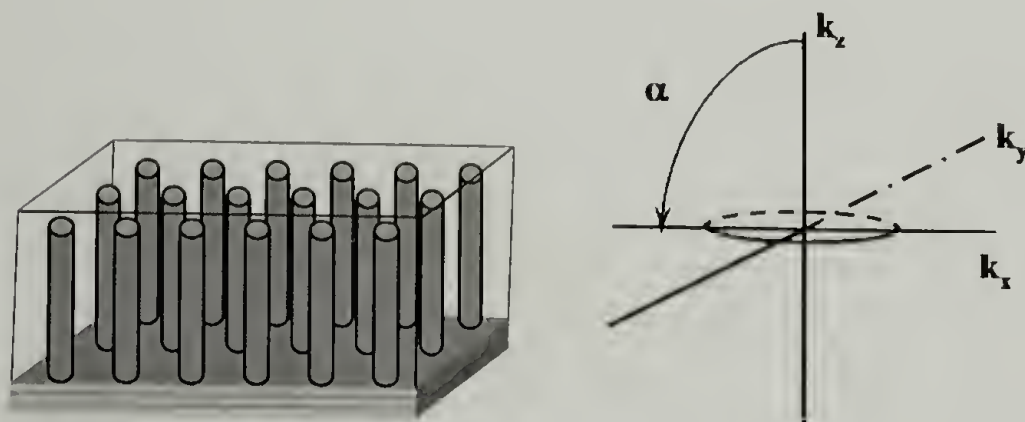
respectively.^{13,20} The rings result from many grains of cylindrical microdomains oriented randomly in the plane of the film.

Figure 5.1 Schematic diagram of hexagonally packed cylinders (a) parallel and (b) perpendicular to the surface in the real and reciprocal space. (c) The geometry of SANS measurement.

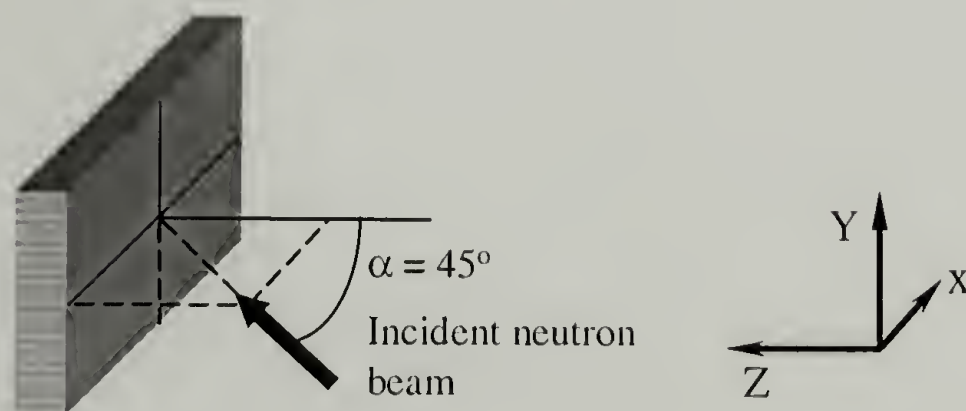
a



b



c



By varying the incidence angle (α) of the neutron beam, defined with respect to the substrate normal as $\alpha = 0$, different points on the two diffraction

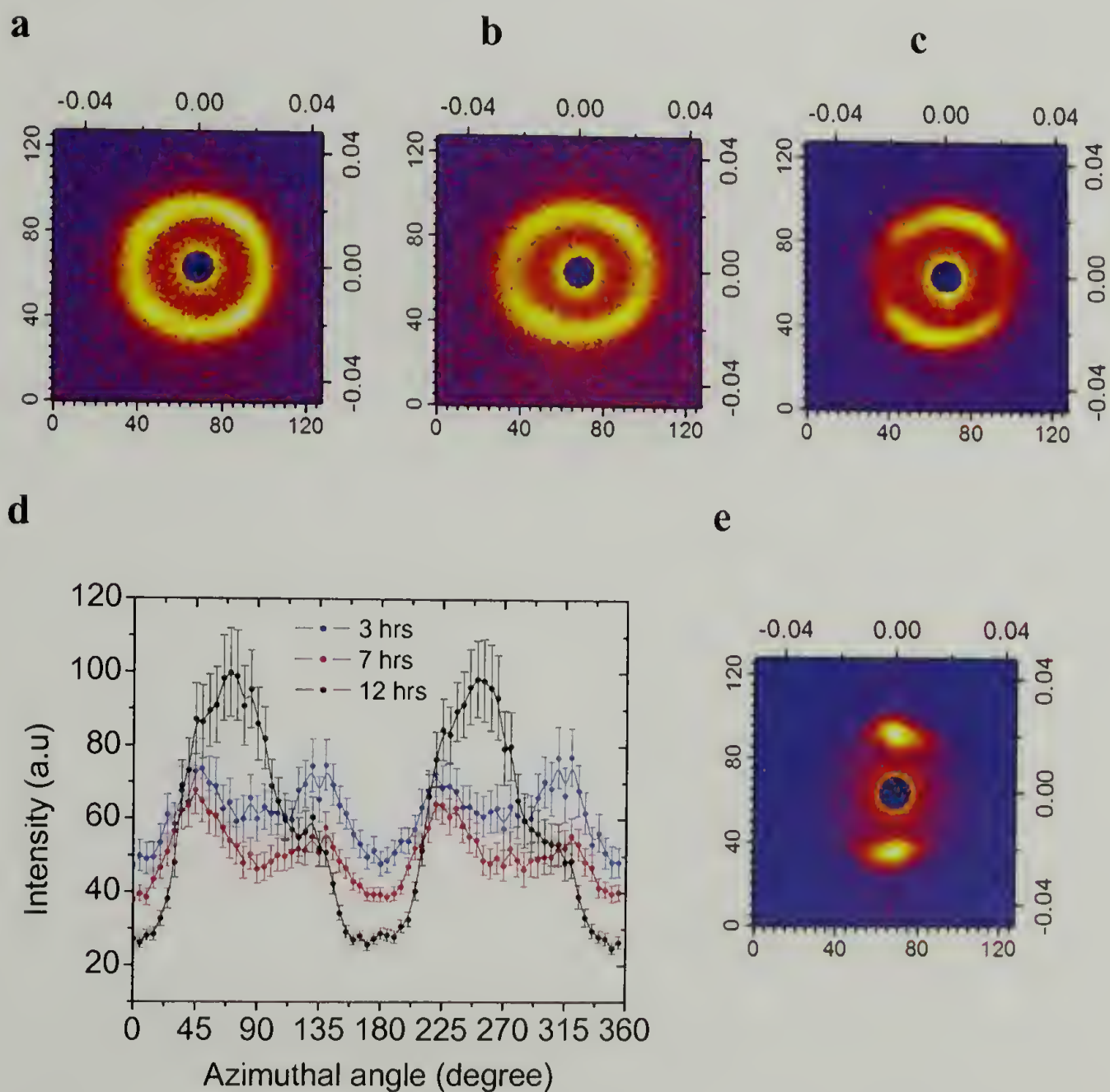
rings are observed. If the cylinders are oriented normal to the surface as shown in Figure 5.1b, the characteristic reflections appear in the K_x, K_y plane. Since there are different grains of the hexagonally-packed cylinders in the plane of the film, a ring of scattering is seen for $\alpha = 0^\circ$. For any other incidence angle, two arcs (or spots) on the axis of rotation (here the vertical axis) are seen. For an isotropic sample, the scattering pattern consists of a homogeneous ring independent of the incidence angle. All the measurements shown here were taken at $\alpha = 45^\circ$ using the geometry shown in Figure 5.1c. With this setup, a four-point scattering pattern with reflections at $45^\circ, 135^\circ, 225^\circ$ and 315° indicates oriented cylinders parallel to the surface, and a two-spot pattern in the vertical direction indicates cylinders normal to the surface.

The alignment process was studied using a ~ 500 nm as-cast dPS-*b*-PMMA (47K) film that was annealed at 170°C under $\sim 40\text{V}/\mu\text{m}$ electric field for different times. The film was dried to remove residual solvent with the initial state being kinetically trapped and poorly ordered. Figure 5.2a-c shows the 2-D SANS patterns of the film annealed at 170°C under $\sim 40\text{V}/\mu\text{m}$ electric field for 3, 7, 14 hrs, respectively. The modified substrate has a lower interfacial interaction with PS than that of PMMA. The SANS pattern shown in Figure 5.2a is after the sample was annealed under electric field for 3 hrs. Overall, a ring pattern was seen indicating that the cylindrical microdomains were randomly oriented. The integrated peak intensity as a function of azimuthal angle in Figure 5.3 shows higher scattering intensities at $\sim 45^\circ, 90^\circ, 135^\circ, 225^\circ, 270^\circ$, and 315° . The scattering pattern was a superposition of a ring, a two-spot pattern indicating

microdomains normal to the surface, and a four-spot pattern indicating cylindrical microdomains parallel to the surface. The two-spot pattern originated from the fact the biasing of the concentration fluctuations by the applied field in the center of the film as shown by Thurn-Albrecht *et al.*²⁰ The copolymers near the interface were strongly biased by the interface and thus, microphase separated with a parallel orientation initially, which contributed to the four-spot pattern in SANS.²⁷ Thus, similar to that of symmetric diblock copolymer thin films, the alignment process is a competition between two fields: a surface field and an electric field where the surface field showed a dominant effect at the early stages of the alignment process in thin films.^{23,24} In the absence of an electric field, a parallel microdomain orientation was found. Here, with the applied field, cylindrical microdomains were slowly aligned along the field direction as shown in Figure 5.2b, c. The intensity visible in Figure 5.2b is lower than the intensity in Figure 5.2a. This is because only some of the grains of the microdomains contributed to the scattering intensity at a fixed incidence angle. However, the degree of orientation in Figure 5.2c is much lower than that usually obtained and may be due to the sample preparation.^{3,13} Figure 5.2a-c were obtained from one sample by annealing the sample for a predetermined time. After SANS measurements, the sample was put back into an oven preheated to 170°C with an applied electric field. Due to the difference in thermal expansion coefficients between crosslinked PDMS and Kapton film, there were always air bubbles between the top electrodes and film surface in the first 5-10 minutes. The presence of air bubbles effectively reduced the electric field strength

dramatically. With no or low electric field, the surface field oriented the cylindrical microdomains parallel to the surface. Orienting these microdomains in the applied field direction was a much slower process, as discussed below, reducing the degree of orientation. Figure 5.2d shows a 2-D SANS pattern of another ~ 500 nm film after annealing at 170°C under a $\sim 40\text{V}/\mu\text{m}$ electric field for 16 hrs. A high degree of orientation is clearly seen.

Figure 5.2. 2-D SANS patterns of a ~ 500 nm dPS-*b*-PMMA (47K) film annealed at 170°C under a $\sim 40\text{V}/\mu\text{m}$ electric field for (a) 3, (b) 7, (c) 14 hrs. (d) The integrated peak intensity as a function of azimuthal angle of SANS patterns in a, b and c. (e) 2-D SANS pattern of another dPS-*b*-PMMA (47K) film annealed at 170°C under a $\sim 40\text{V}/\mu\text{m}$ electric field for 16 hrs.



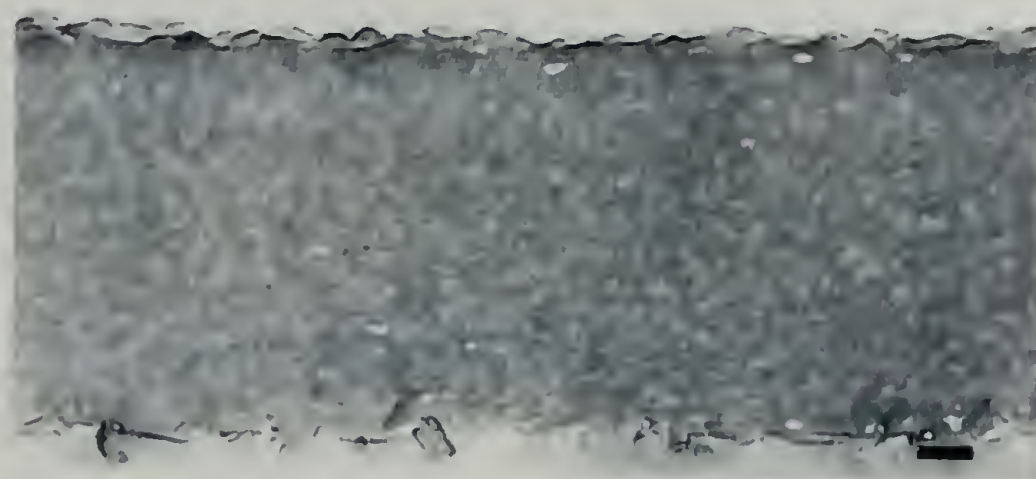
Shown in Figure 5.3b-d are a set of cross-sectional TEM images of ~700 nm PS-*b*-PMMA (120K) films after annealing at $185\pm 5^\circ\text{C}$ under $\sim 40\text{V}/\mu\text{m}$ electric field for 9, 12, 16 hrs, respectively. The samples were identical except for the annealing time under the applied electric field. Cross-sections were microtomed at $90\pm 2^\circ$ with respect to the substrate as shown in Figure 5.4a. After annealing under an electric field for 9 hrs, cylindrical microdomains were seen with mainly random orientations. Particularly, cylindrical microdomains adjacent to copolymer/substrate interfaces were not parallel even with the lower interfacial interactions between PS blocks with the modified substrate. This is clearly different from symmetric diblock copolymer thin films where under the same treatment, the lamellae were oriented parallel to the surface first and only mixed orientations could be achieved if the interfacial interactions were not balanced. This can be ascribed to the free energy barrier related to a surface induced cylinder to lamellar transition and the stretching and compression of polymer chains to pack the cylinders onto a flat surface.^{28,29} After annealing under electric field for 12 hrs, ellipsoidal-shaped objects were seen with long axis oriented along the field direction throughout of the image shown in Figure 5.4c. TEM images reflect the projection of microdomains with different orientations and there are always different possibilities to give the same image. The TEM image shown here can be explained with either a fraction of cylinders normal to the surface tilted out of the imaging plane or ellipsoidal-shaped microdomains. Projections of the tilted cylinders will give ellipsoids of different lengths for different angles.

Figure 5.3. (a) Schematic diagram of TEM sample preparation. Cross-sectional TEM images of ~ 700 nm PS-*b*-PMMA (120K) films after annealing at $185 \pm 5^\circ\text{C}$ under a $\sim 40\text{V}/\mu\text{m}$ electric field for (b) 9, (c) 12, (d) 16 hrs. Scale bar: 100nm.

a



b



c



d



At one cutting angle, a TEM image may show ellipsoids with different aspect ratios due to different grain orientations. Here, images similar to Figure 5.4c were seen across hundreds of micrometers with a uniform aspect ratio of the ellipsoids. These TEM images most likely show the ellipsoidal shape microdomains. Further annealing (16hrs) leads to cylinders aligned along the field direction throughout the film as shown in Figure 5.3c.

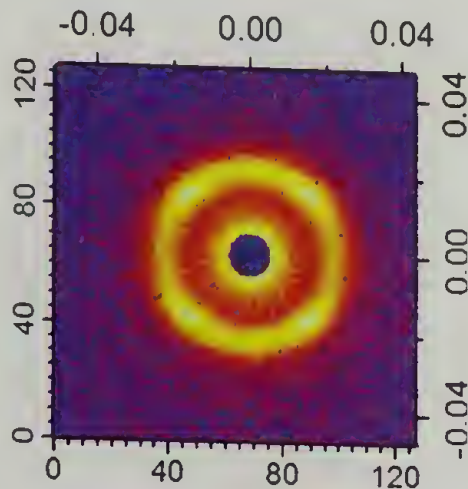
Starting from a poorly ordered state, copolymers form cylindrical microdomains with the orientations biased initially by the surface field and electric field. With time, the electric field breaks the cylindrical microdomains into ellipsoids with a size comparable to the equilibrium period that connect to form cylinders along the electric field direction. The cylindrical microdomains do not align parallel to the surface in the early stage due to the free energy associated with packing curved objects onto a flat substrate. Consequently, complete alignment of cylindrical microdomains along the field direction could be achieved even when the interfacial interactions are not balanced. The electric field alignment process in thin films occurs by the local arrangement of the cylindrical microdomains and is much slower compared with those in thick or bulk samples.

Figure 5.4a shows the SANS pattern of a ~500 nm dPS-*b*-PMMA (47K) film annealed at 170°C for 72 hrs. Previous studies showed that the propagation of the lamellar parallel orientation depends on the strength of the surface field. For a finite surface field, there is a certain distance beyond which the parallel

orientation gets lost and the microdomain orientation randomizes. This is the case for cylindrical microdomains too.³⁰

Figure 5.4. (a) 2-D SANS pattern and (b) cross-sectional TEM image of a ~500nm dPS-*b*-PMMA (47K) film annealed at 170°C under vacuum for 72 hrs.

a



b

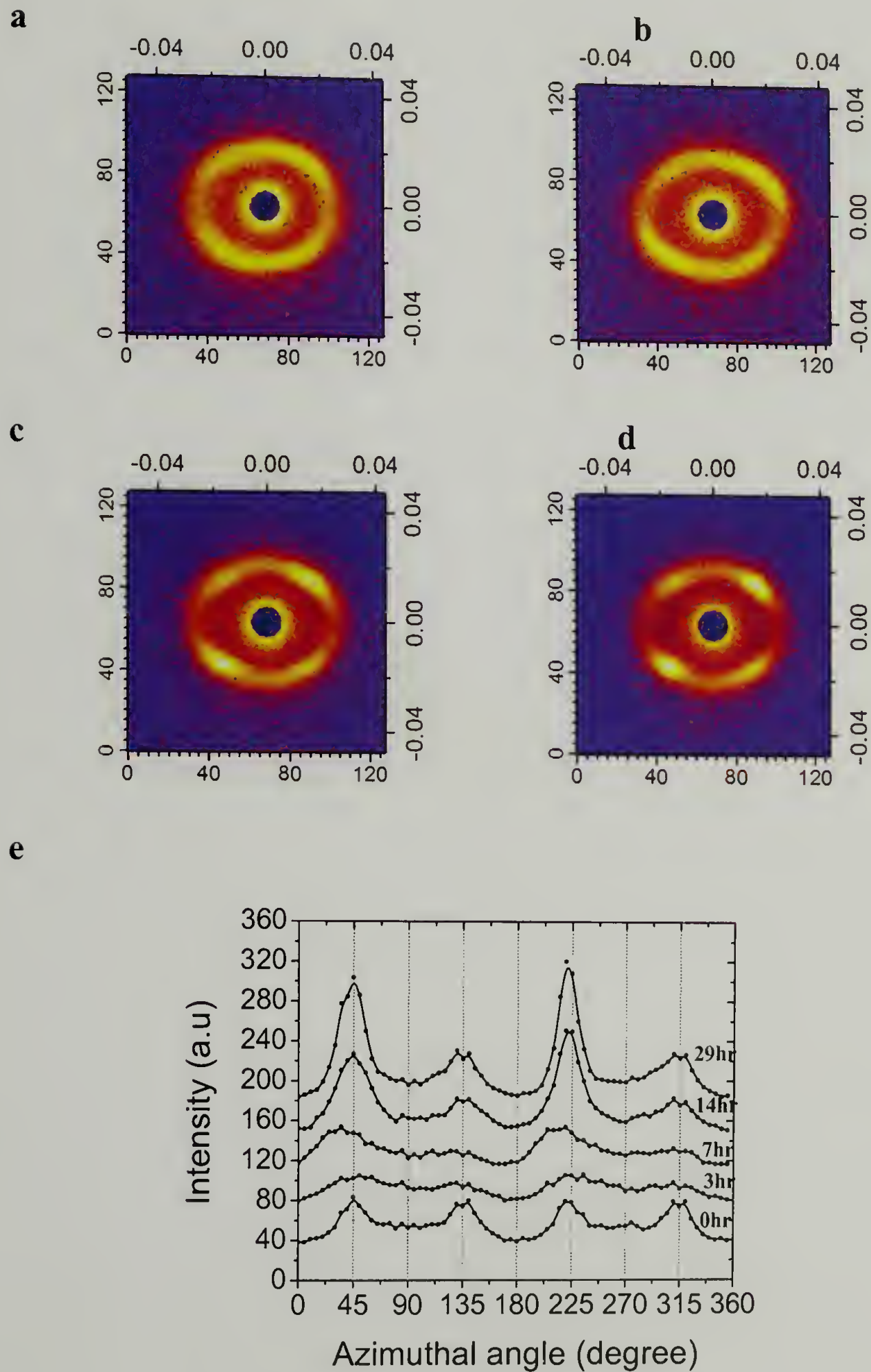


In Figure 5.4a, the four-spot scattering pattern indicates that the cylindrical microdomains were mainly oriented parallel to the surface. The parallel orientation was not perfect and there were also cylindrical microdomains with random orientations giving rise to the ring pattern. This was confirmed by the cross-sectional TEM image shown in Figure 5.4b. The cylindrical microdomains were parallel to the surface at the copolymer/substrate interface and were randomly oriented in the center of the film. Projections of cylinders

with different orientations were seen in one image and the in-plane grain size of the parallel cylinders was small.

Figure 5.5a is the SANS pattern after annealing the films in Figure 5.4a under an electric field ($\sim 40\text{V}/\mu\text{m}$) for 3 hrs. The four-spot scattering pattern can still be seen. However, the shape of the spots has changed dramatically. The streaking of the spots can be explained by deformation of the cylindrical microdomains in the direction of the applied electric field, i.e. the cylindrical microdomains are deformed by the applied electric field. The integrated peak intensity as a function of azimuthal angle is plotted in Figure 5.5e. The plots were shifted for clarity. After annealing for 7 hrs under an applied electric field, the scattering intensity increased for the reflections at $\sim 38^\circ$ and $\sim 217^\circ$ with full width at half maximum (FWHM) of 33° as shown in Figure 5.5b. The reflection position shifted to $\sim 45^\circ$ and 222° (FWHM of $\sim 20^\circ$) and intensified with further annealing as shown in Figure 5.5c, d. Detailed information on the peak intensity and position can be seen in Figure 5.5e. After annealing under electric field for up to 29 hrs, the cylindrical microdomains have not been reoriented normal to the surface. Instead, the SANS pattern indicates that the cylindrical microdomains were mainly oriented at $\sim 45^\circ$ with respect to the electric field direction. Compared with the as cast films, the reorientation was a much slower process. However, the details on the alignment were not immediately evident from the SANS results.

Figure 5.5. 2-D SANS patterns of a pre-annealed dPS-*b*-PMMA (47K) film annealed under a $\sim 40\text{V}/\mu\text{m}$ electric field for (a) 3, (b) 7, (c) 14, (d) 29 hrs. (d) The integrated peak intensity as a function of azimuthal angle of SANS patterns in a, b, c and d. The plots were shifted 40 units with each other for clarity.



A detailed study on the reorientation of cylindrical microdomains parallel to the surface was performed using TEM. Figure 5.6a shows a cross-sectional TEM image after annealing the film under a $\sim 40\text{V}/\mu\text{m}$ electric field for 7 hrs (the same sample as that in Figure 5.5b). Compared to Figure 5.4b, the projections of parallel cylinders were no longer seen within the field of view and only spherical objects were seen. Considering the small grain size in Figure 5.4b, it is unlikely that the spherical objects were edge-on cylindrical microdomains. Instead, the electric field may enhance fluctuations at the interfaces of the cylindrical microdomains with a wavelength D , the center to center distance between cylindrical microdomains, and break the cylinders into spheres. The process of electric field induced cylinder-to-sphere transition is very similar to the thermoreversible order-order transition (OOT) that has been studied thoroughly.³¹⁻³⁹ There are striking similarities between Figure 5.6a with those TEM images of OOT shown by Lodge and Hashimoto.^{39,40} The (100) plane of hexagonally packed cylinders becomes the (110) plane of body centered cubic (BCC) packed spheres and the long axis of the cylinder is the $\langle 111 \rangle$ direction of BCC spheres that is parallel to the surface in diblock copolymer thin films. Figure 5.6a shows the projections of the distorted hexagonal array of the spherical microdomains.

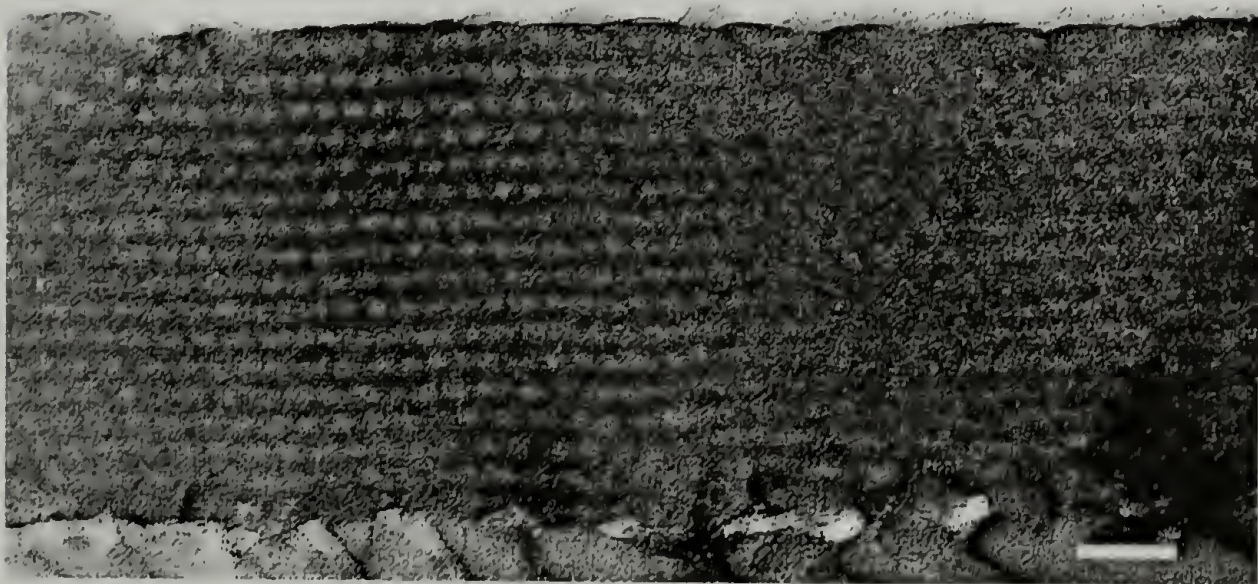
The intermediate state of spherical microdomains under an applied electric field was not stable and the spheres connected to form cylinders oriented along the electric field direction to lower the free energy as shown before.⁴¹

Figure 5.6. Cross-sectional TEM images of a ~ 500 nm pre-annealed dPS-*b*-PMMA (47K) thin film after annealing under a ~ 40 V/ μ m electric field for (a) 7, (c) 7, (d) 29 hrs. Scale bar: 100nm.

a



b



c



Figure 5.6b shows how spheres were connected. On the right side of the image, spheres with distorted hexagonal packing were clearly seen. In the center of the film, the spheres were deformed into ellipsoids and connected to each other at an angle of $\sim 45^\circ$ with respect to the applied field direction instead of along the field direction. This may explain the SANS observations in Figure 5.5 that the reflections at 45° and 222° intensified with further annealing under electric field. The copolymer morphologies having cylinders tilted at a 45° with respect to the field direction were not energetically favorable and cylinders will be reoriented along the field direction with further annealing under the applied electric field. Figure 5.6c captured a region that was undergoing this step after annealing under the electric field for 29 hrs. In the center of the film, the tilted cylinders were undergoing a transition from being tilted at 45° to the surface to being oriented normal to the surface. A superposition texture of cylinder at 45° and normal to the surface was seen. With further annealing, the cylindrical microdomains will be aligned along the field direction. However, this reorientation process is much slower and takes tens of hours. Adjacent to the copolymer/substrate interface, spherical microdomains that had not yet connected to form cylinders were still seen. The presence of the surface field suppresses the fluctuations and slowed the reorientation process.

Regarding the question of why the cylinders were tilted at 45° with respect to the field direction, instead of along the field direction, there are two possible reasons. First, the spheres need to be deformed into ellipsoids to connect with other spheres. The further apart the neighboring spheres are, the more the

spheres need to be deformed. The distance to reach another sphere along the field direction is $\sqrt{2} D$. The closest spheres ($\sqrt{3}/2 D$) are at $\sim 45^\circ$ with respect to the field direction. Deforming spheres further means more interfaces between two blocks and stretching or compressing polymer chains and, consequently, a higher energetic barrier. Though deforming spheres along the electric field direction is thermodynamically favored, it is much easier kinetically for spheres to connect with closest neighbors. Another possibility is the trace amount of ionic impurities such as lithium ions in the diblock copolymers from anionic copolymerization.²² If there are dissociated lithium ions, they may locate mainly in PMMA microdomains.^{22,42} When cylinders were broken into spheres, under electric field, there will be positive charges at one end and negative charges at the other end of the spherical microdomains, forming an effective dipole. Laterally, there will be attractive forces between two oppositely charged ends of the ellipsoids. This generates dipole-dipole interactions and thus another field parallel to the surface. Combined with the electric field normal to the surface, the overall field direction will be at an angle with respect to the electric field direction. Thus, the spheres are connected to form tilted cylinders. The experimental observations shown here are very possibly because of the combination of both.

Conclusions

Electric field alignment of cylindrical microdomains in diblock copolymer thin films (~ 500 nm) was studied using SANS and TEM. The alignment processes were followed with different initial states. Starting from a

poorly ordered state, the cylindrical microdomain orientations were biased by the surface field and the electric field and, in the early stage, the surface field dominated. With further annealing, the cylinders were locally disrupted to form ellipsoidal-shaped microdomains that, with time, connected into cylindrical microdomains in the field direction. Starting from an ordered state with cylinders parallel to the surface, the applied electric field enhanced fluctuations at the interfaces of the microdomains with a wavelength comparable to D , the center to center distance of the cylindrical microdomains. The enhancement of the fluctuations broke cylindrical microdomains into spherical microdomains. This electric field induced sphere to cylinder transition was similar to thermoreversible cylinder to sphere order-order transition. With time, the spheres deformed into ellipsoids and reconnected forming cylindrical microdomains oriented at $\sim 45^\circ$ with respect to the applied field direction. Further annealing aligned the tilted cylinders along the applied field direction. This reorientation process was much slower than that from poorly ordered state.

References

- (1) Huang, E.; Rockford, L.; Russell, T. P.; Hawker, C. J. *Nature* **1998**, *395*, 757.
- (2) Park, M.; Harrison, C.; Chaikin, P. M.; Register, R. A.; Adamson, D. *Science* **1997**, *276*, 1401.
- (3) Thurn-Albrecht, T.; Schotter, J.; Kastle, C. A.; Emley, N.; Shibauchi, T.; Krusin-Elbaum, L.; Guarini, K.; Black, C. T.; Tuominen, M. T.; Russell, T. P. *Science* **2000**, *290*, 2126.
- (4) Anastasiadis, S. H.; Russell, T. P.; Satija, S. K.; Majkrzak, C. F. *Physical Review Letters* **1989**, *62*, 1852.
- (5) Fredrickson, G. H. *Macromolecules* **1987**, *20*, 2535.
- (6) Amundson, K.; Helfand, E.; Davis, D. D.; Quan, X.; Patel, S. S.; Smith, S. D. *Macromolecules* **1991**, *24*, 6546.
- (7) Amundson, K.; Helfand, E.; Quan, X.; Smith, S. D. *Macromolecules* **1993**, *26*, 2698.
- (8) Amundson, K.; Helfand, E.; Quan, X. N.; Hudson, S. D.; Smith, S. D. *Macromolecules* **1994**, *27*, 6559.
- (9) Ashok, B.; Muthukumar, M.; Russell, T. P. *J Chem Phys* **2001**, *115*, 1559.
- (10) Boker, A.; Elbs, H.; Hansel, H.; Knoll, A.; Ludwigs, S.; Zettl, H.; Urban, V.; Abetz, V.; Muller, A. H. E.; Krausch, G. *Physical Review Letters* **2002**, *89*, 135502.
- (11) Kyrylyuk, A. V.; Sevink, G. J. A.; Zvelindovsky, A. V.; Fraaije, J. G. E. M. *Macromol Theor Simul* **2003**, *12*, 508.
- (12) Morkved, T. L.; Lu, M.; Urbas, A. M.; Ehrichs, E. E.; Jaeger, H. M.; Mansky, P.; Russell, T. P. *Science* **1996**, *273*, 931.
- (13) Thurn-Albrecht, T.; DeRouchey, J.; Russell, T. P.; Jaeger, H. M. *Macromolecules* **2000**, *33*, 3250.
- (14) Tsori, Y.; Andelman, D. *Macromolecules* **2002**, *35*, 5161.
- (15) Pereira, G. G.; Williams, D. R. M. *Macromolecules* **1999**, *32*, 8115.

- (16) Thurn-Albrecht, T.; Steiner, R.; DeRouchey, J.; Stafford, C. M.; Huang, E.; Bal, M.; Tuominen, M.; Hawker, C. J.; Russell, T. P. *Adv. Mater.* **2000**, *12*, 1138.
- (17) Xu, T.; Kim, H. C.; DeRouchey, J.; Seney, C.; Levesque, C.; Martin, P.; Stafford, C. M.; Russell, T. P. *Polymer* **2001**, *42*, 9091.
- (18) Fukuda, J.; Onuki, A. *J Phys II* **1995**, *5*, 1107.
- (19) Kyrylyuk, A. V.; Zvelindovsky, A. V.; Sevink, G. J. A.; Fraaije, J. G. E. M. *Macromolecules* **2002**, *35*, 1473.
- (20) Thurn-Albrecht, T.; DeRouchey, J.; Russell, T. P.; Kolb, R. *Macromolecules* **2002**, *35*, 8106.
- (21) Tsori, Y.; Tournilhac, F.; Leibler, L. *Macromolecules* **2003**, *36*, 5873.
- (22) Tsori, Y.; Tournilhac, F.; Andelman, D.; Leibler, L. *Physical Review Letters* **2003**, *90*, 145504.
- (23) Xu, T.; Hawker, C. J.; Russell, T. P. *Macromolecules* **2003**, *36*, 6178.
- (24) Xu, T.; Zhu, Y.; Gido, S. P.; Russell, T. P. *Macromolecules* **2004**, accepted.
- (25) Hawker, C. J. *Macromolecules* **1996**, *29*, 2686.
- (26) Mansky, P.; Liu, Y.; Huang, E.; Russell, T. P.; Hawker, C. *Science* **1997**, *275*, 1458.
- (27) Mansky, P.; Russell, T. P.; Hawker, C. J.; Mays, J.; Cook, D. C.; Satija, S. K. *Physical Review Letters* **1997**, *79*, 237.
- (28) Suh, K. Y.; Lee, H. H. *Journal of Polymer Science: Part B: Polymer Physics* **2001**, *39*, 2217.
- (29) Karim, A.; Singh, N.; Sikka, M.; Bates, F. S. *J Chem Phys* **1994**, *100*, 1620.
- (30) Xu, T.; Hawker, C. J.; Russell, T. P. **2004**, in preparation.
- (31) Silva, A. S.; Mitchell, C. A.; Tse, M. F.; Wang, H. C.; Krishnamoorti, R. *Journal of Chemical Physics* **2001**, *115*, 7166.
- (32) Sakurai, S.; Hashimoto, T.; Fetters, L. J. *Macromolecules* **1996**, *29*, 740.
- (33) Ryu, C. Y.; Vigild, M. E.; Lodge, T. P. *Physical Review Letters* **1998**, *81*, 5354.

- (34) Matsen, M. W. *Journal of Chemical Physics* **2001**, *114*, 8165.
- (35) Leibler, L. *Macromolecules* **1980**, *13*, 1602.
- (36) Kimishima, K.; Koga, T.; Hashimoto, T. *Macromolecules* **2000**, *33*, 968.
- (37) Krishnamoorti, R.; Modi, M. A.; Tse, M. F.; Wang, H. C. *Macromolecules* **2000**, *33*, 3810.
- (38) Krishnamoorti, R.; Silva, A. S.; Modi, M. A.; Hammouda, B. *Macromolecules* **2000**, *33*, 3803.
- (39) Ryu, C. Y.; Lodge, T. P. *Macromolecules* **1999**, *32*, 7190.
- (40) Sota, N.; Sakamoto, N.; Saijo, K.; Hashimoto, T. *Macromolecules* **2003**, *36(12)*, 4534.
- (41) Xu, T.; Russell, T. P. **2004**, in preparation.
- (42) Kim, C. S.; Oh, S. M. *Electrochim. Acta* **2000**, *45*, 2101.

CHAPTER 6

ELECTRIC FIELD INDUCED SPHERE TO CYLINDER TRANSITION IN DIBLOCK COPOLYMER THIN FILMS

Introduction

Diblock copolymers are composed of chemically different polymers covalently coupled at one end that microphase separate into morphologies ranging from spheres to cylinders to lamellae (and other morphologies) depending on the volume fraction of the each block.^{1,2} The Flory-Huggins interaction parameter, χ , which characterizes the interactions between segments in each block, is inversely proportional to the temperature. By increasing temperature, χN decreases and transitions between different morphologies, called order-to-order transitions (OOT), are possible. Thermoreversible order-order transitions in the weak segregation limit were theoretically predicted years ago.³ Experimentally, different transitions, such as cylinder to gyroid and sphere to cylinder have been reported in bulk copolymer systems.⁴⁻¹² For example, Sakurai *et al.* reported the thermoreversible OOT between spheres in a body-centered cubic lattice to hexagonal cylinders for a polystyrene-*b*-polyisoprene diblock copolymer. The cylinders were transformed into a series of spheres, where the axes of the cylinders defined the direction of the bcc-spheres upon heating. The spheres deformed and interconnected to cylinders upon cooling.¹⁰

Electric fields have been shown as an effective method of controlling copolymer microdomains orientations.¹³⁻¹⁷ Experimental results and theoretical calculations show that the electric field enhances fluctuations along the interface between two blocks due to the difference in dielectric constants of the

microdomains and aligns the microdomains in the direction of the applied field to lower the free energy.¹⁸⁻²⁰ Numerous studies have described the mechanism by which the electric field reorients the anisotropic microdomains.²¹⁻²⁵ However, it should also be possible to induce an order-to-order transition, such as the sphere to cylinder transition, with an applied field.

Landau showed that a spherical dielectric can be deformed into ellipsoids under the influence of an applied electric field.²⁶ Recently, Tsori *et al* suggested that the presence of dissociated ions in block copolymers, as opposed to simply differences in the dielectric constants, can be used to induce morphological changes under an electric fields and lead to phase transitions.²⁷ In both cases, under sufficiently high electric fields, it should be possible to deform spherical microdomains into ellipsoids and, for the block copolymer thin films with multiple layers of spheres, the ellipsoids can be sufficiently stretched such that they interconnect to form cylinders that penetrate through the film. Taking the volume conservation into account, the diameters of the cylinders will be smaller than those of the spherical microdomains. Such a transition may offer a simple route to generate cylinders with high aspect ratios from symmetric spherical microdomains. As shown by Kramer and Register *et al.*, it is possible to generate thin films with exceptional long-range order using block copolymers with spherical microdomains. Thus, by using a sphere to cylinder transition, a simple route in achieving highly ordered arrays of nanoscopic cylindrical domains having large aspect ratio may be possible.^{28,29}

Experimental

Materials

Diblock copolymers polystyrene-*b*-poly(methyl methacrylate), denoted as PS-*b*-PMMA, was prepared by anionic synthesis having a molecular weight of 151,000 g/mol, a polydispersity of 1.06, and a PS volume fraction of 0.9, as measured by H^1 NMR. In the bulk, the diblock copolymer microphase separates into spherical microdomains of PMMA in a PS matrix. The copolymers were precipitated in methanol and the elemental concentration of residual lithium impurities from the initiator was less than 1 ppm (Measured by Quantitative Technologies, Inc) with 1 ppm resolution.³⁰

Sample Preparation

Smooth ~400 nm thick films of PS-*b*-PMMA were prepared by spin coating 6% (w/v) solutions of the copolymer in toluene onto the modified Si substrate. The silicon wafer was modified by anchoring a hydroxyl-terminated random copolymer of styrene and methyl methacrylate with a styrene fraction of 0.58 as described previously. Interactions between the PS and PMMA blocks with this modified surface are balanced.³¹ An aluminized Kapton film comprised the top electrode. A thin layer (20-25 μ m) of crosslinked PDMS (SylgardTM) was used as a buffer layer between the Kapton electrode and the copolymer thin film to ensure physical contact between the electrode and copolymer films. The copolymer films were heated to 170°C under N₂ with an applied electric field of ~40V/ μ m for 20hrs, and then quenched to room temperature before removing the electric field. For transmission electron microscopy, the samples were embedded

in epoxy, peeled off the substrate by dipping into liquid N₂, microtomed with a diamond knife at room temperature onto a water surface and retrieved with a copper grid. The thin sections were exposed to ruthenium tetroxide for 15 min to enhance the contrast. Electron microscopy experiments were performed on a JEOL 200KV TEM at an accelerating voltage of 200KV. Tapping mode AFM was performed with a Dimension 3100, Nanoscope III from Digital Instruments Corp. Grazing incidence small angle x-ray scattering (GISAXS) was performed at the National Synchrotron Light Source, (NSLS, Brookhaven National Laboratory), using x-rays with a wavelength of 1.567Å. The exposure times were 30 seconds per sample.

Results and Discussion

To confirm the copolymer thin films formed spherical microdomains, a ~50nm film was spin coated onto a silicon wafer having a native silicon oxide layer and annealed at 170°C under vacuum for 48hrs. The film was then exposed to UV and rinsed with acetic acid to selectively remove the PMMA block.¹⁷ Figure 6.1a shows the in-plane view AFM phase image. Spherical domains with liquid-like packing can be seen due to the comparable surface tension of PS and PMMA and film thickness constraint.³² The diameter of the PMMA microdomains is ~22nm with a center to center distance ~41nm. The surface of films thicker than several equilibrium periods was covered by the PS blocks, the lower surface energy component, and showed no structure.

Figure 6.1(a) AFM phase image of a $\sim 50\text{nm}$ PS-*b*-PMMA film annealed 48hrs at 170°C under vacuum, then exposed to UV and rinsed with acetic acid. Image size: $1 \times 1 \mu\text{m}^2$. (b) Cross-sectional TEM image and (c) Grazing incidence small angle x-ray scattering pattern of a $\sim 400\text{ nm}$ PS-*b*-PMMA film annealed 48hrs at 170°C under vacuum. Scale bar: 100 nm.

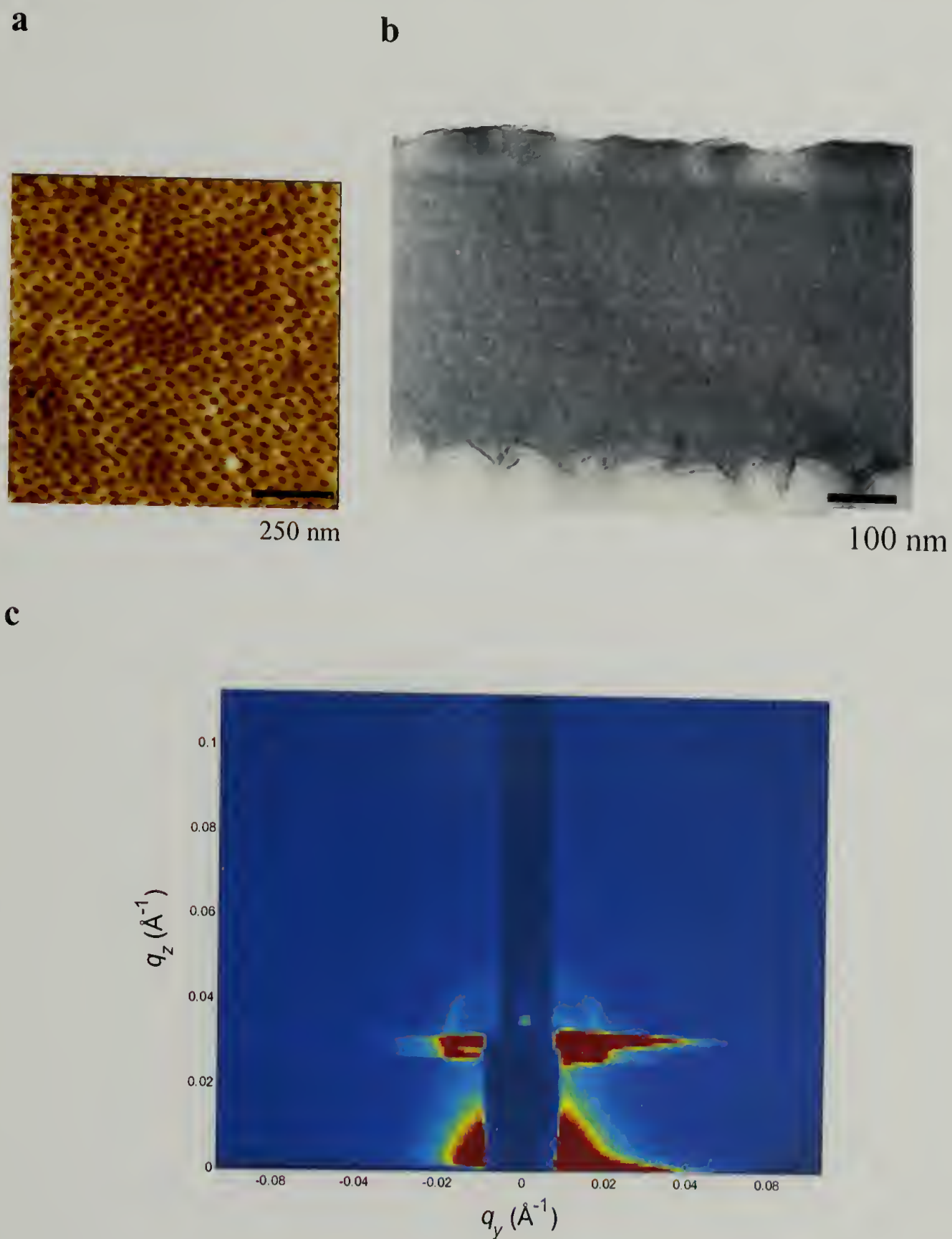


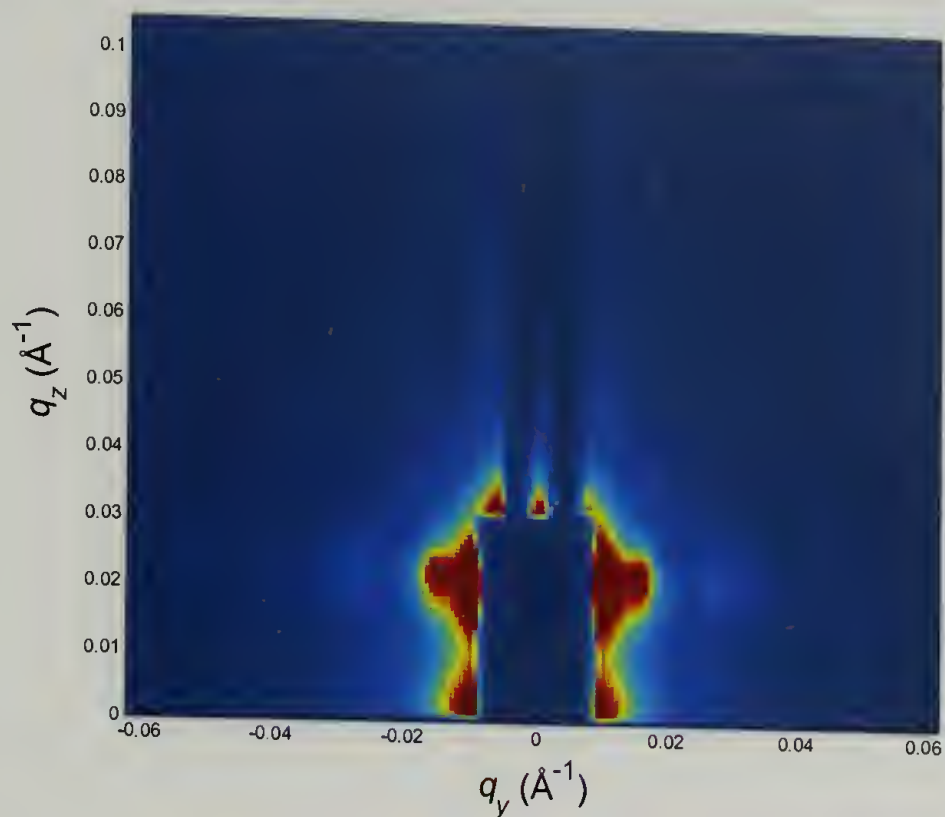
Figure 6.1b is the cross-sectional TEM image of a $\sim 400\text{ nm}$ film annealed at 170°C under vacuum for 48hrs. Layers of spherical microdomains induced by

the substrate (or air)/copolymer interfaces are clearly seen.^{33,34} From the side-view, the packing of the spherical microdomains is not well-defined. Shown in Figure 6.1c is the grazing incidence small angle x-ray scattering pattern of the film. The halo in the data confirms the random packing of the spherical microdomains. The scattering intensity is low due to the small electron density difference between PS and PMMA. In addition, the volume fraction of the spherical domains is only 0.1.

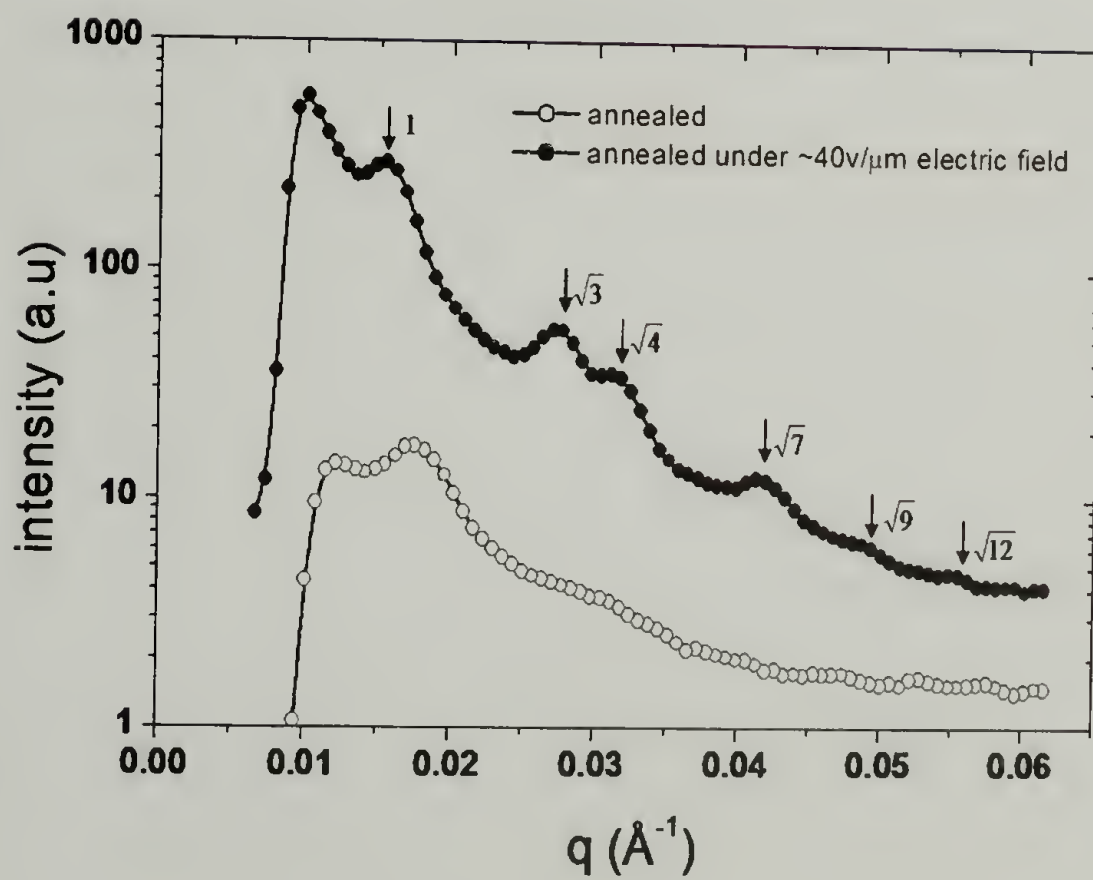
Figure 6.2a shows the grazing incident small angle X-ray scattering pattern taken at an incidence angle of ~ 0.2 degree of a ~ 400 nm film after annealing under ~ 40 V/ μ m electric field for ~ 20 hrs. The point-type scattering signal in along q_z direction is a resolution limited reciprocal space signature of the infinitely long line-type form factor. No maximum in the scattering is seen along q_z direction. Thus, interferences normal to the surface, and, hence, the layered structure of the spherical domains seen initially, have vanished. However, along q_y (in the plane of the film) multiple reflections are evident. This suggests that microdomains are aligned normal to the substrate and are no longer spherical. A q_y scan at $q_z \approx 0.022 \text{ \AA}^{-1}$ is shown in Figure 6.2b. After annealing under an electric field, a first order peak is seen at $q \approx 0.0154 \text{ \AA}^{-1}$ and higher order reflections with peak positions relative to the first order are seen at $1 : \sqrt{3} : \sqrt{4} : \sqrt{7} : \sqrt{9} : \sqrt{12}$. This indicates that the microdomains oriented normal to the surface are laterally packed into a hexagonally array.

Figure 6.2 (a) Grazing incidence small angle x-ray scattering pattern of a $\sim 400\text{nm}$ PS-*b*-PMMA film annealed at 170°C under $\sim 40\text{V}/\mu\text{m}$ electric field for 24hrs. (b) The q_y scan at $q_z \approx 0.022 \text{ \AA}^{-1}$ of the left side of the GISAXS pattern of the films annealed with and without electric field.

a



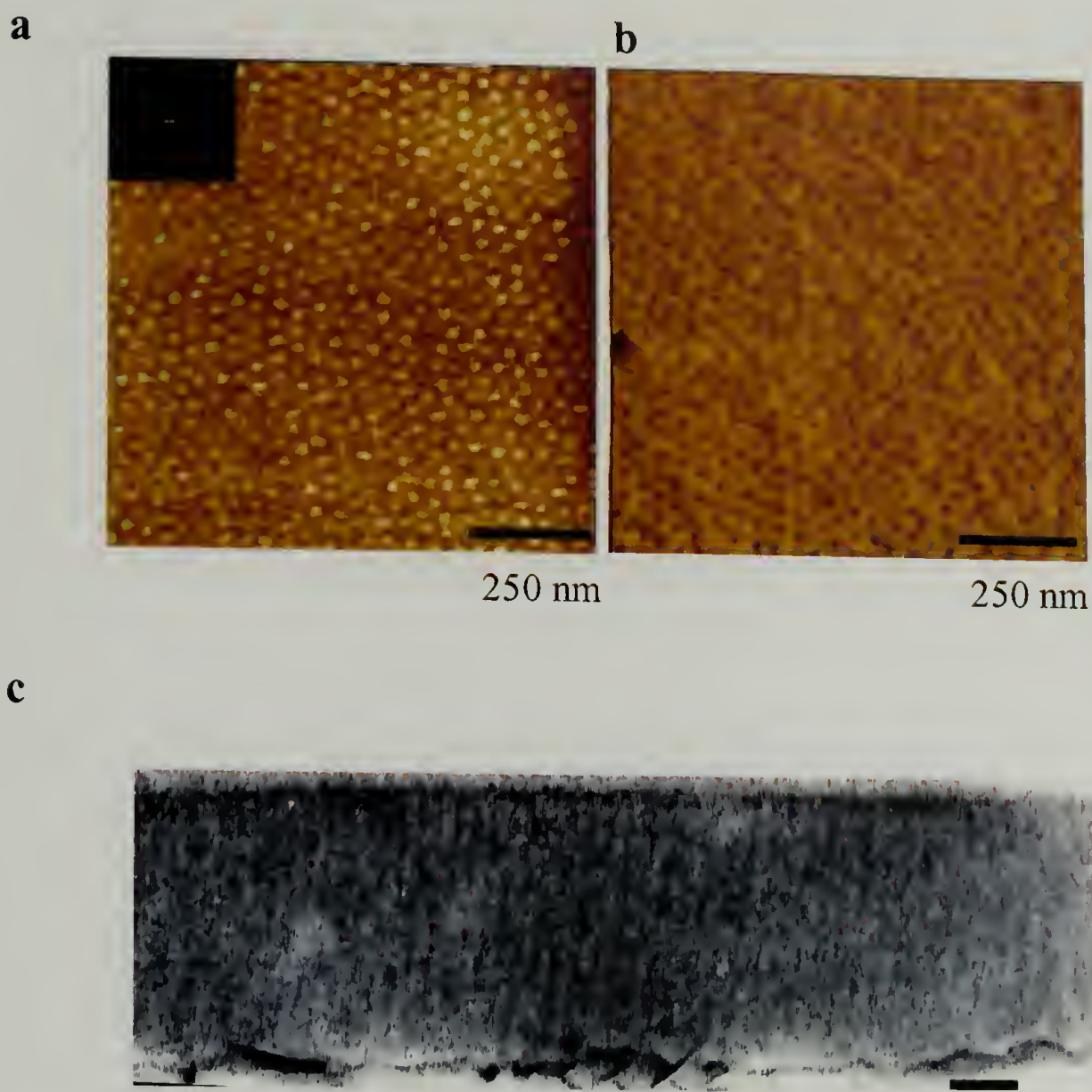
b



A q_y scan from the left side of the GISAXS image in Figure 1c was also plotted for comparison. For the film annealed without electric field, only the first order peak at $q \approx 0.0174 \text{ \AA}^{-1}$ with a diffuse shoulder is seen suggesting a morphology consistent with lattice-disordered spheres (LDS).^{10,35} Thus by applying an electric field normal to the surface, the spherical microdomains were transformed into cylindrical microdomain oriented normal to the surface. However, with GISAXS, it is not possible to discern whether the alignment of the microdomains extends completely to the interfaces.

Figure 6.3a shows the AFM phase image of a copolymer film after annealing under electric field at 170°C under N₂ for ~20hrs. The Fast Fourier Transform (FFT) of part of the image is shown in the inset. Hexagonally packed PMMA domains in PS matrix are seen. After deep UV exposure and rinsing with acetic acid, the AFM image in Figure 6.3b was obtained showing a nanoporous film with pores ~14nm in diameter. Figure 6.3c shows the cross-section TEM image of the film. The brighter PMMA cylinders oriented normal to the substrate are seen to penetrate through the entire film. The roughness on the surface is due to the fracture separation of the film from the neutral surface by dipping into liquid N₂.

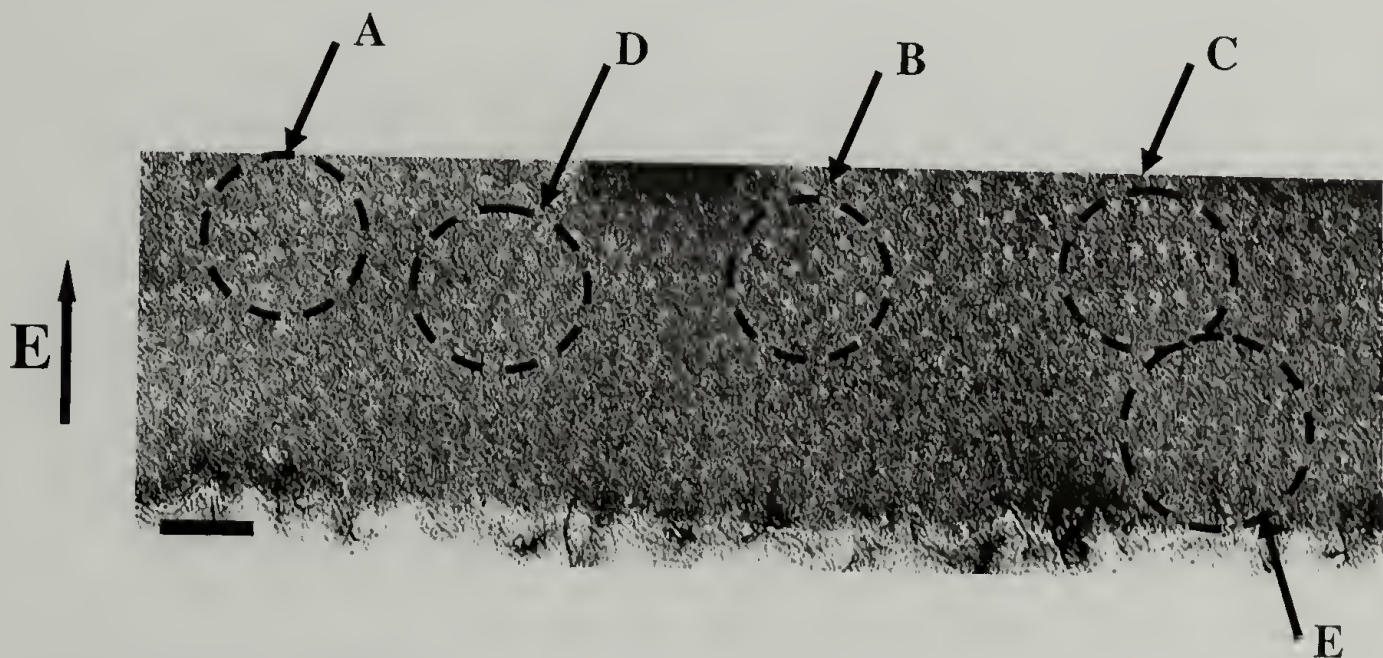
Figure 6.3 AFM phase image of a $\sim 400\text{nm}$ PS-*b*-PMMA film annealed at 170°C under $\sim 40\text{V}/\mu\text{m}$ electric field for 24hrs. (a) before and (b) after UV exposure and acetic acid rinsing to remove PMMA blocks. (c) cross-sectional TEM image of the film.



The process by which the sphere-to-cylinder transition occurs can be elucidated by the cross-sectional TEM image in Figure 4. This copolymer film has been annealed under electric field for 10hrs, shorter than the time necessary to produce the cylindrical microdomains shown in Figure 2. A mixed morphology of un-deformed spheres (A, B), deformed spheres (C, D) and interconnected spheres or ellipsoids (E) are seen in one image. Based on these different observations, the transition process can be deduced. In the early stage of the alignment, the diblock copolymer forms spherical microdomain even in the

presence of electric field. In A, B, the spherical microdomains have not yet been deformed. After annealing under an electric field for a longer time, the spherical microdomains in region A are deformed into ellipsoids (C, D) with their long axis oriented in the direction of the applied electric field. The ellipsoids, in turn, due most likely to induced polarization charges interconnect (E). These interconnections are not oriented in the field direction but, rather, are dictated by the proximity of poles of the ellipsoids of different sign. Eventually, they interconnect to cylindrical domains that become oriented along the field lines.

Figure 6.4 Cross-sectional TEM image of a $\sim 400\text{nm}$ PS-*b*-PMMA film annealed at 170°C under $\sim 40\text{V}/\mu\text{m}$ electric field for $\sim 10\text{hrs}$. Different morphologies are discernable. Region A, B: undeformed spherical microdomains. Region C, D; deformed spherical microdomains. Region E: deformed spherical microdomain connected into cylinders.



The electric field induced transition from spherical microdomains to cylinders was theoretically predicted to be $\sim 70\text{ V}/\mu\text{m}$ for the PS/PMMA system based on dielectric constants difference ($\epsilon_{\text{PS}} \approx 2.5$, $\epsilon_{\text{PMMA}} \approx 6$)²⁷. It was argued, that presence of the dislocated Li ions in the block copolymer may require considerably lower electric fields for this transition. Here, we present that transition occurred at an electric field of $\sim 40\text{V}/\mu\text{m}$, lower than the calculated

critical field strength. This may very possible be due to presence of trace lithium ion from anionic copolymerization. The measured elemental concentration of lithium impurity is less than 1 ppm. 1 ppm is the best resolution we can achieve and is much higher than the concentration necessary to reduce the critical electric field. Further experiments are carrying on quantifying the effect of lithium ion on the electric field alignment of diblock copolymer thin films.

Conclusions

Thus, an electric field induced sphere to cylinder transition in PS-*b*-PMMA diblock copolymer thin films has been observed. In the absence of an applied electric field, thin films of the asymmetric diblock copolymer were found to consist of layers of spherical microdomains with poor in-plane long-range ordering. Under a $\sim 40\text{V}/\mu\text{m}$ applied electric field, hexagonally-packed cylindrical microdomains oriented normal to the surface were found. After selectively remove the minor component, AFM images reveal cylindrical microdomains with diameters smaller than the original spherical microdomains. Cross-sectional transmission electron microscopy images of intermediate stages of the alignment indicate that under electric field, the asymmetric diblock copolymer forms the spherical microdomains that are deformed into ellipsoids that, with time interconnected to form cylindrical microdomains oriented in the direction of the applied electric field.

References

- (1) Bates, F. S.; Fredrickson, G. H. *Annual Reviews of Physics and Chemistry* **1990**, *41*, 5252.
- (2) Park, M.; Harrison, C.; Chaikin, P. M.; Register, R. A.; Adamson, D. *Science* **1997**, *276*, 1401.
- (3) Leibler, L. *Macromolecules* **1980**, *13*, 1602.
- (4) Wang, C. Y.; Lodge, T. P. *Macromolecules* **2002**, *35*, 6997.
- (5) Wang, C. Y.; Lodge, T. P. *Macromol Rapid Comm* **2002**, *23*, 49.
- (6) Sakurai, S.; Hashimoto, T.; Fetters, L. J. *Macromolecules* **1996**, *29*, 740.
- (7) Sakamoto, N.; Hashimoto, T.; Han, C. D.; Kim, D.; Vaidya, N. Y. *Macromolecules* **1997**, *30*, 1621.
- (8) Matsen, M. W. *J Chem Phys* **2001**, *114*, 8165.
- (9) Krishnamoorti, R.; Silva, A. S.; Modi, M. A.; Hammouda, B. *Macromolecules* **2000**, *33*, 3803.
- (10) Kimishima, K.; Koga, T.; Hashimoto, T. *Macromolecules* **2000**, *33*, 968.
- (11) Hajduk, D. A.; Gruner, S. M.; Rangarajan, P.; Register, R. A.; Fetters, L. J.; Honeker, C.; Albalak, R. J.; Thomas, E. L. *Macromolecules* **1994**, *27*, 490.
- (12) Ryu, C. Y.; Vigild, M. E.; Lodge, T. P. *Physical Review Letters* **1998**, *81*, 5354.
- (13) Amundson, K.; Helfand, E.; Davis, D. D.; Quan, X.; Patel, S. S.; Smith, S. D. *Macromolecules* **1991**, *24*, 6546.
- (14) Boker, A.; Knoll, A.; Elbs, H.; Abetz, V.; Muller, A. H. E.; Krausch, G. *Macromolecules* **2002**, *35*, 1319.
- (15) Mansky, P.; DeRouchey, J.; Russell, T. P.; Mays, J.; Pitsikalis, M.; Morkved, T.; Jaeger, H. *Macromolecules* **1998**, *31*, 4399.
- (16) Morkved, T. L.; Lu, M.; Urbas, A. M.; Ehrichs, E. E.; Jaeger, H. M.; Mansky, P.; Russell, T. P. *Science* **1996**, *273*, 931.
- (17) Thurn-Albrecht, T.; Steiner, R.; DeRouchey, J.; Stafford, C. M.; Huang, E.; Bal, M.; Tuominen, M.; Hawker, C. J.; Russell, T. P. *Adv. Mater.* **2000**, *12*, 1138.

- (18) Onuki, A.; Fukuda, J. *Macromolecules* **1995**, *28*, 8788.
- (19) Lin, Z. Q.; Kerle, T.; Baker, S. M.; Hoagland, D. A.; Schaffer, E.; Steiner, U.; Russell, T. P. *J Chem Phys* **2001**, *114*, 2377.
- (20) Schaffer, E.; Thurn-Albrecht, T.; Russell, T. P.; Steiner, U. *Nature* **2000**, *403*, 874.
- (21) Thurn-Albrecht, T.; DeRouchey, J.; Russell, T. P.; Jaeger, H. M. *Macromolecules* **2000**, *33*, 3250.
- (22) Thurn-Albrecht, T.; DeRouchey, J.; Russell, T. P.; Kolb, R. *Macromolecules* **2002**, *35*, 8106.
- (23) Pereira, G. G.; Williams, D. R. M. *Macromolecules* **1999**, *32*, 8115.
- (24) Amundson, K.; Helfand, E.; Quan, X.; Smith, S. D. *Macromolecules* **1993**, *26*, 2698.
- (25) Amundson, K.; Helfand, E.; Quan, X.; Hudson, S. D.; Smith, S. D. *Macromolecules* **1994**, *27*, 6559.
- (26) Landau, L. D.; Lifshitz, E. M.; Pitaevshii, L. P. *Electrodynamics of continuous media* **1984**, New York, vol. 8.
- (27) Yoav Tsori; Francois Tournilhac; David Andelman; Leibler, L. *Physical Review Letters* **2003**, *90*, 145504.
- (28) Segalman, R. A.; Yokoyama, H.; Kramer, E. J. *Adv Mater* **2001**, *13*, 1152.
- (29) Register, R. A.; al., e. *Abstracts of the American Physical Society* **2001**.
- (30) The lithium elemental concentration was measured by quantitative technology Inc.. Website: <http://www.QTionline.com>.
- (31) Mansky, P.; Liu, Y.; Huang, E.; Russell, T. P.; Hawker, C. *Science* **1997**, *275*, 1458.
- (32) Fasolka, M. J.; Banerjee, P.; Mayes, A. M.; Pickett, G.; Balazs, A. C. *Macromolecules* **2000**, *33*, 5702.
- (33) Henkee, C. S.; Thomas, E. L.; Fetters, L. J. *J Mater Sci* **1988**, *23*, 1685.
- (34) Yokoyama, H.; Mates, T. E.; Kramer, E. J. *Macromolecules* **2000**, *33*, 1888.
- (35) Sota, N.; Sakamoto, N.; Saijo, K.; Hashimoto, T. *Macromolecules* **2003**, *36*, 4534.

CHAPTER 7

SEQUENTIAL, ORTHOGONAL FIELDS: A PATH TO LONG-RANGE, 3-D ORDER IN BLOCK COPOLYMER THIN FILMS

Introduction

The long-range orientation and ordering of microdomains in thin films of diblock copolymers are requisite for applications that require spatial definition of structures in three dimensions. Thin films of block copolymers with microdomains oriented normal to the surface are finding increasing uses as templates and scaffolds for functional nanoscopic materials.¹ Many methods have been developed, such as shear and elongational flow fields, electric fields, surface fields and solvent flow, to achieve the desired microdomain orientation.²⁻

⁹ Shear and elongational flow fields, that result in nearly single crystal-like textures of the microdomains, as, for example produced in roll-casting processes, have proven successful in achieving long-range ordering in bulk samples.^{10,11} Copolymer films with lamellar and cylindrical microdomains, prepared by these methods, typically contain microdomains parallel to the shear or elongation direction, i.e. parallel to the surface of the sample. Many emerging applications for thin films of diblock copolymer require an orientation of the microdomains normal to the surface that can not be achieved by the methods developed for bulk samples. In thin films, electric fields have been effectively used to achieve an orientation of the microdomains normal to the surface.^{12,13} However, such fields are unidirectional causing a high degree of orientation along the field line direction, but lacking any preferred orientation in the plane normal to this direction. Consequently, a second field is required orthogonal to this field to

achieve a morphology where the microdomain orientation can be controlled in three dimensions.

Winey, *et al.* investigated the influence of the thermal history on the microdomain orientation in a lamellar diblock copolymer subsequent to shearing, and showed that large grains grew from nuclei formed during the shearing process.¹⁴ This observation points towards a route to achieve three dimensional ordering in diblock copolymer thin films. Using a shear field to generate oriented nuclei, a second field applied normal to the shearing direction can be used to further orient the growing microphase separated morphology and, thereby, produce a near single crystal texture.

Here, a simple process is shown that combines an elongational flow field with an applied electric field where the three-dimensional control over the orientation of lamellar microdomain orientation in thin films of poly(styrene-*b*-methyl methacrylate) diblock copolymers is achieved. Roll-pressing was done below order-disorder transition (ODT) but above the glass transition temperatures of both blocks where oriented nuclei of the microdomains form. Subsequent annealing under an electric field applied normal to the film surface produced a lamellar microdomain morphology with a high degree of long-range order and orientation as evidenced by small angle x-ray scattering and transmission electron microscopy.

Experimental

Materials

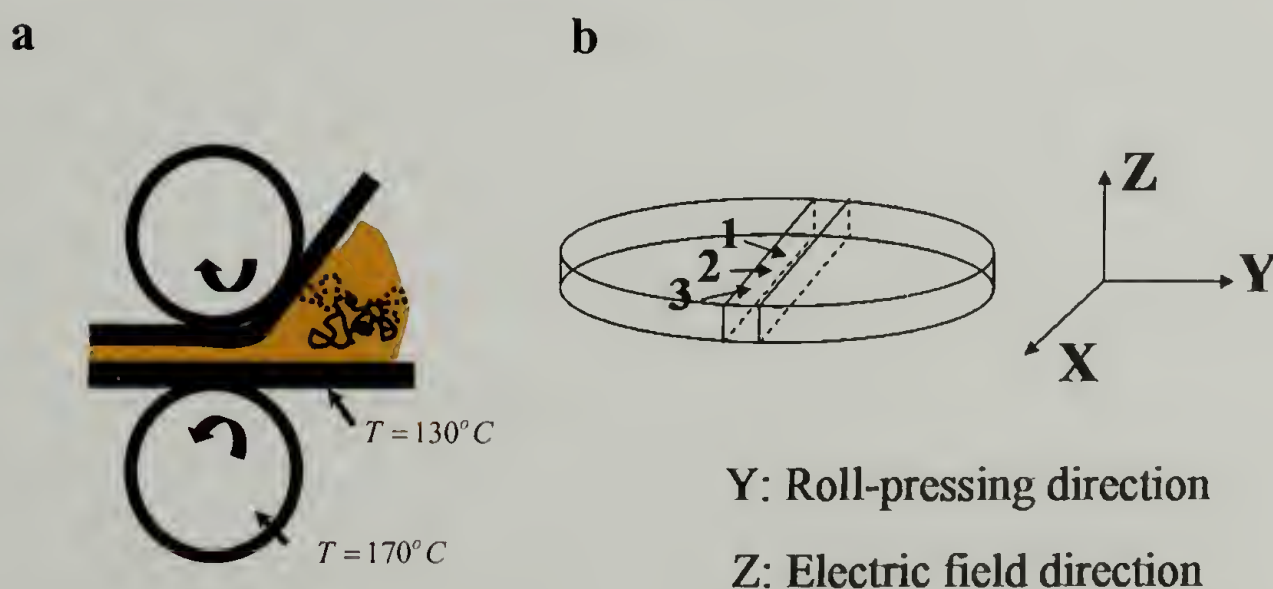
Symmetric polystyrene-*block*-poly(methyl methacrylate) diblock copolymers, PS-*b*-PMMA, were prepared by standard anionic polymerization methods, with $M_n = 45,600$ and a polydispersity $M_w/M_n = 1.08$. The equilibrium period of the lamellar microdomain morphology in the bulk is 18.7 nm, corresponding to the scattering vector $q^* = 0.336 \text{ nm}^{-1}$, determined by small angle x-ray scattering. Here $q = 4\pi/\lambda \sin\theta$, where λ is the wavelength of the x-rays and 2θ is the scattering angle.

Sample Preparation

Copolymer films were prepared by roll-pressing which is schematized in Figure 7.1a. A powder of the copolymer was sandwiched between two Kapton sheets and heated at 130°C for 5 minutes before rolling. The rollers were heated at 170°C and rotated at 5 mm·sec⁻¹. Clear, uniform films of the copolymers, ~ 300 μm thick, were obtained after 4-6 passes through the rollers. Two or three additional rolling passes were done to reduce the film thickness to ~30 μm. The length of the film increased approximately 8 times in the rolling direction while the width increased only slightly (typically less than a factor of two). The final shape of the film is shown schematically in Figure 7.1b. The flow patterns in the film vary across the width of the film during rolling. Near the center of the film (position 1), the orientation is uniaxial, whereas near the edge of the film (position 2 and 3), it is biaxial. Other, more complex orientations occur elsewhere across the film. The experiments shown here were performed using samples taken from the center of the film.

After roll-pressing, the film was placed between two aluminized Kapton electrodes (each 25.4 μm thick) and annealed at 170°C for 14 hours under an applied electric field of $\sim 20 \text{ V}\cdot\mu\text{m}^{-1}$. Small angle x-ray scattering (SAXS) was performed with nickel-filtered copper K_{α} radiation from a Rigaku rotating anode, operated at 8 kW. A gas-filled area detector (Siemens Hi-Star) was used. Scattering patterns were obtained with the beam incident normal to the sample surface with a counting time of 30 minutes. For transmission electron microscopy, a thin layer of carbon (10-20nm) was evaporated onto the surface to prevent the epoxy from diffusing into the copolymer films. The film was then embedded in epoxy and cured at 60°C for 12 hrs. The samples were microtomed with a diamond knife at room temperature and retrieved with a copper grid from the water surface. The thin sections were exposed to Ruthenium tetroxide for 35 min to enhance the contrast. The images were taken with a JEOL 100CX TEM at an acceleration voltage of 100KV.

Figure 7.1 (a) Schematic drawing of the roll-pressing and (b) the typical shape of copolymer thin films after roll-pressing.



Results and Discussion

Figure 7.2a shows the transmission SAXS pattern from the center of the sample after roll processing. A diffuse reflection is observed with peak position at $q^* = 0.342 \text{ nm}^{-1}$ and half-peak width of 0.051 nm^{-1} . The breadth of the reflection indicates that microphase separation is not complete during the roll-pressing and a non-equilibrium morphology is frozen-in when the film is quenched to room temperature upon exiting the rollers. Transmission electron microscopy (TEM) showed an ill-defined, microphase separated morphology (not shown here). The intensity of the SAXS along the ring of scatterings, i.e. the azimuthal angular dependence of the scattering, showed weak broad equatorial peaks indicating that the oriented nuclei have formed during the roll-pressing.

Figure 7.2 (a) SAXS pattern of a copolymer thin film after roll-pressing and (b) the integrated peak intensity as a function of azimuthal angle Ω .

a



b

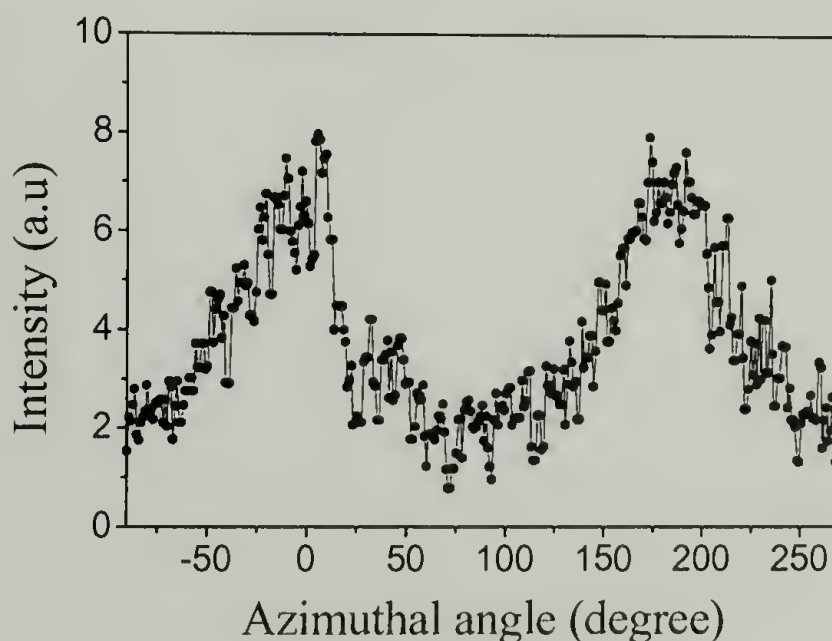


Figure 7.3 shows the SAXS pattern of the roll-pressed, thin film after annealing at 170°C under an applied electric field ($\sim 20 \text{ V}/\mu\text{m}$). Two sharp

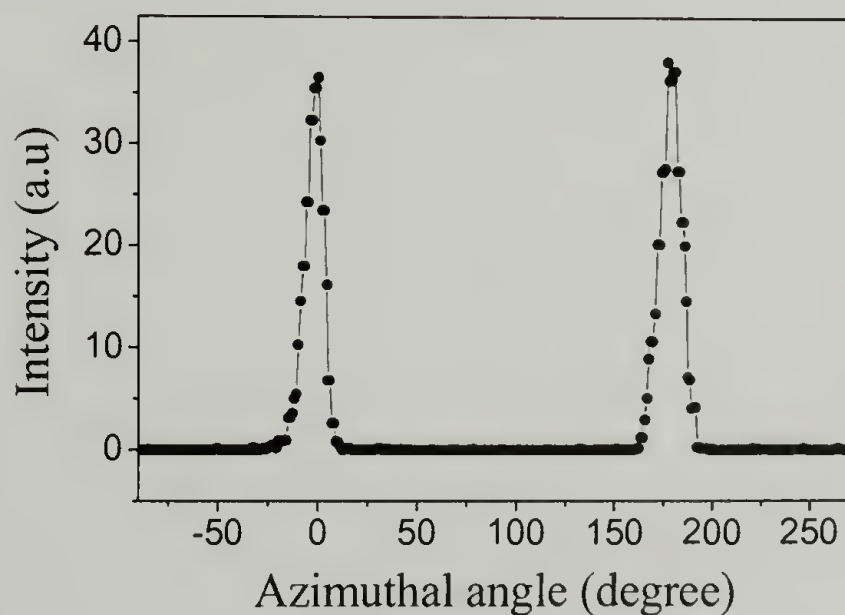
equatorial reflections, with peak position at $q^* = 0.336 \text{ nm}^{-1}$ and half-peak width of 0.026 nm^{-1} , are seen indicating a high degree of orientation of the lamellae normal to the surface and along the direction of flow. This is in contrast to thin films annealed only with an applied electric field, i.e. without roll-pressing elongational flow field, an isotropic ring of scattering is seen due to the random orientation of grains of the lamellae oriented normal to the surface.

Figure 7.3 (a) SAXS pattern of copolymer thin films after roll-pressing and applying a subsequent electric field normal to the film surface. (b) The integrated peak intensity as a function of azimuthal angle Ω .

a



b



To quantify the degree of the alignment, the order parameter or orientation function, f , was calculated.

$$f = \frac{3\langle \cos^2 \Omega \rangle - 1}{2}$$

with

$$\langle \cos^2 \Omega \rangle = \frac{\int_0^\pi d\Omega (I_q(\Omega) \cos^2 \Omega \sin \Omega)}{\int_0^\pi d\Omega (I_q(\Omega) \sin \Omega)}$$

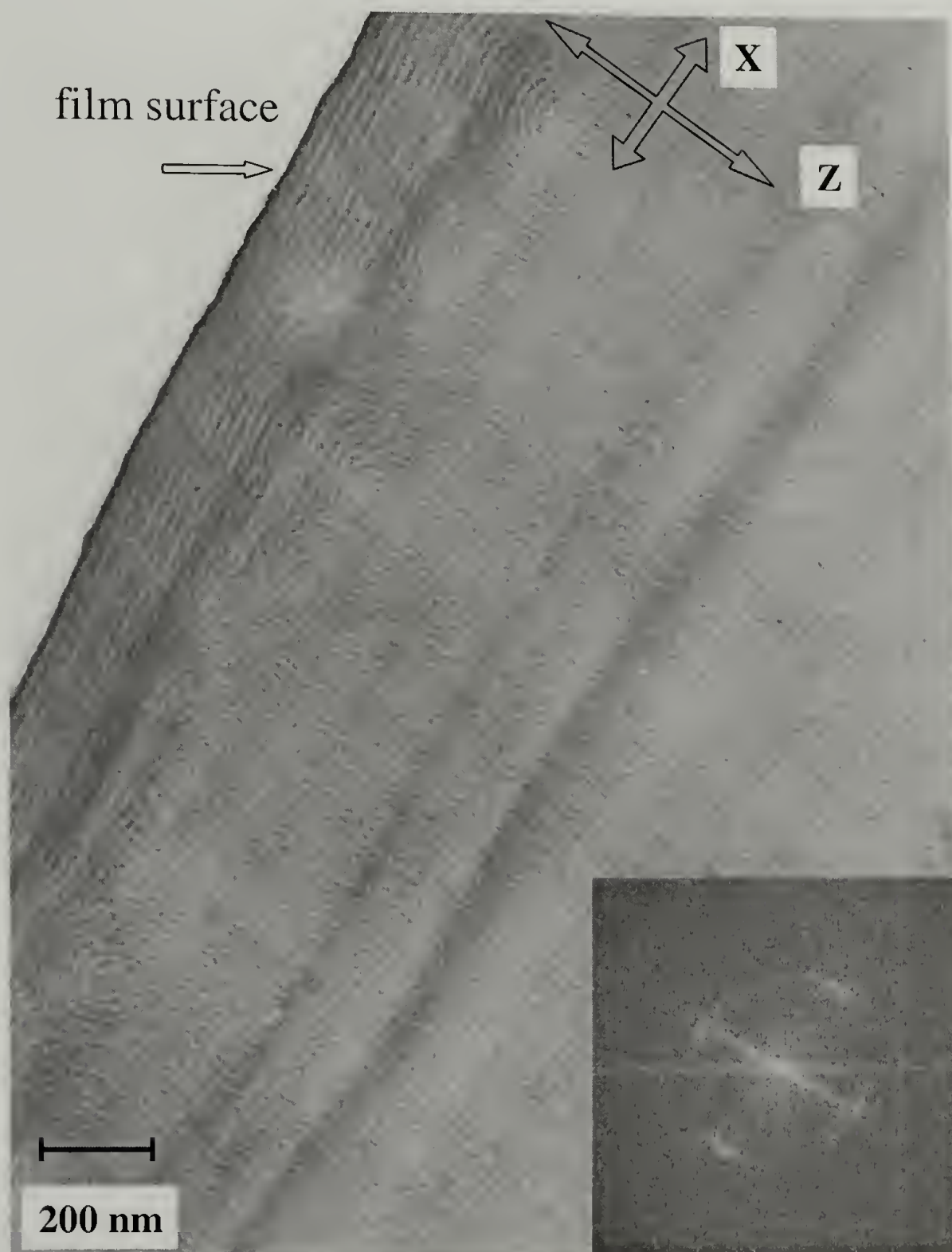
Where Ω is the azimuthal angle defined from the orientation direction ($\Omega=0$) and $I_q(\Omega)$ is the intensity at a given Ω integrated over its full width in q . f has limits of $-1/2$ and 1 , corresponding to orientation of lamellae normal to and parallel to the flow direction and 0 corresponds to a random orientation. From the data in Figure 7.3b, $f = 0.9$, i.e the lamellae are almost fully oriented in the flow direction. Thus, three dimensional control over the microdomain orientation was achieved with the lamellar planes oriented parallel to the flow direction and normal to the surface.

SAXS data shows that a global orientation of microdomains in the diblock copolymer thin film has been achieved. On a more local level, TEM was used as a probe. Figure 7.4 shows the cross-sectional TEM images of the copolymer film viewed into the flow direction, i.e the XZ plane in Figure 7.1b. Figure 7.4a is a typical TEM image at both surfaces of the thin film where a mixed orientation can be seen. At both surfaces, the lamellae orient parallel to the surface of the electrodes. This arises from a preferential wetting of PMMA on the electrodes as discussed previously.¹⁵ In the center of the film, the lamellae are oriented perpendicular to the substrate (parallel to the electric field direction).

Four-spot fourier transform (FFT) pattern of this micrograph, resulting from the mixture orientation, is shown in the inset.

Figure 7.4 TEM cross-sectional images of (a) the copolymer/substrate interface and (b) the interior of the film.

a



Continued next page

Figure 7.4, Continued

b



Figure 7.4b shows a typical TEM cross-sectional image for rest of the film along Z direction. Over very large areas, the orientation and order are defect-free. Only one grain was found within the field of view. This result is

quite remarkable in comparison to previous results using only an electric field where many grains are found.¹⁶ The Fourier transform (FFT) of this micrograph is shown in the inset. Two sharp spots are observed in the pattern, showing the presence of only one large grain of lamellae, with a uniform separation distance between the lamellae, oriented normal to the surface and in the flow direction. The uniformity of the spacing in the micrograph also reflects the perfection in orientation, since different orientations of the lamellae would result in different widths of the lamellae in the TEM image. To characterize the extent of the ordering, TEM images were taken every $\sim 3 \mu\text{m}$ along the X and Z directions of the sample. The FFT of each of these TEM images is shown in Figure 7.5.

Again, the interlamellar spacing is constant across the film and no deviation of the orientation along Z was observed. In the X direction, the ordering extends over hundreds of microns. Only a small fraction of the FFT's is shown here.

Though the order and orientation extends very large distances, defects still exist with frequently-observed defects being shown in Figure 7.6. Shown in the inset is the FFT transform of the micrograph. However, from the SAXS measurements, it is apparent that the number of defects is very small.

SAXS and TEM results confirm that 3-dimensional control over lamellar microdomain orientation can be achieved by using two orthogonal fields, namely an elongational flow and an electric field, applied sequentially. The copolymer thin film was biased first by an elongational flow field that produced oriented nuclei during the roll-pressing at a temperature below the ODT. Complete ordering of the copolymer in an applied external electric field yielded a lamellar

microdomain morphology where there was a three-dimensional control over the orientation.

Figure 7.5 FFT patterns of TEM images at different positions of the film. The TEM images were taken every $\sim 3\mu\text{m}$ (a) normal to the film surface (along the Z direction in Fig. 7.4a), the first images on the left side of the sequence was taken right after Fig. 7.4a., and subsequent images were taken towards the other side of the film. The last image on the right of the z-axis sequence (top) exhibits a 4-point pattern due to the mixed orientation of the lamellar microdomains at the film edge. (b) The first image was taken in the center of the film and subsequent images were taken normal to the flow direction (along the X direction in Fig. 7.4a). The grain size is too large to be shown all and only small portion was shown.

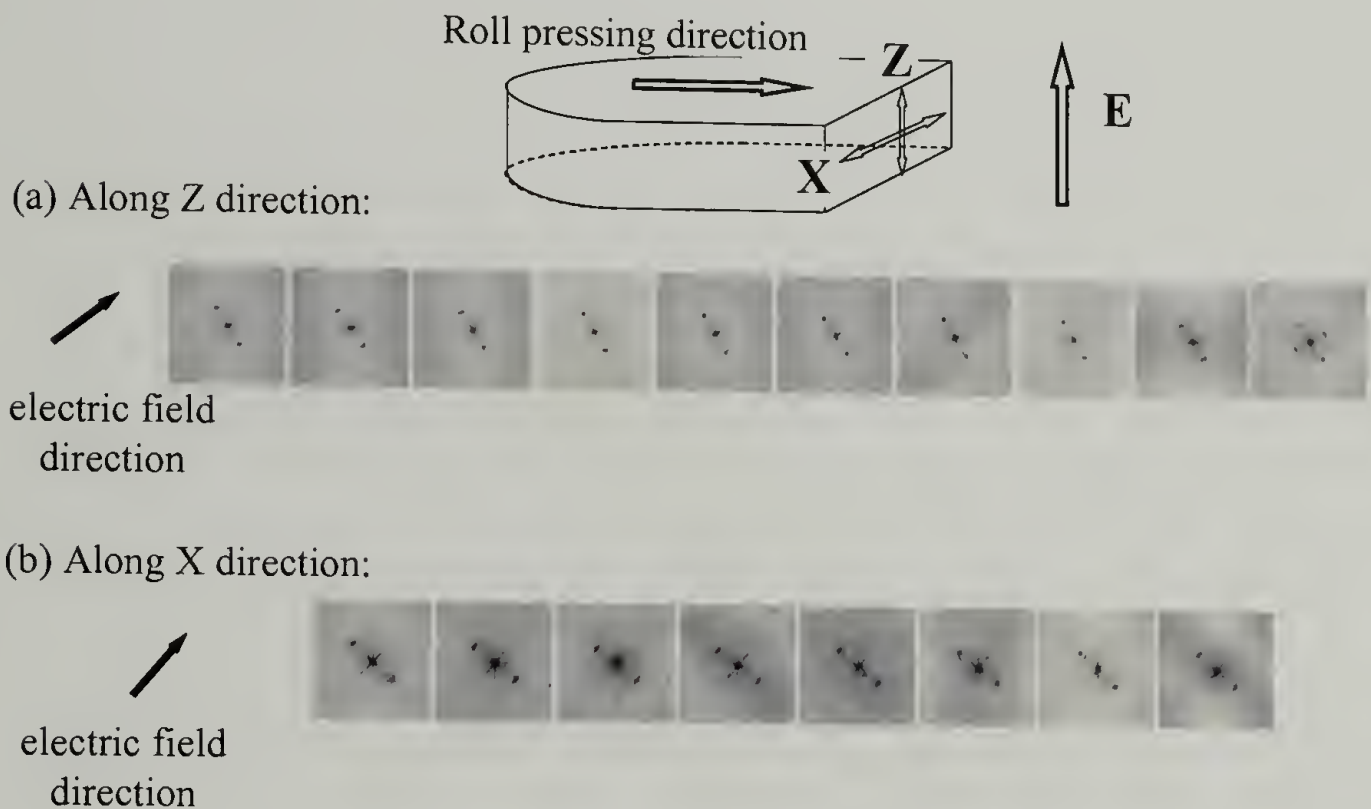


Figure 7.6 Cross-sectional TEM image of typical defects. While there were few defects, the defects shown were observed the most frequently.



Several important parameters affected the degree of orientation and ordering in these samples. The influence of the electric field strength on the microdomain alignment along the applied electric field direction has been studied and there is a critical electric field strength required to achieve the alignment.^{7,17} A similar situation is found with the elongational flow field where a high degree

of in-plane ordering is achieved only when the strain rate is high. The ordering parameter decreases with decreasing strain rate. The high degree of in-plane shown was obtained with the strain rate ~ 8 . Lower degree of orientation was obtained using lower strain rate. However, a simple squeeze flow generates the in-plane orientation. Thus, three dimensional ordering could only be achieved when both field strengths are sufficiently high. These results shown here were acquired from the samples in the center where there is a high degree of uniaxial stretching. Other locations in the sample that are subjected to different flow fields do not exhibit such order and orientation. Different SAXS patterns were found that show a direct correlation between the flow-direction and the in-plane microdomain orientation. Consequently, the in-plane orientation of the microdomains can be tailored by varying the flow pattern.

The experiments shown here have been done with copolymer films that were ~ 20 - $50\mu\text{m}$ thick. For many applications, films with thickness $\leq 1\mu\text{m}$ are desirable. Fundamentally, the mechanism behind the method reported here should be applicable for such thin films also. Slight modifications in producing an elongational flow field are necessary, since such thin films would be supported on a rigid substrate. This can be solved by use of novel shearing techniques, as, for example that recently developed by Chaikin and coworkers to achieve long range ordering in thin block copolymer films with spherical or cylindrical microdomains or by use of highly oriented flow fields in solution, as recently discussed by Kimura *et al.*^{18,9} In either case, oriented nuclei in thin films

can be generated that can then be used to initiate the growth of microdomains under an applied electric field.

Conclusions

It has been shown that the orientation of lamellar microdomains in PS-*b*-PMMA can be controlled in three dimensions by use of two orthogonal external fields. An elongational flow field was applied to a copolymer melt to control the in-plane orientation and a subsequent external electric field was applied to control orientation normal to the film surface. Excellent, long-range order and orientation of the lamellar microdomains was observed by SAXS and TEM.

References

- (1) Thurn-Albrecht, T.; Schotter, J.; Kastle, G. A.; Emley, N.; Shibauchi, T.; Krusin-Elbaum, L.; Guarini, K.; Black, C. T.; Tuominen, M. T.; Russell, T. P. *Science* **2000**, *290*, 2126.
- (2) Cohen, Y.; Albalak, R. J.; Dair, B. J.; Capel, M. S.; Thomas, E. L.; *Macromolecules* **2000**, *33*, 6502.
- (3) Honeker, C. C.; Thomas, E. L.; *Macromolecules* **2000**, *33*, 9407.
- (4) Keller, A.; Pedemonte, E.; Willmouth, F. M.; *Nature*, **1970**, *225*, 538.
- (5) Kobori, Y.; Kwon, Y. K.; Okamoto, M.; Kotaka, T.; *Macromolecules* **2003**, *36*, 1656.
- (6) Amundson, K.; Helfand, E.; Davis, D. D.; Quan, X.; Patel, S. S.; Smith, S. D. *Macromolecules* **1991**, *24*, 6546.
- (7) Morkved, T.; Lu, M.; Urbas, A. M.; Ehrichs, E. E.; Jaeger, H. M.; Mansky, P.; Russell, T. P. *Science*, **1996**, *273*, 931.
- (8) Huang, E.; Rockford, L.; Russell, T. P.; Hawker, C. J.; Mays, J.; *Nature* **1998**, *395*, 757.
- (9) Kimura, M.; Misner, M. J.; Xu, T.; Kim, S. H.; Russell, T. P.; *Langmuir*, **2003**, *19*, 9910.
- (10) Albalak, R. J.; Thomas, E. L.; *J. Polym. Sci., B: Polym. Phys.* **1994**, *31*, 37.
- (11) Albalak, R. J.; Thomas, E. L.; *J. Polym. Sci., B: Polym. Phys.*, **1993**, *32*, 341.
- (12) Thurn-Albrecht, T.; DeRouchey, J.; Russell, T. P.; Kolb, R.; *Macromolecules*, **2002**, *35*, 8106.
- (13) Boker, A.; Knoll, A.; Elbs, H.; Abetz, V.; Muller, A. H. E.; Krausch, G.; *Macromolecules* **2002**, *35*, 1319.
- (14) Winey, K. I.; Patel, S.; Larson, R. G.; Watanabe, H.; *Macromolecules*, **1993**, *26*, 2376.
- (15) Xu, T.; Hawker, C. J.; Russell, T. P.; *Macromolecules*, **2003**, *36*, 6178.
- (16) Amundson, K.; Helfand, E.; Quan, X.; Hudson, S. D.; Smith, S. D.; *Macromolecules* **1994**, *27*, 6559.
- (17) Thurn-Albrecht, T.; DeRouchey, J.; Jaeger, H. M.; Russell, T. P.; *Macromolecules*, **2000**, *33*, 3250.

- (18) Chaikin, P. *et.al*, *American Physics Society*, Annual Meeting, Austin, TX, **2003**.

BIBLIOGRAPHY

- (1) Albalak, R. J.; Thomas, E. L. *J Polym Sci Pol Phys* **1993**, *31*, 37.
- (2) Albalak, R. J.; Thomas, E. L. *J Polym Sci Pol Phys* **1994**, *32*, 341.
- (3) Amundson, K.; Helfand, E.; Davis, D. D.; Quan, X.; Patel, S. S.; Smith, S. D. *Macromolecules* **1991**, *24*, 6546.
- (4) Amundson, K.; Helfand, E.; Quan, X.; Smith, S. D. *Macromolecules* **1993**, *26*, 2698.
- (5) Amundson, K.; Helfand, E.; Quan, X. N.; Hudson, S. D.; Smith, S. D. *Macromolecules* **1994**, *27*, 6559.
- (6) Anastasiadis, S. H.; Russell, T. P.; Satija, S. K.; Majkrzak, C. F. *Physical Review Letters* **1989**, *62*, 1852.
- (7) Anastasiadis, S. H.; Russell, T. P.; Satija, S. K.; Majkrzak, C. F. *J Chem Phys* **1990**, *92*, 5677.
- (8) Ashok, B.; Muthukumar, M.; Russell, T. P. *J Chem Phys* **2001**, *115*, 1559.
- (9) Bates, F. S.; Fredrickson, G. H. *Annual Reviews of Physics and Chemistry* **1990**, *41*, 5252.
- (10) Boker, A.; Elbs, H.; Hansel, H.; Knoll, A.; Ludwigs, S.; Zettl, H.; Urban, V.; Abetz, V.; Muller, A. H. E.; Krausch, G. *Physical Review Letters* **2002**, *89*, 135502.
- (11) Boker, A.; Knoll, A.; Elbs, H.; Abetz, V.; Muller, A. H. E.; Krausch, G. *Macromolecules* **2002**, *35*, 1319.
- (12) Boker, A.; Elbs, H.; Hansel, H.; Knoll, A.; Ludwigs, S.; Zettl, H.; Zvelindovsky, A. V.; Sevink, G. J. A.; Urban, V.; Abetz, V.; Muller, A. H. E.; Krausch, G. *Macromolecules* **2003**, *36*, 8078.
- (13) Brown, G.; Chakrabarti, A. *J Chem Phys* **1994**, *101*, 3310.
- (14) Coulon, G.; Deline, V. R.; Russell, T. P.; Green, P. F. *Macromolecules* **1989**, *22*, 2581.
- (15) Coulon, G.; Daillant, J.; Collin, B.; Benattar, J. J.; Gallot, Y. *Macromolecules* **1993**, *26*, 1582.
- (16) DeRouchey, J.; Russell, T. P. *Unpublished results* **2003**.
- (17) Fasolka, M. J.; Banerjee, P.; Mayes, A. M.; Pickett, G.; Balazs, A. C. *Macromolecules* **2000**, *33*, 5702.
- (18) Fasolka, M. J.; Mayes, A. M. *Ann Rev Mater Res* **2001**, *31*, 323.
- (19) Fredrickson, G. H. *Macromolecules* **1987**, *20*, 2535.
- (20) Hajduk, D. A.; Gruner, S. M.; Rangarajan, P.; Register, R. A.; Fetters, L. J.; Honeker, C.; Albalak, R. J.; Thomas, E. L. *Macromolecules* **1994**, *27*, 490.

- (21) Hasegawa, H.; Hashimoto, T. *Macromolecules* **1985**, *18*, 589.
- (22) Hawker, C. J. *Macromolecules* **1996**, *29*, 2686.
- (23) Henkee, C. S.; Thomas, E. L.; Fetters, L. J. *J Mater Sci* **1988**, *23*, 1685.
- (24) Huang, E.; Rockford, L.; Russell, T. P.; Hawker, C. J. *Nature* **1998**, *395*, 757.
- (25) Huang, E.; Russell, T. P.; Harrison, C.; Chaikin, P. M.; Register, R. A.; Hawker, C. J.; Mays, J. *Macromolecules* **1998**, *31*, 7641.
- (26) Karim, A.; Singh, N.; Sikka, M.; Bates, F. S. *J Chem Phys* **1994**, *100*, 1620.
- (27) Keller, A.; Pedemonte, E.; Willmouth, F. M. *Nature* **1970**, *225*, 538.
- (28) Kim, C. S.; Oh, S. M. *Electrochim. Acta* **2000**, *45*, 2101.
- (29) Kimishima, K.; Koga, T.; Hashimoto, T. *Macromolecules* **2000**, *33*, 968.
- (30) Krishnamoorti, R.; Modi, M. A.; Tse, M. F.; Wang, H. C. *Macromolecules* **2000**, *33*, 3810.
- (31) Krishnamoorti, R.; Silva, A. S.; Modi, M. A.; Hammouda, B. *Macromolecules* **2000**, *33*, 3803.
- (32) Kunz, M.; Shull, K. *Polymer* **1993**, *34*, 2427.
- (33) Kyrylyuk, A. V.; Zvelindovsky, A. V.; Sevink, G. J. A.; Fraaije, J. G. E. M. *Macromolecules* **2002**, *35*, 1473.
- (34) Lambooy, P.; Russell, T. P.; Kellogg, G. J.; Mayes, A. M.; Gallagher, P. D.; Satija, S. K. *Physical Review Letters* **1994**, *72*, 2899.
- (35) Landau, L. D.; Lifshitz, E. M.; Pitaevshii, L. P. *Electrodynamics of continuous media* **1984**, New York Vol: 8.
- (36) Leibler, L. *Macromolecules* **1980**, *13*, 1602.
- (37) Lin, Z. Q.; Kerle, T.; Baker, S. M.; Hoagland, D. A.; Schaffer, E.; Steiner, U.; Russell, T. P. *J Chem Phys* **2001**, *114*, 2377.
- (38) Lin, Z. Q.; Kerle, T.; Russell, T. P.; Schaffer, E.; Steiner, U. *Macromolecules* **2002**, *35*, 6255.
- (39) Lin, Z. Q.; Kerle, T.; Russell, T. P.; Schaffer, E.; Steiner, U. *Macromolecules* **2002**, *35*, 3971.
- (40) Liu, Y.; Zhao, W.; Zheng, X.; King, A.; Singh, A.; Rafailovich, M. H.; Sokolov, J. *Macromolecules* **1994**, *27*, 4111.
- (41) Mansky, P.; Russell, T. P. *Macromolecules* **1995**, *28*, 8092.
- (42) Mansky, P.; Liu, Y.; Huang, E.; Russell, T. P.; Hawker, C. *Science* **1997**, *275*, 1458.
- (43) Mansky, P.; Russell, T. P.; Hawker, C. J.; Mays, J.; Cook, D. C.; Satija, S. K. *Physical Review Letters* **1997**, *79*, 237.

- (44) Mansky, P.; Liu, Y.; Huang, E.; Russell, T. P.; Hawker, C. *Science* **1997**, *275*, 1458.
- (45) Mansky, P.; DeRouchey, J.; Russell, T. P.; Mays, J.; Pitsikalis, M.; Morkved, T.; Jaeger, H. *Macromolecules* **1998**, *31*, 4399.
- (46) Matsen, M. W. *Current Opinion in Colloid & Interface Science* **1998**, *3*, 40.
- (47) Matsen, M. W. *J Chem Phys* **2001**, *114*, 8165.
- (48) Menelle, A.; Russell, T. P.; Anastasiadis, S. H.; Satija, S. K.; Majkrzak, C. F. *Physical Review Letters* **1992**, *68*, 67.
- (49) Milner, S. T.; Morse, D. C. *Physical Review E* **1996**, *54*, 3793.
- (50) Morkved, T. L.; Lu, M.; Urbas, A. M.; Ehrichs, E. E.; Jaeger, H. M.; Mansky, P.; Russell, T. P. *Science* **1996**, *273*, 931.
- (51) Nonomura, M.; Ohta, T. *Physica A* **2002**, *304*, 77-84.
- (52) Onuki, A.; Fukuda, J. *Macromolecules* **1995**, *28*, 8788.
- (53) Park, M.; Harrison, C.; Chaikin, P. M.; Register, R. A.; Adamson, D. *Science* **1997**, *276*, 1401.
- (54) Pereira, G. G.; Williams, D. R. M. *Macromolecules* **1999**, *32*, 8115.
- (55) Register, R. A.; al., e. *Abstracts of the American Physical Society* **2001**.
- (56) Ryu, C. Y.; Vigild, M. E.; Lodge, T. P. *Physical Review Letters* **1998**, *81*, 5354.
- (57) Ryu, C. Y.; Lodge, T. P. *Macromolecules* **1999**, *32*, 7190.
- (58) Sakamoto, N.; Hashimoto, T.; Han, C. D.; Kim, D.; Vaidya, N. Y. *Macromolecules* **1997**, *30*, 1621.
- (59) Sakamoto, N.; Hashimoto, T.; Han, C. D.; Kim, D.; Vaidya, N. Y. *Macromolecules* **1997**, *30*, 5321.
- (60) Sakurai, S.; Hashimoto, T.; Fetters, L. J. *Macromolecules* **1996**, *29*, 740.
- (61) Schafer, E.; Thurn-Albrecht, T.; Russell, T. P.; Steiner, U. *Europhys Lett* **2001**, *53*, 518.
- (62) Schaffer, E.; Thurn-Albrecht, T.; Russell, T. P.; Steiner, U. *Nature* **2000**, *403*, 874.
- (63) Segalman, R. A.; Yokoyama, H.; Kramer, E. J. *Adv Mater* **2001**, *13*, 1152.
- (64) Silva, A. S.; Mitchell, C. A.; Tse, M. F.; Wang, H. C.; Krishnamoorti, R. *J Chem Phys* **2001**, *115*, 7166.
- (65) Sivaniah, E.; Hayashi, Y.; Iino, M.; Hashimoto, T.; Fukunaga, K. *Macromolecules* **2003**, *36*, 5894.
- (66) Sota, N.; Sakamoto, N.; Saijo, K.; Hashimoto, T. *Macromolecules* **2003**, *36*, 4534.

- (67) Suh, K. Y.; Lee, H. H. *Journal of Polymer Science: Part B: Polymer Physics* **2001**, *39*, 2217.
- (68) Thomas, E. L.; Kinning, D. J.; Alward, D. B.; Henkee, C. S. *Macromolecules* **1987**, *20*, 2934.
- (69) Thurn-Albrecht, T.; DeRouchey, J.; Russell, T. P.; Jaeger, H. M. *Macromolecules* **2000**, *33*, 3250.
- (70) Thurn-Albrecht, T.; Steiner, R.; DeRouchey, J.; Stafford, C. M.; Huang, E.; Bal, M.; Tuominen, M.; Hawker, C. J.; Russell, T. P. *Adv. Mater.* **2000**, *12*, 1138.
- (71) Thurn-Albrecht, T.; Schotter, J.; Kastle, C. A.; Emley, N.; Shibauchi, T.; Krusin-Elbaum, L.; Guarini, K.; Black, C. T.; Tuominen, M. T.; Russell, T. P. *Science* **2000**, *290*, 2126.
- (72) Thurn-Albrecht, T.; Steiner, R.; DeRouchey, J.; Stafford, C. M.; Huang, E.; Bal, M.; Tuominen, M.; Hawker, C. J.; Russell, T. *Adv Mater* **2000**, *12*, 787.
- (73) Thurn-Albrecht, T.; DeRouchey, J.; Russell, T. P.; Kolb, R. *Macromolecules* **2002**, *35*, 8106.
- (74) Tsori, Y.; Andelman, D. *Macromolecules* **2002**, *35*, 5161.
- (75) Tsori, Y.; Tournilhac, F.; Andelman, D.; Leibler, L. *Physical Review Letters* **2003**, *90*, 145504.
- (76) Tsori, Y.; Tournilhac, F.; Leibler, L. *Macromolecules* **2003**, *36*, 5873.
- (77) Wang, C. Y.; Lodge, T. P. *Macromol Rapid Comm* **2002**, *23*, 49.
- (78) Wang, C. Y.; Lodge, T. P. *Macromolecules* **2002**, *35*, 6997.
- (79) Winey, K. I.; Patel, S. S.; Larson, R. G.; Watanabe, H. *Macromolecules* **1993**, *26*, 4373.
- (80) Xu, T.; Kim, H. C.; DeRouchey, J.; Seney, C.; Levesque, C.; Martin, P.; Stafford, C. M.; Russell, T. P. *Polymer* **2001**, *42*, 9091.
- (81) Xu, T.; Hawker, C. J.; Russell, T. P. *Macromolecules* **2003**, *36*, 6178.
- (82) Xu, T.; Zhu, Y.; Gido, S. P.; Russell, T. P. *Macromolecules* **2004**, accepted.
- (83) Xu, T.; Hawker, C. J.; Russell, T. P. **2004**, in preparation.
- (84) Xu, T.; Russell, T. P. **2004**, in preparation.
- (85) Yoav Tsori; Francois Tournilhac; David Andelman; Leibler, L. *Physical Review Letters* **2003**, *90*, 145504.
- (86) Yokoyama, H.; Mates, T. E.; Kramer, E. J. *Macromolecules* **2000**, *33*, 1888.
- (87) Zvelindovsky, A. V.; A., S. G. J. *Physical Review Letters* **2003**, *90*, 49601.

